博士論文

Thermal properties of PDMS composite containing aligned CNTs

(配向 CNT－PDMS 複合材料の熱物性)

車　振赫

Thermal properties of PDMS composite containing aligned CNTs

(配向 CNT－PDMS 複合材料の熱物性)

Jin Hyeok Cha

工学系研究科機械工学専攻

Department of Mechanical Engineering
School of Engineering

A THESIS SUBMITTED IN PARTIAL FULILLMENT OF

THE REQUIREMENTS FOR THE DEGREE OF

***Philosophiæ Doctor* (*Ph. D.*)**

August 2014

THE UNIVERSITY OF TOKYO

This thesis entitled "Thermal properties of PDMS composite containing aligned CNTs", submitted by JinHyeok Cha, is approved by the undersigned members of this committee:

Shigeo Maruyama, Professor
Thesis Advisor and Committee Chair
Department of Mechanical Engineering
The University of Tokyo, Japan.

Hideaki Murayama, Associate Professor
Department of Systems Innovation
The University of Tokyo, Japan.

Junichiro Shiomi, Associate Professor
Department of Mechanical Engineering
The University of Tokyo, Japan.

Reo Kometani, Lecturer
Department of Mechanical Engineering
The University of Tokyo, Japan.

Shohei Chiashi, Lecturer
Department of Mechanical Engineering
The University of Tokyo, Japan.

Declaration

I, hereby declare that the investigation presented in the thesis entitled "Thermal properties of PDMS composite containing aligned CNTs" submitted to The University of Tokyo, Japan for the award of Doctoral degree is the record of work carried out by me during the period from April 2011 to August 2014 under the supervision of Dr. Shigeo Maruyama. The work is original and has not been submitted earlier as a whole or in part for a degree at this or any other academic institutions.

Cha Jin Myeok

Tokyo, August 2014

Table of Contents

Acknowledgment

During the course of this thesis, I have been privileged to receive the advice and assistance from numerous people. I would like to thank them all, but mentioning only a few is allowed here.

First and foremost, I would like to express my sincere heart of gratitude to my advisor, Prof. Shigeo Maruyama for his support and encouragement to complete my research successfully throughout the course. No matter how many questions, how hard it is, and how much time takes for discussion, he always joined the discussion and suggested me a rough idea to let me solve the problems in various perspectives. Through the process, I have learned how to think and create idea when facing to some problems. Not only that, but he has concerned my whole life staying in Japan that his kind consideration helped me to overcome the situation when I was in trouble.

I am particularly grateful to Dr. Shohei Chiashi who gave consistent feedback on my research throughout my stay in Japan. His valuable suggestions and guidance filled me with courage and confidence whenever I was let down by various problems during the research. His attitude of mind toward scientific research has been an inspiration to me. I would also like to thank Prof. Junichiro Shiomi who gave me very useful and sophisticated comments systematical ways of thinking which made me improve weak points on my research, particularly my staying at Massachusetts Institute of Technology in U.S.A. Also, I specially thank to lab. members in Maruyama laboratory that I've

spent about six years in this lab. with almost 100 people. Without them, nothing left in my mind, and my lab life was exciting because of lots of discussion, argument, drinking, and funny things with them.

I also wish to thank Prof. Suguru Noda, Dr. Kei Hasegawa, and laboratory members in the Department of Applied Chemistry at Waseda University, who allowed me to use their experimental setup to synthesize millimeter long carbon nanotubes significantly used in this research.

I would also like to thank Prof. Brian L Wardle for giving me the great chance to study mechanical densification for vertical aligned CNT forests and mechanical property of polymer composites and with wonderful colleagues, Jeonyoon Lee, Itai Stein, and others.

Finally, I would like to thank my family that I could not have reached this milestone without their support and tolerance. In particular, I want to express my hearty gratitude to my wife, Haehyun Lee, for her kind support, encouragement, understanding, and patience throughout my fulfillment of the thesis research. I am particularly grateful to my lovely son, Geonwoo, has refreshed and recovered me when I came back home from work every day.

Abstract

The generation of micro/nanotechnology has required "*cooling*" as one of the major challenges. In the field of micro and nano electronics, those devices undoubtedly produce heat, which need to be minimized with efficient cooling to prevent the failure of performance. For decade, electronic devices such as integrated chips tend to reduce size and increase the speed and performance, which drive the thermal management more important due to the necessity for the sufficient cooling system. So far, cooling by air convection for electronics is the most widely used method, but this method has a serious limitation which is unable to increase degree of heat flux.

Thermal interface materials (TIMs) are one of the main bottlenecks for efficient heat transfer from integrated chips to heat sinks and ambient environment by filling micro-gap-interface between two contacting materials to improve thermal conduction instead of air gap: thermal grease, thermal gel, phase change materials, thermal conductive adhesive, thermal tapes ad pads. Among carbon allotropes-based TIMs, *carbon nanotubes* (CNTs) with high thermal conductivity and high aspect ratio is one of the most expected candidates acting as fillers since they enables to extend the study down to a further smaller scale than before.

Over the past few decades, CNTs have been studied to be used in various

fields due to outstanding electrical, mechanical, and thermal properties since the discovery. The electric current density of metallic CNTs is found to be 4×10^9 A/cm^2 in theoretical study, about 1000 times than that of metals such as copper. In addition, the structure of sp^2 chemical bonding – stronger than that of sp^3 found in diamond – gives CNTs have exceptionally high mechanical property, up to 1.2 TPa for Young's modulus and 50 – 200 GPa for the tensile strength. Since it is difficult to measure directly thermal properties of an individual CNT due to the technical difficulties in nanoscale, thermal properties of CNTs have been investigated by theoretical simulation and calculation. Thermal conductivity of CNTs has been measured up to ~ 6000 W/mK surpassing that of diamond, even though the results of measured thermal conductivities are largely scattered.

CNTs contained in polymer enable to enhance thermal property of the polymer composite. Various factors have an impact on degree of improvement for the thermal property such as fabrication method, orientation, density, and types of CNTs. The fabrication methods are categorized into three types such as solution mixing, melt blending, in situ polymerization, and latex technology which have each advantages and limitations. In addition, the orientation of CNTs in polymer matrix is a critical factor due to their anisotropic structure, which leads to determine the thermal property of the composite. Enhanced thermal property of the composite is dependent on weight/volume percent of CNTs, however, their excess inclusion lead to debilitate thermal property rather than to improve.

Either SWNT or MWNT should be chosen for a proper purpose of the composite with consideration of their difference for thermal behavior.

Electronic devices with the necessary to reduce size and increase the speed and performance have led cooling to be more important. This thesis work is motivated by potential applications that polymer composite containing CNTs as fillers is expected to be used for thermal interface material. Prior to study for the thermal performance of the composite, thermal behavior of CNT forest without polymer are investigated with several potential factors such as volume fraction, types of CNTs, and temperature. In addition, thermal conductivity of an individual CNT also is estimated with additional information. Then, thermal properties of polymer composite containing CNT forest are evaluated to be used for potential thermal applications. Moreover, this thesis work also focus on the development for a new fabrication method for polymer composites with CNT forests available applying for the size of tens of μm to enhance thermal transfer. Through a series of above studies, this PhD thesis aims to provide engineering knowledge to understand thermal behavior of both CNTs and polymer composite containing CNT forests, which can help to describe improved various applications by using the composites in the field of micro and nanotechnology.

The contact-free laser flash analysis (LFA) technique proposed by Parker *et al* measured thermal diffusivity of vertically aligned CNT (VACNT) forests with various volume fractions. As-grown VACNT forests have the volume

fraction at most up to ~ 5 %, which represents the degree of the number of CNTs occupying the forest. Wardle *et al* introduced the mechanical densification to control the volume fraction of CNT forests. In this study, 4.15 % volume fraction of millimeter-long as-grown SWNT forest was squeezed up to 25.2 %. Measured thermal diffusivity for each volume fraction of SWNT forests should have been identical even though they are in different volume fraction, since it is intrinsic thermal property of a material representing the rapidity of the heat propagation thorough it. Hence, the result is unnatural that the increase of volume fraction resulted in high thermal diffusivity of SWNT forests. This potentially occurred because the suspending SWNTs in the forest, not directly involved in the thermal propagation from front to rear surfaces during the measurement of LFA, became to contribute for thermal transfer rather than to disturb, which causes to have higher thermal diffusivity. Indirectly, thermal conductivity of SWNT forest can be derived with additional information such as the specific heat and density. In addition, obtained thermal diffusivity and conductivity for MWNT forest were compared to those of SWNT forests. The comparison indicated that the CNT forest when composed of MWNTs has higher thermal properties than SWNTs. Marconnet *et al* reported the role of inner-walls of MWNTs for thermal transfer that conducts phonons efficiently with less interacting to surrounding materials than outer shell. However this cannot be the suitable reason to explain this phenomena since CNTs existed without surrounding materials. In fact, the result is potentially concluded that the effect of suspending CNTs cause the increase of thermal diffusivity rather

than from that of inner-walls, and can be clarified by considering the intrinsic structural difference between SWNTs and MWNTs such as inherent waviness resulting from the synthesis process.

PDMS composite with VACNT forest were fabricated that the phenomenon of PDMS wetting CNTs is apparently close to the in-situ polymerization except the functionalized surface that CNTs are incorporated into liquefied polymer matrix in which cross-linking agent was added, resulting from capillary motion. The slow infusion of PDMS from the side direction potentially leads to prevent the composites from void-trap. Since the thickness of the CNT forests are relatively long up to 1 mm, it is possible to fully wet the CNT forests, up to the tip, by controlling quantities of PDMS. Remained voids trapped in the composites are removed by giving enough time to polymerize in a vacuum desiccator. Since the infiltration of polymer matrix into CNT forest is one of the main factors to determine the quality of the composite when using the technique to pour polymer on to CNT forest, scanning electron microscopy characterized the degree of PDMS infiltration in CNT forest. On the other hand, thermal diffusivity of the composites was enhanced by the various volume fractions of VACNT forests up to 7.86 mm^2/s with 20.3 % of SWNTs, and 6.65 mm^2/s with 12.2 % for MWNTs. Derived thermal conductivity of each SWNT and MWNT forest was discussed by comparing to the theoretical prediction model of the composite for aligned continuous CNTs proposed by Nan *et al.*

A facile fabrication method, called *side-intrusion method* was proposed to use for applying to tens of μm long VACNT forests, which is practical size-scale in TIMs for such integrated chips. The method enables to make the polymer composite uniform and well-aligned, but requires no treatment. The composites fabricated from the side-intrusion method are characterized the degree of PDMS infiltration into CNT forest, and vertical alignment of CNTs in PDMS composite by Raman spectroscopy. As a result, it was confirmed that PDMS uniformly infiltrated into the VACNT forest by capillarity even without deteriorating the aligned morphology.

The obtained result in this thesis work possibly provides engineering knowledge to understand thermal behavior of both CNTs and polymer composite containing CNT forests, which potentially help to imagine various applications with improved thermal property by using the composites in the field of micro and nanotechnology.

List of Tables

List of Figures

Chapter 1:

Introduction

Since the discovery of *carbon nanotubes* (CNTs), numerous studies have been reported for the applications in various fields due to their outstanding mechanical, electrical, and thermal properties. The structure of sp^2 chemical bonding – stronger than that of sp^3 found in diamond – gives CNTs have exceptionally high mechanical property, up to 1.2 TPa for Young's modulus and 50 – 200 GPa for the tensile strength. In addition, electric current density of metallic CNTs is found to be 4×10^9 A/cm^2 in theoretical study, about 1000 times than that of metals such as copper. On the other hand, thermal properties of CNTs have been investigated by theoretical simulation and calculation since it is difficult to measure directly thermal properties of an individual CNT due to the technical difficulties in nanoscale. Although the results of measured thermal conductivities are scattered, thermal conductivity of CNTs has been measured up to ~6000 W/mK which surpasses that of diamond.

In terms of thermal applications, CNTs are one of the most expected candidates for thermal management in such integrated chips as cooling solution such as thermal interface materials (TIMs). Polymer composites containing vertically aligned CNTs (VACNTs) possibly enables to fully take extraordinary anisotropic thermal property of CNTs. For that, this work investigates thermal properties of VACNT forests with various volume fraction, and then those of the composites. In addition, it introduces a facile method to fabricate polymer composites with VACNT forests applying for potential thermal applications.

In chapter 1, it describes the concept of sp^2 carbon allotropes such as fullerene, carbon nanotube, graphene, and graphite comparing physical properties of them each other. In

particular, the unique structure of CNTs rolling up from the graphene sheet has an influence to determine either metallic or semiconducting. In addition, this chapter involves the explanation of polydimethylsiloxane (PDMS) which is used as a base polymer matrix in this Ph.D. work.

Chapter 2 investigates the dependence of thermal properties on the volume fraction of CNT forests, single- and multi-walled carbon nanotubes. The volume fraction of CNT forest is varied by the mechanical densification introduced by Wardle *et al* that squeezes interstitial spaces between vertically aligned CNTs without any destruction. Thermal properties of SWNT and MWNT forest are evaluated that thermal diffusivity of the CNT forests along axial direction are measured by laser flash analysis technique, and then thermal conductivity are derived with additional information such as specific heat and density, which potentially estimates the role of suspending CNTs in CNT forest for thermal transfer. Comparing thermal properties of between SWNT and MWNT probably proposes better material for potential application such as thermal interface materials (TIMs).

In chapter 3, thermal properties are investigated for the PDMS composites containing CNT forest with various volume fractions. Since the infiltration of polymer matrix into CNT forest is one of the main factors to determine the quality of the composite when using the technique to pour polymer on to CNT forest, scanning electron microscopy characterizes the degree of PDMS infiltration in CNT forest. In addition, thermal conductivity of CNTs is estimated in PDMS by applying the model for aligned continuous CNTs in effective medium theory proposed Nan *et al*.

Chapter 4 introduces a facile fabrication method, called *side-intrusion method* in this study, of polymer composites available for applying to tens of μm long VACNT forests (i.e. practical size-scale in thermal interface materials for such integrated chips) which make the composite uniform and well-aligned, but requires no treatment. The composites fabricated from the side-intrusion method are characterized the degree of PDMS infiltration into CNT forest, and vertical alignment of CNTs in PDMS composite by Raman spectroscopy.

Chapter 5 summarizes the content of each chapter, and concludes this thesis work that the effect of thermal properties of CNT forests on volume fraction in chapter 2, enhanced thermal properties of PDMS composites containing VACNT forests in chapter 3, and the side-intrusion method, for the fabrication of PDMS composite with tens of μm long VACNT forests, practical size-scale in thermal interface materials in chapter 4.

1.1 Needs for Cooling on Electronics

The generation of micro/nanotechnology has required "cooling" as one of the major challenges. In the field of micro and nano electronics, those devices undoubtedly produce heat, which need to be minimized with efficient cooling to prevent the failure of performance. For decade, electronic devices such as integrated chips tend to reduce size and increase the speed and performance, which drive the thermal management more important due to the necessity for the sufficient cooling system. So far, cooling by air convection for electronics is the most widely used method, but this method has a serious limitation which is unable to increase degree of heat flux [29].

On the other hand, thermal interface materials (TIMs) are one of the main bottlenecks for efficient heat transfer from the integrated chips to heat sinks and ambient environment by filling micro-gap-interface between two contacting materials to improve thermal conduction instead of air gap. There are several categories for TIMs such as thermal grease, thermal gel, phase change materials, thermally conductive adhesives, thermal tapes and pads [30].

One of the major trends in the field of thermal interface material research is to include high thermally conductive fillers. Thermal interface materials based on the carbon allotropes such as diamond, graphite, fullerenes and carbon nanotubes, have attracted new types for TIMs, which enables to extend the study down to an even smaller scale than before. In particular, carbon nanotubes (CNTs) is one of the most expected candidates acting as fillers due to their high thermal conductivity, and high aspect ratio.

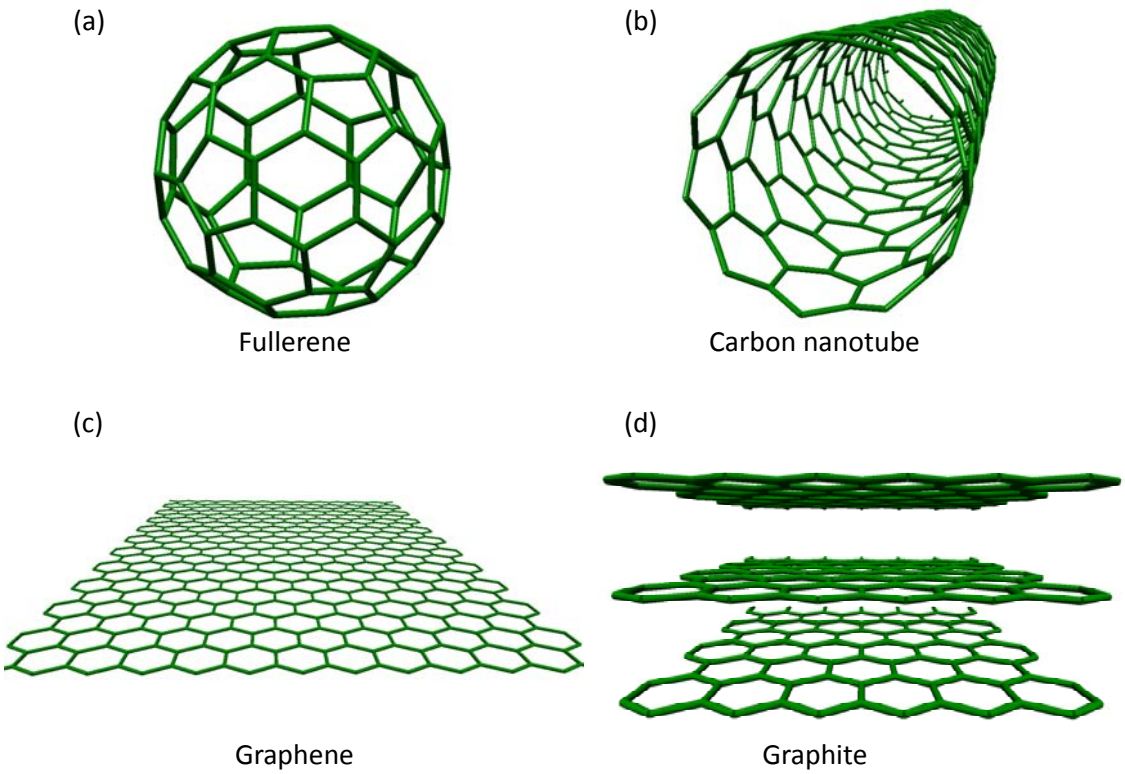

Figure 1.2.1: Schematic images of sp^2 carbon allotropes: (a) fullerene, (b) carbon nanotube, (c) graphene, and (d) graphite.

1.2 Carbon Nanotubes (CNTs)

1.2.1 Family of Carbon Materials

Carbon, a base of earth life, represented as a symbol **C** is a member of 14th group in the periodic table of the elements, and which is a non-metallic material. A single carbon atom is allowed to have capability for four chemical bonds. There are well-known carbon allotropes such as diamonds, graphite, fullerenes and carbon nanotubes shown in Fig. 1.2.1.

Table 1.1: Physical properties of carbon allotropes [1]. Reproduced with permission. Copyright 2010, Elsevier.

	Fullerene	CNT	Graphite	Diamond
Specific Gravity (g/cm^3)	1.7	0.8 – 1.8	1.9 – 2.3	3.5
Electrical Conductivity (S/cm)	10^{-5}	10^2–10^6	~ 4000	10^{-2} – 10^{-15}
Electron Mobility (cm^2/Vs)	0.5 – 6	~ 10^5	2.0×10^4	1800
Thermal Conductivity (W/mK)	0.4	~ 6000	298	~ 2320
Thermal Stability in air (°C)	~ 600	> 600	450 – 650	< 600

In diamond, carbon forms four bonds with other carbon atoms. The diamond is electrically an insulator since every electron belongs in single chemical bonds which carbon is sp^3 hybridized. In contrast to graphite, each carbon atom in graphene and fullerene has an extra electron arising from sp^2 hybridization which plays as a charge carrier, hence they are electrically conductive. In three dimensions, the carbon atoms are arranged as crystalline in diamond whereas carbon atoms forms planar or curved planar in the sp^2 hybridized materials such as graphene or fullerene.

Graphite is composed of graphene sheets with parallel alignment. The in-plane properties of the graphite are 1.02 TPa of tensile modulus [31], 4000 S/m of an electrical conductivity, and 1.9 – 2.3 W/mK of thermal conductivity [32,33]. All these physical properties of graphite differ from those of an individual graphene despite structural similarity. In particular, graphite is not a very strong material because the stacked graphene layers tend to slip each other, however, the tensile modulus of an individual graphene have been measured to be 130 GPa [34], approximately 200 times. In addition, electrical conductivity of graphene, measured to be ~2×10^4 [35], is

considerably higher than that of graphite.

Fullerene, so-called *buckyball*, was discovered in 1980s by Harold Kroto, Robert Curl and Richard Smalley from Rice University. Fullerene involves planar sp^2 of carbon atoms, which can be rolled into either a spheroidal or a tubular structure. Only specific number of carbon atoms enables to compose buckyball, and C_{60} and C_{70} are the most common of them. Although the discovery was awarded the *1996 Nobel Prize* in Chemistry, there are only few commercial applications of buckyball.

1.2.2 Geometry, Synthesis, and Physical Properties

In 1991, Iijima *et al* observed the existence of tube-like graphite structures with close ends by transmission electron microscopy, which is well-known as multi-walled carbon nanotubes (MWNTs) [36]. Two years later, Iijima *et al* discovered single-walled carbon nanotubes (SWNTs) [37] with a much smaller diameter than MWNTs, which considered as an ideal CNT composing perfect single-layer. Due to their extraordinary electrical, mechanical, thermal properties [38], it has been regarded as a promising material to be used in nanotechnology.

CNTs can be specifically categorized according by the wall-number of a CNT such as an SWNT, double-walled carbon nanotubes (DWNTs), a few-walled carbon nanotube (FWNT), and MWNT. Typically, the diameters of SWNTs, DWNTs and FWNTs are ranging from 0.7 – 4 nm, 0.7 – 10 nm, and 0.7 – 20 nm, respectively. However, since it is frequently ambiguous to classify according by the diameter or the number of walls,

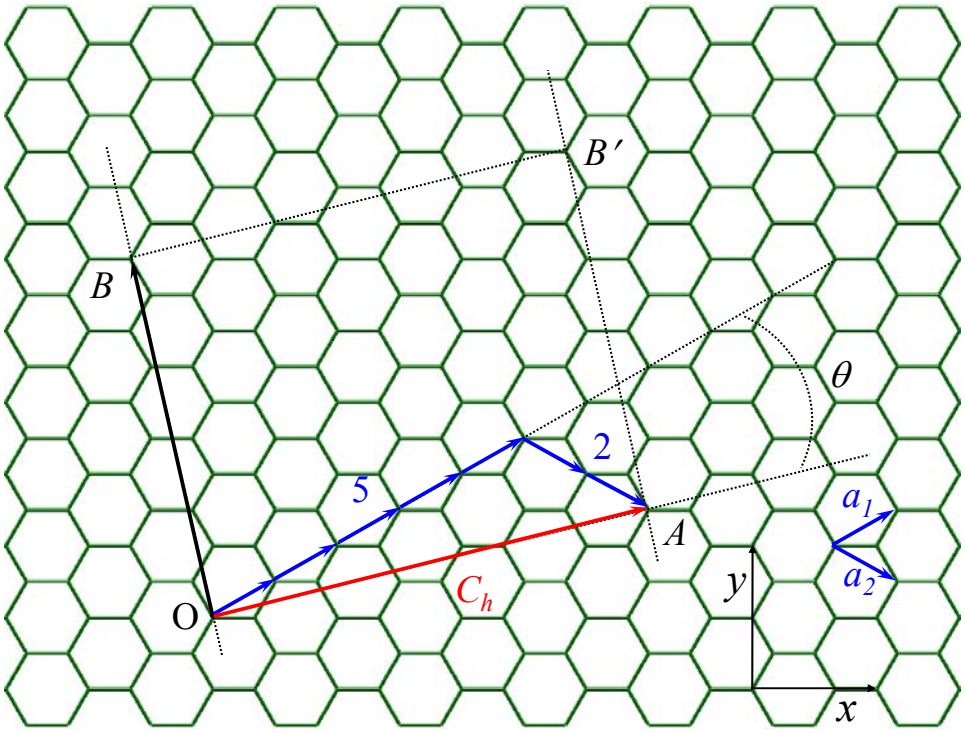

Figure 1.2.2 Geometry of graphene sheet shows the chiral vector $\boldsymbol{C}_h$ for an SWNT with (n,m) = (5,2). The chiral angle is shown by θ.

hence CNTs here are only separated into either SWNTs or MWNTs by whether they contain single-layer or more than that in this study.

An SWNT forms a cylindrical tube from a single graphene sheet rolled up with the diameter ranging from 0.7 – 4 nm, and the length up to tens of mm. In particular, since its length-to-diameter ratio, *aspect ratio*, is significantly larger than any other material, it is regarded as a quasi-one-dimensional material. Figure 1.2.2 represents the sp^2 hybridization of carbon structure in two-dimensional graphene sheet as a hexagonal lattice. Based on Cartesian coordinates, vectors a_1 and a_2 represents the unit vectors of the cell as,

$$\boldsymbol{a}_1 = \left(\frac{\sqrt{3}}{2} a, \frac{a}{2} \right), \quad \boldsymbol{a}_2 = \left(\frac{\sqrt{3}}{2} a, -\frac{a}{2} \right) \tag{1.1}$$

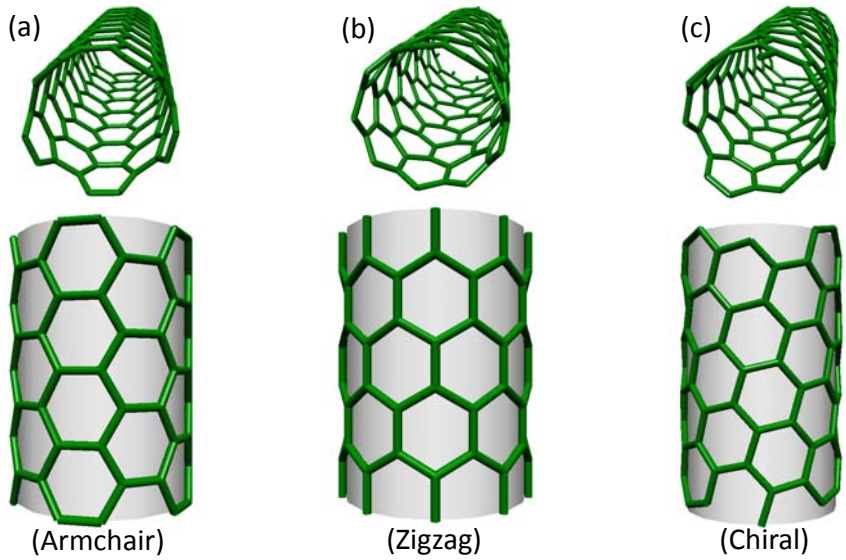

Figure 1.2.3: Different geometries of SWNTs: (a) armchair, (b) zigzag, and (c) chiral.

where $a \equiv |\boldsymbol{a}_1| = |\boldsymbol{a}_2| = \sqrt{3} \times a_{\text{c-c}}$, and $a_{\text{c-c}}$ of the distance between neighboring carbon atoms is 1.452 Å. The lattice vectors of graphene specify the structure of a carbon nanotube, so-called *chiral vector* described as $\boldsymbol{C}_h$. (see Fig. 1.2.2). The chiral vector $\boldsymbol{C}_h$ is expressed as real-space unit vectors $\boldsymbol{a}_1$ and $\boldsymbol{a}_2$ and two positive integers, n and m ($0 \leq m \leq n$) as

$$\boldsymbol{C}_h = n\boldsymbol{a}_1 + m\boldsymbol{a}_2 \equiv (n,m) \tag{1.2}$$

The length of $\boldsymbol{C}_h$ indicates the circumferential length of the SWNT, hence the diameter of the SWNT, d_t can be described as

$$d_{\text{t}} = \frac{|C_h|}{\pi} = \frac{\sqrt{C_h \cdot C_h}}{\pi} = \frac{a\sqrt{n^2 + m^2 + nm}}{\pi} \tag{1.3}$$

The angle formed between the chiral vector $\boldsymbol{C}_h$ and the unit vector $\boldsymbol{a}_1$, chiral angle θ, varies from 0 to 30 ° resulting from hexagonal symmetry of the honeycomb lattice. This produces three different geometries of SWNTs such as armchair, zigzag, and chiral (see Figure 1.2.3), which is expressed as

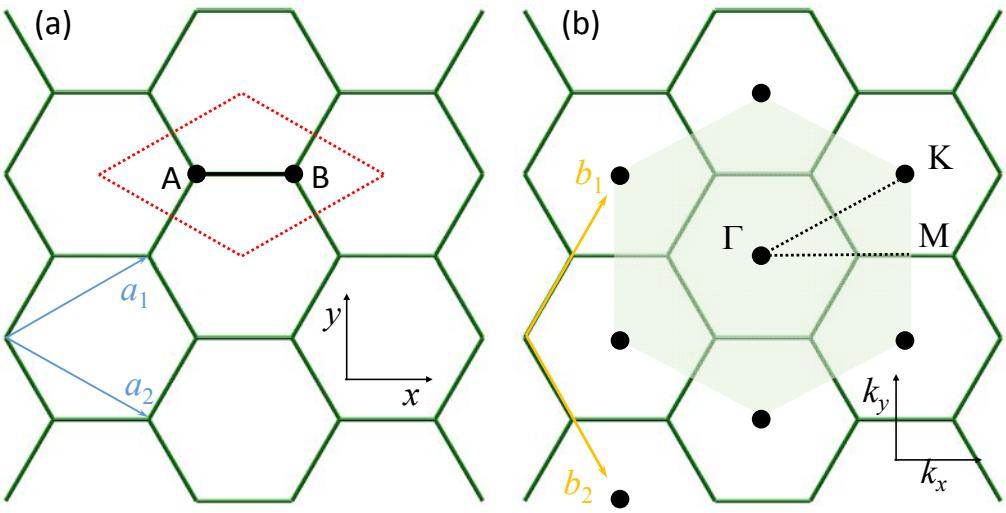

Figure 1.2.4: (a) The unit cell in real space of graphene (enclosed by the dashed rhombus) contains two atoms A and B. (b) The Brillouin zone (green region), and the high-symmetric points **Γ**, **M**, and **K** in reciprocal space. The unit vectors of real and reciprocal space are represented by $\boldsymbol{a}_i$ and $\boldsymbol{b}_i$ (i=1,2), respectively.

$$\cos\theta = \frac{C_h \cdot a_1}{|C_h||a_1|} = \frac{2n+m}{2\sqrt{n^2+m^2+nm}} \tag{1.4}$$

From the relationship $\boldsymbol{C}_h \cdot \boldsymbol{T} = 0$, the translational vector $\boldsymbol{T}$ can be obtained as below,

$$\boldsymbol{T} = t_1\boldsymbol{a}_1 + t_2\boldsymbol{a}_2 \equiv (t_1,t_2), \tag{1.5}$$

$$(t_1 = \frac{2m+n}{d_R},\ t_2 = -\frac{2n+m}{d_R})$$

where the value d_R is the greatest common divisor (gcd) of ($2m$+n) and ($2n$+m). It results in

$$d_R = \begin{cases} d & if\ (n-m)\ is\ mutiple\ of\ 3d \\ 3d & if\ (n-m)\ is\ not\ mutiple\ of\ 3d \end{cases} \tag{1.6}$$

In Fig. 1.2.2, the rectangle OAB′B is defined by the vectors $\boldsymbol{C}_h$ and $\boldsymbol{T}$, which encloses the unit cell of the SWNT. The number of hexagons, N, in the unit cell can be obtained as below

$$N = \frac{|C_h \times T|}{|a_1 \times a_2|} = \frac{2(n^2 + m^2 + nm)}{d_R} \tag{1.7}$$

With the translational vector $\boldsymbol{T}$ and the chiral vector $\boldsymbol{C}_h$, the unit cell of an SWNT can be determined in the real space of the graphene sheet as shown in Fig. 1.2.4 (a). In similar, the reciprocal-space vectors can be described with the reciprocal space basis vectors $\boldsymbol{b}_1$ and $\boldsymbol{b}_2$ (see Fig. 1.2.4(b)), which are expressed as

$$\boldsymbol{b}_1 = \left(\frac{2\pi}{\sqrt{3}a}, \frac{2\pi}{a}\right), \boldsymbol{b}_2 = \left(\frac{2\pi}{\sqrt{3}a}, -\frac{2\pi}{a}\right) \tag{1.8}$$

The high-symmetric points of the Brillouin zone at the center, corner, and the midpoint of neighboring corners are described as **Γ**, **M**, and **K**, respectively.

One of the most important characteristics of SWNTs is that chirality determines

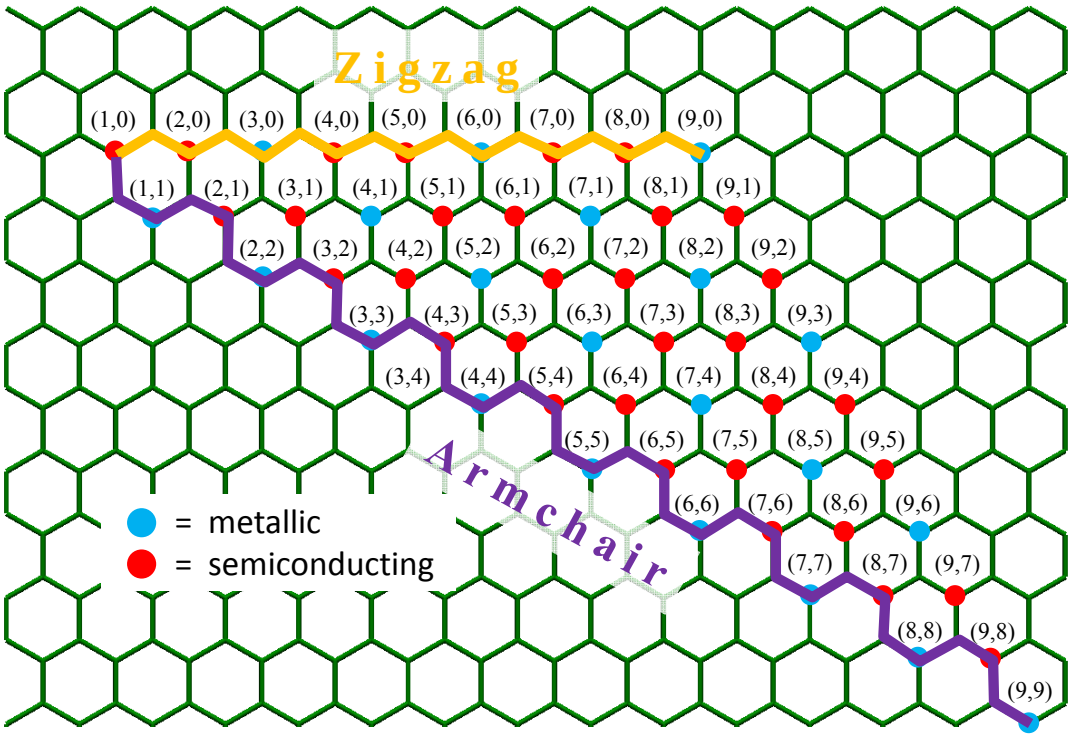

Figure 1.2.5: Representation of the symmetry-dependent electrical properties of SWNTs. Each blue for metallic and red for semiconducting dot corresponds to a specific chirality.

metallic/semiconducting transport properties. Figure 1.2.5 represents the symmetry-dependent electrical properties of SWNTs that a specific chirality with either blue or red dot corresponds to metallic or semiconducting, respectively.

There are three typical techniques to synthesize CNTs which electric arc discharge method, laser ablation method, and chemical vapor deposition (CVD) method. Electric arc discharge method involves the generation of electric arc between two graphitic electrodes. Anode is filled with catalytic metal powders such as Fe, Ni, and Co, and CNTs are obtained from cathodes. This method can directly, easily, perfectly produce both SWNTs and MWNTs with lengths of up to 50 μm but with few structural defects [39].

Laser ablation method was firstly used in the synthesis of fullerenes. Over the years, it has been improved for synthesis of CNTs. A pulsed laser vaporized a graphite target in a high-temperature reactor, and the CNTs are developed on the cooler side of the reactor. The process was developed by R. E. Smalley's Group at Rice University, and the best yield to synthesize SWNTs was from the mixture of Co and Ni [40].

CVD, which is employed method to synthesize in this study, involves the process that gaseous molecules, so-called precursors, transform to solid materials with the temperature ranging from 550 to 900 °C on a substrate. Deposited catalytic particles on the substrate in this process decompose hydrocarbon gas to form carbon and hydrogen. The catalysts act as a template on which CNTs can be synthesized. There are many challenges to control the diameter and length of CNTs by controlling the size of

catalysts and the reaction time.

Due to their outstanding physical properties such as mechanical, electrical, and thermal properties, CNTs have been expected to be used in various fields. In terms of application, the exceptional mechanical property becomes the primary reason, which is related to both the nature of chemical bonds between carbon atoms and given aspect ratio. The structure of sp^2 chemical bonding – stronger than that of sp^3 found in diamond – gives CNTs have exceptionally high mechanical property. Although there have not had the agreement for the exact value of mechanical property, many theoretical and experimental studies have shown the results up to 1.2 TPa for Young's modulus and 50 – 200 GPa for the tensile strength [41]. These make CNTs the strongest and stiffest materials in earth. They also have extraordinary electrical property that electric current density of metallic CNTs is found to be 4×10^9 A/cm^2 in theoretical study, about 1000 times than that of metals such as copper [42]. On the other hand, thermal conductivity of SWNTs and MWNTs has been measured ~2000 W/mK [11] and ~3000 W/mK [43], respectively. Many studies about thermal properties of CNTs have been investigated by theoretical simulation and calculation [44–48] since it is difficult to measure directly thermal properties of an individual CNT due to the technical difficulties in nanoscale. Hence, the results of measured thermal conductivities are scattered, usually ranging from 2000 to 6000 W/mK.

1.3 Polymer Composite Containing CNTs

1.3.1 Polydimethylsiloxane (PDMS)

PDMS is one of the most widely used silicon-based polymer which belongs to a group of polymeric organosilicon compounds, referred to as silicones. The empirical formula of PDMS is $(C_2H_6OSi)_n$, and fragmented formula is $CH_3(Si(CH_3)_2O)CH_3$, where n is the repeating number of the monomer. Figure 1.3.1 shows the string of monomer of PDMS illustrated by *Jmol*. The non-cross-linked PDMS acts as an almost liquid or semi-solid depending on with poor n or with large n, respectively, and after the crosslinking, PDMS becomes a hydrophobic elastomer.

PDMS is commonly used to fabricate various micro-devices due to its outstanding properties such as optical transparency, biocompatibility, flexibility, thermal stability, nontoxicity, and low price [49,50]. For its particular flexibility among the unique properties, PDMS is the most expected candidate polymer for flexible electronic device applications, which causes the PDMS-based devices to preserve flexibility and elasticity even after the fabrication [51–54]. PDMS is viscoelastic, and acting like a viscous liquid,

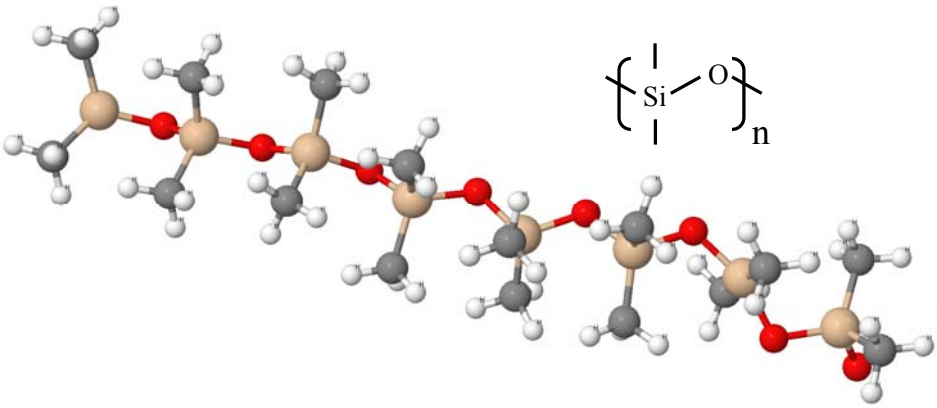

Figure 1.3.1: Illustration shows the string of monomer of PDMS.

similar to honey at long flow time. When it is left on a certain surface overnight, PDMS flows to cover the surface and mold to any surface imperfections. Due to its physical behavior during cross-linking process, PDMS is a potential candidate for PDMS-based applications such as thermal interface materials, however, its low thermal conductivity ~0.18 W/mK [55] has been a critical obstacle. PDMS-based thermal greases with particles loading have thermal conductivity ranging from 0.7 to 3 W/mK, and 5 W/mK with silver particles as the highest [30].

1.3.2 CNTs/Polymer Composites

Many kinds of natural or synthetic polymers have been used in various fields such as

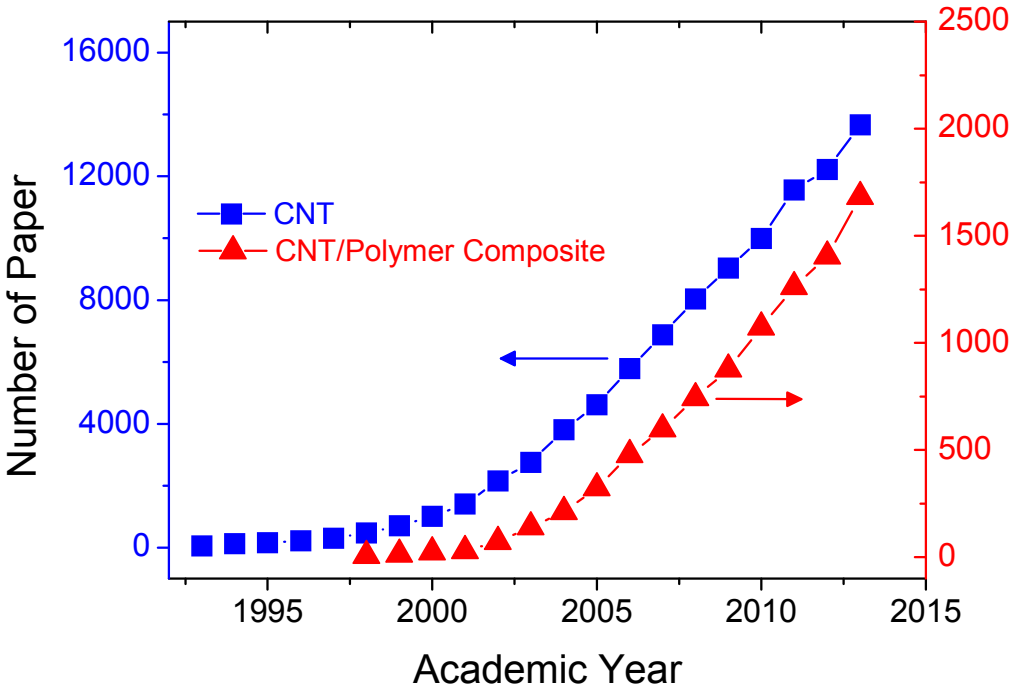

Figure 1.3.2: Number of published papers for CNT (blue squares for left axis) and CNT/polymer composites (red squares for right axis), searched with the keyword, "CNT" and "CNT/polymer composite" on Web of Science, Thomson Reuters.

human life, environment, and industries as essential materials. For example, common plastic bottles for containing soft drinks are made from polyethylene terephthalate (PET), and epoxide resin is used for adhesives or paints for building construction material. Valid uses of them considering their specific advantages have become more important with the evolution of micro/nanotechnology. However, there are still needs for new types of polymers to be develop because of using for emerging new industrial applications although there have been a large number of kinds. For that, the combination of multiple material having well-known physical properties is one of the most common methods to have new purposed material. For example, as containing additives in polymers matrix resulting in structural modification or improvement, it is possible to overcome the limitation of physical properties or modify intrinsic properties of polymers.

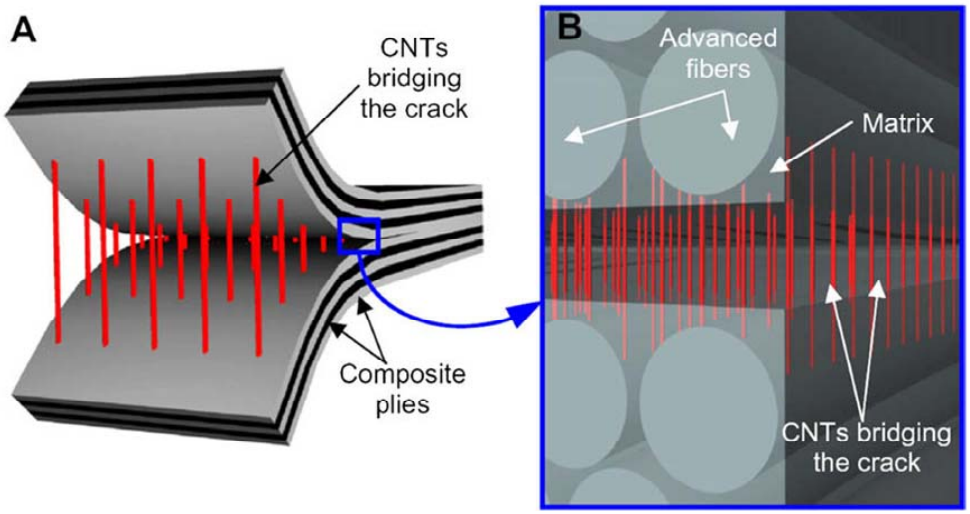

Figure 1.3.3: Illustration of the ideal hybrid interlaminar architecture: (A) VACNTs placed in between two plies of a laminated composite; (B) close-up of the crack, showing VACNTs bridging the crack between the two plies [2]. Reproduced with permission Copyright 2008, Elsevier.

CNTs with large aspect ratio and outstanding physical properties such as mechanical, electrical, and thermal properties are regarded as ideal fillers for the composite generation. Figure 1.3.2 shows the number of published papers searched with the keyword, "CNT" and "CNT/polymer composite" on Web of Science, Thomson Reuters. By containing CNTs in polymer improved thermal [56], electrical [57], and mechanical [58], properties of composite. For example, bridging the crack between composite piles by placing VACNTs increased fracture toughness 1.5 – 2.5 times as described in Fig. 1.3.3 [59]. Many studies have reported the enhanced electrical conductivity of polymer composites with CNTs, even specific designed structure with exposed both tips of VACNTs more enhanced up to ~10^5 S/m [60] (see Fig. 1.3.4).

On the other hand, various factors have an impact on degree of improvement for the

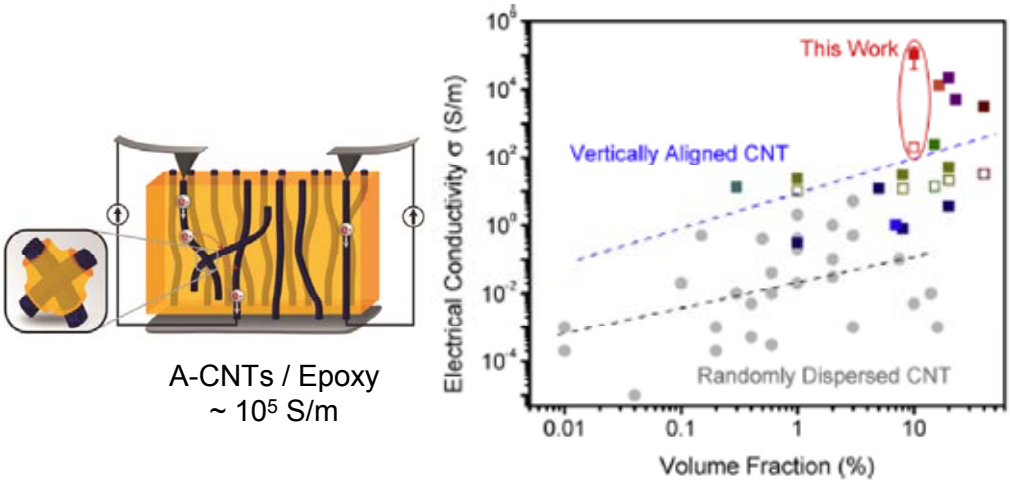

Figure 1.3.4: Schematic of mechanism of electron transport within CNTs/epoxy composites (left), and comparison of obtained result in this study to other reported data for electrical conductivity of randomly dispersed and aligned CNT/epoxy (polymer) composites (right) [60]. Reproduced with permission Copyright 2013, Elsevier.

physical properties such as fabrication method, orientation, density, and types of CNTs. The fabrication methods are categorized into three types such as solution mixing, melt blending, in situ polymerization, and latex technology which have each advantages and limitations, described in detail in chapter 3. The orientation of CNTs in polymer matrix is also a critical factor due to their anisotropic structure, which leads to determine the physical property of the composite. Enhanced physical properties of composite depend on weight/volume percent of CNTs, however, their excess inclusion lead to debilitate physical properties than to improve. In addition, either SWNT or MWNT should be chosen for a proper purpose of the composite with consideration of their different physical properties.

1.4 Objective of This PhD Thesis

Over decade, electronic devices with the necessary to reduce size and increase the speed and performance have led cooling to be more important. This thesis work is motivated by potential applications that polymer composite containing CNTs as fillers is expected to be used for thermal interface material.

Prior to study for the thermal performance of the composite, thermal behavior of CNT forest without polymer are investigated with several potential factors such as volume fraction, types of CNTs, and temperature. In addition, thermal conductivity of an individual CNT also is estimated with additional information. At last, thermal properties of polymer composite containing CNT forest are evaluated to be used for potential thermal applications. This thesis work also focus on the development for the fabrication method of polymer composite with CNT forests in relatively smaller size up to tens of μm to enhance thermal transfer, which is expected to be practical size-scale in thermal interface materials for such integrated chips.

Through a series of above studies, this PhD thesis aims to provide engineering knowledge to understand thermal behavior of both CNTs and polymer composite containing CNT forests, which can help to describe improved various applications by using the composites in the field of micro and nanotechnology.

Chapter 2:

Thermal Properties of CNT Forests with Various Volume Fractions

2.1 Prior Works for Thermal Property of Carbon Nanotubes

The discovery of carbon nanotubes (CNTs) by Iijima in 1991 [36] has generated a large number of research due to its outstanding mechanical, electrical, and thermal properties. In particular, their very high thermal conductivity is believed to surpass even that of diamond [61], hence numerous experimental and numerical studies have so far reported for thermal properties of CNTs with different forms and types such as forest or individual CNTs, and SWNTs or MWNTs.

In the beginning, direct and quantitative experimental measurement of thermal transport property of an individual CNT remained challenging due to technological difficulties in

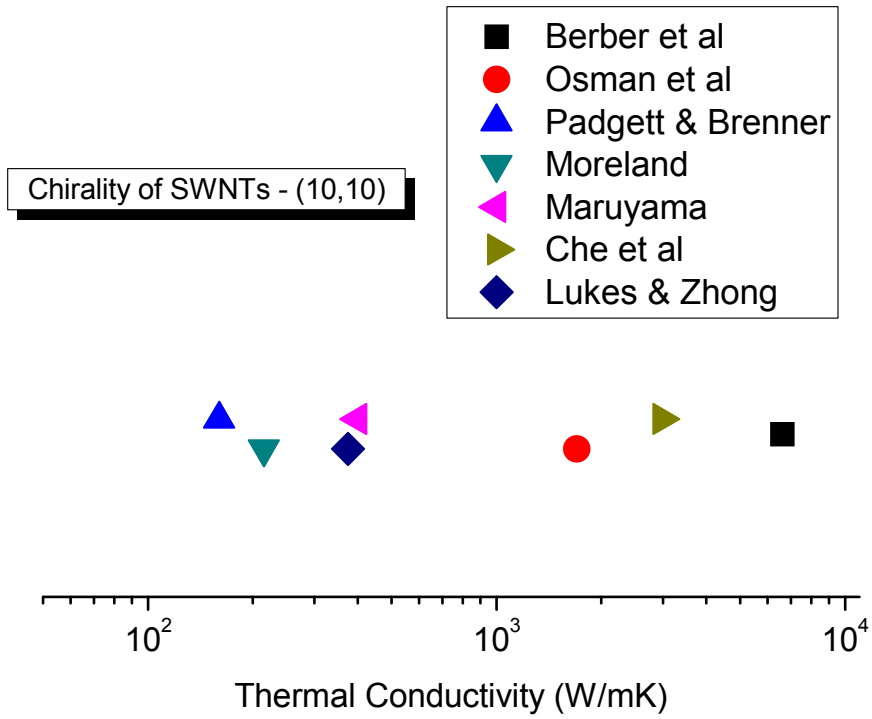

Figure 2.1.1: Thermal conductivities of SWNT with chirality (10,10) in literature obtained by molecular dynamics simulation [3–9].

nanoscale [62]. Thus, approach to study thermal conductivity of CNTs is using molecular dynamics (MD) simulations, which calculate the thermal transport based on the interaction potentials between carbon atoms. MD simulation is generally classified into three ways to compute the thermal transport: equilibrium molecular dynamics (EMD), non-equilibrium molecular dynamics (NEMD), and homogeneous non-equilibrium molecular dynamics (HNEMD). There are several studies for thermal conductivity of CNTs by MD simulations [3–9], and shown in Fig. 2.1.1.

Berber *et al* investigated thermal conductivity for an isolated SWNT, which reached a maximum at 100 K and decreases to 6600 W/mK at room temperature [3]. Although lower thermal conductivity of 1700 W/mK at room temperature, Osman *et al* reported similar tendency with maximized thermal conductivity at 400 K [4]. Other studies found even lower values of thermal conductivity of 160 [5], and 215 W/mK [6] than previously calculated. On the other hand, Maruyama *et al* [7] reported length-dependent thermal conductivity ranging from 250 to 400 W/mK, and Che *et al* found thermal conductivity of 2980 W/mK for 40 nm-long SWNT [8]. Lukes and Zhong also reported thermal conductivity with length dependence of 375 W/mK [9]. Various conditions for the simulation such as length of CNT, boundary condition, and interaction potentials lead to scatter the obtained values of thermal conductivities for CNTs.

Not only by using numerical method, but thermal property of CNTs also has to be investigated with experimental approach for practical use in nanotechnology. Each type and form of CNTs such as forest or individual CNTs, and SWNTs or MWNTs, varies a wide range of thermal conductivities. Figure 2.1.2 shows thermal conductivities

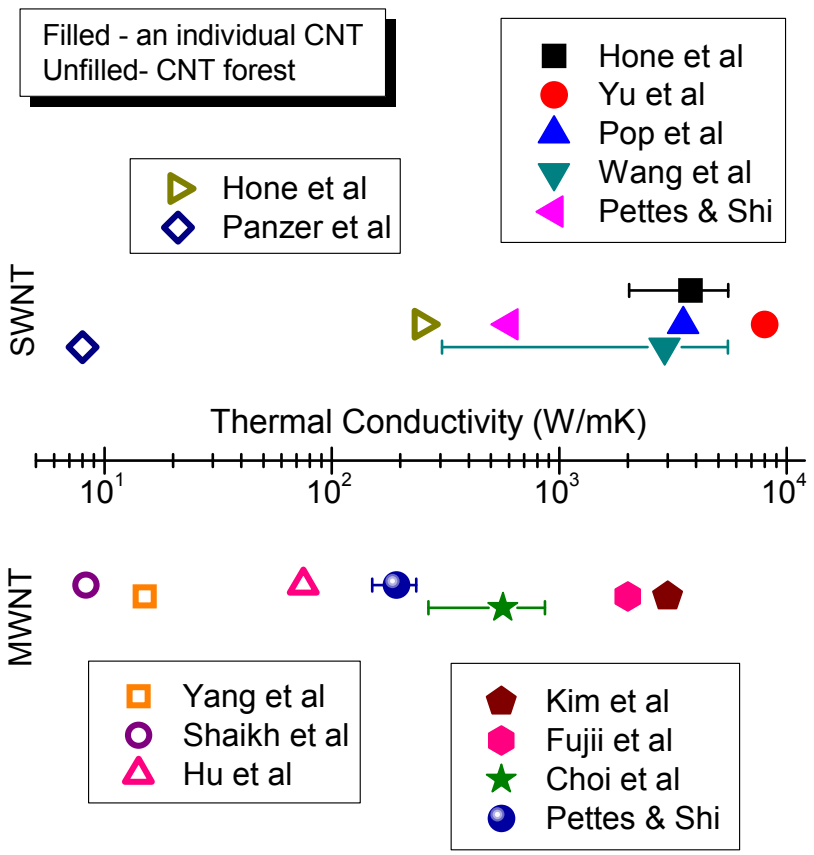

Figure 2.1.2.: Thermal conductivities of CNTs with different types and forms in literature obtained by experiment [10–19].

obtained from many studies which are exhibited according by each type and form of CNTs [11–15,63].

In terms of thermal conductivity of an individual CNT, Hone *et al* found thermal conductivity at room temperature ranging from 1750 to 5800 W/mK of which type measured was SWNT mat such tangled nanotube bundles [61]. In addition, Yu *et al* found thermal conductivity of 8000 W/mK, and Pop *et al* also measured 3500 W/mK for thermal conductivity of SWNT suspended on trenches [11,12]. On the other hand, thermal conductivity were reported 3000 W/mK by Kim *et al* for an individual MWNT suspended [43], and Fujii *et al* also measured thermal conductivity for MWNT up to

2000 W/mK using T-type nanosensor [16]. Using the two-pad 3ω technique, Choi *et al* reported a thermal conductivity as low as 300 W/mK for an individual MWNT [17].

For thermal conductivity of CNT forest, Hone *et al* found greater thermal conductivity than 250 W/mK for dense and thick aligned SWNT forest in parallel to axis [63]. Panzer *et al* used metal coated vertically-aligned SWNT arrays and measured thermal conductivity up to 8 W/mK using a thermoreflectance technique [18]. In addition, thermal conductivity of MWNT forest was also investigated by several studies, Yang *et al* reported the result of 15 W/mK using a pulsed photothermal reflectance technique [19], those of 8.3 W/mK and 75 W/mK measured by Shaikh *et al* [64] and Hu *et al* [65], respectively.

2.2 Synthesis of Millimeter-Long CNT Forests from Catalytic CVD (CCVD)

2.2.1 Effect of Catalyst (Fe) Size on the Number of CNT Walls

Catalysts for the synthesis of CNTs are one of the most crucial factors to determine such wall-number, and even quality of CNTs. Through the combinatorial methods [66,67], Noda *et al* found optimized catalysts loading on substrate during the chemical vapor deposition (CVD) process to synthesize millimeter-thick carbon nanotube forests. In previous study, the process of CNT synthesis using CVD method has been described in detail in previous study [68–70]. This work chose the specific condition to synthesize vertically-aligned and highly-dense carbon nanotubes for an aim to study thermal transfer phenomenon in CNT forests, and when contained in polymer composite.

Silicon wafers with a thermal oxide layer on the surface were pretreated by dipping into

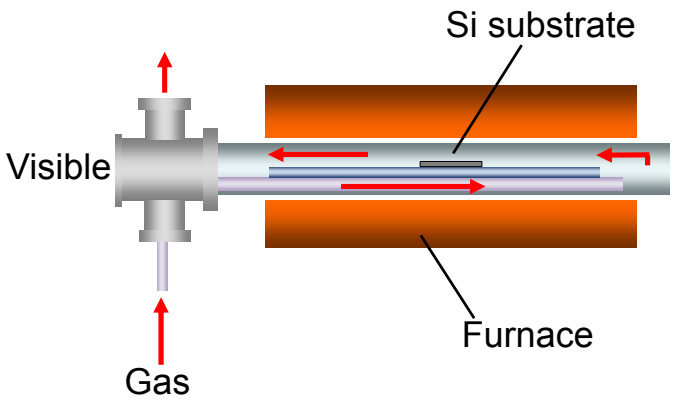

Figure 2.2.1: Schematic of CVD apparatus for the synthesis of millimeter-long vertically-aligned CNTs [20]. Reproduced with permission Copyright 2009, Elsevier.

a H_2SO_4/H_2O_2 solution. 15-nm-thick Al layer with partial oxidized layer and 0.8-nm-layer of Fe were deposited onto the substrate in order by sputtering, which acts as catalysts for the synthesis of SWNTs. In addition, 2.0-nm-layer of Fe was deposited on 15-nm-thick Al_2O_x layer for the synthesis of MWNTs. This is because the diameter and wall-number of CNTs depends on the size of Fe [70].

Si substrate with catalysts of Fe/Al_2O_x was placed in a tubular CVD reactor was heated up to 800 °C, and kept it for 10 min to be exposed to a 10 vol. % H_2/Ar balance mixture at a flow rate of 500 sccm at ambient pressure. After heat treatment, CVD was carried out by switching the gas to a 0.30 vol. % C_2H_2/Ar balance mixture containing 50 ppmv H_2O at ambient pressure.

2.2.2 Characterization of CNTs by Raman Spectroscopy and TEM

By different Fe loading of catalysts on substrate resulted in the synthesized CNTs with different diameter and wall-number. They are characterized by resonance Raman spectroscopy (Chromex 501is with Andor DV401-FI) with excitation laser wavelength of 488 nm and intensity of 0.1 mW using a ×20 objective lens.

Figure 2.2.2(a) shows Raman scattering spectrum of CNTs with radial breathing mode (RBM), D-band, and G-band, which were synthesized on 0.8 nm-thick-layer Fe catalyst. Clear RBM, G-band and very low D-band/G-band ratio gives concrete proof those SWNTs mostly composed the forest. The inset in Fig. 2.2.2(a) shows the snapshot of 1 mm-long SWNT forest. On the other hand, the Raman spectrum of CNTs synthesized with 2.0 nm-thick-layer of Fe catalyst shows similar forms such RBM, D-band, and

G-band to SWNT forest synthesized from 0.8 nm-thick-layer of Fe catalyst, as shown in Fig. 2.2.2(b) with the snapshot (inset) of CNT forest although it is hard to be distinguished from SWNT forest. However, its relatively higher D-band/G-band ratio of the CNTs than that of SWNTs demonstrates that they include not only SWNTs, but also fairly MWNTs. Only with the information obtained by Raman spectroscopy is not enough to conclude the types of CNTs in forest, hence it needs additional investigation to distinguish CNTs synthesized with different size of Fe catalyst.

For that, transmission electron microscopy (TEM, JEM-2000Ex, JEOL Ltd, 200kV) is used to characterize wall-number distribution and diameter of CNTs. Each four TEM

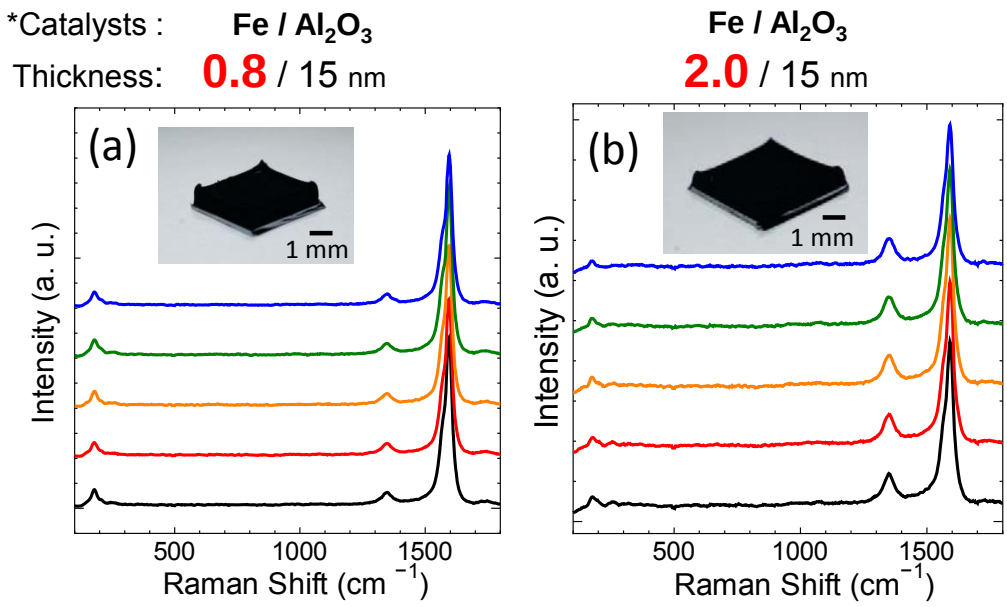

Figure 2.2.2: Characterization of Raman spectra for the synthesized CNT forest. (a) The spectra show typical spectrum of SWNTs with RBM and low D-band/G-band ratio, and (b) the spectra also show similar tendency to (a) except the relatively higher D-band/G-band ratio. Synthesized CNT forests with (a) 0.8 / 15 and (b) 2.0 / 15 nm of Fe / Al_2O_3 as catalysts were VASWNTs and VAMWNTs, respectively.

images of CNTs taken from CNTs synthesized with 0.8 and 2.0 nm-thick-layer of Fe catalysts on substrate are used to count wall-number distribution, and to find diameter of CNTs (see Fig. 2.2.3(a) and (b)). Figure 2.2.3(c) shows wall-number distribution of CNTs in forest that more than 90 % of CNTs are single-walled CNTs, and rest of them are double-,triple-, quadruple-walled CNTs. Although the forest contained some of few-walled CNTs, these CNTs are called SWNTs with average diameter of 3.0 nm in this study.

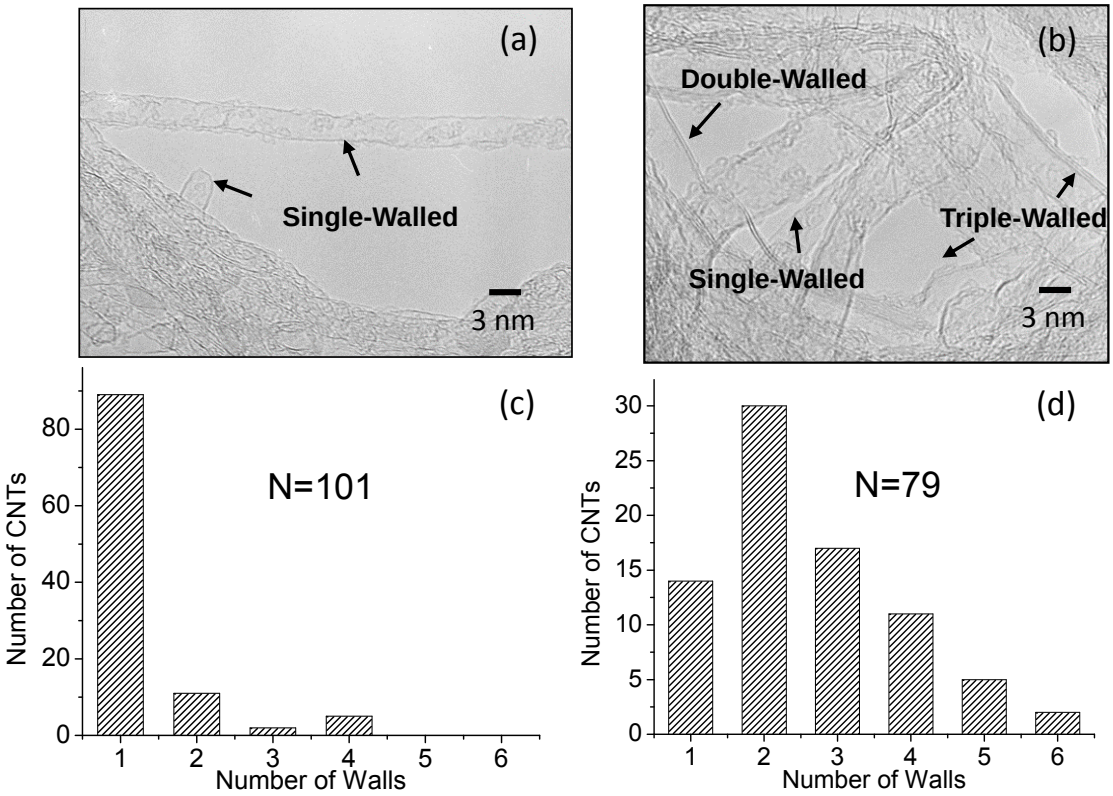

Figure 2.2.3: Wall-number distribution of CNTs counted by using TEM images, (a) and (b). (c) The CNTs consist of mostly single walled CNTs, called SWNTs in this study, which synthesized on 0.8 nm-thick Fe of catalysts. (d) The CNTs contains not only single-walled, but also few-walled CNTs mostly varied from double- to quadruple-walled CNTs, called MWNTs in this study.

For CNTs synthesized with 2.0 nm-thick-layer of Fe catalyst, the forest included partly single-walled CNTs, but mostly double-, triple-, and quadruple-walled CNTs in the forest, which also contains even quintuple-, and sextuple-walled CNTs (see Fig. 2.2.3(d)). The diameter for the CNTs ranged from 4.7 to 7.5 nm, and the average diameter is 6.15 nm. By fine classification for wall-number of CNTs, those CNTs are occasionally called few-walled carbon nanotubes (FWNTs), but this work called MWNTs for apparent separation and simplicity from the term of SWNTs. More information and details about TEM and Raman spectroscopy to characterize CNTs will be described in chapter 4.1.2.

2.3 The Effect of Volume Fraction on Thermal Properties of CNT Forest

2.3.1 Calculation of Volume Fraction

To estimate the volume fraction (V_f) of SWNT forest, it is initially necessary to determine the volume of a single SWNT. Figure 2.3.1(a) shows the employed cross-sectional hexagonal surface of an individual SWNT, which has a diameter of 3.34 nm considering 0.34 nm of Van der Waals distance [70], and a length of 1.2 mm. Consequently, the volume of an single SWNT is calculated to be 1.16×10^{-20} m^3. The number of SWNTs in forest can be estimated as dividing the density of SWNT forest by SWNT linear mass density supposed by the atomic model [71]. By multiplying the

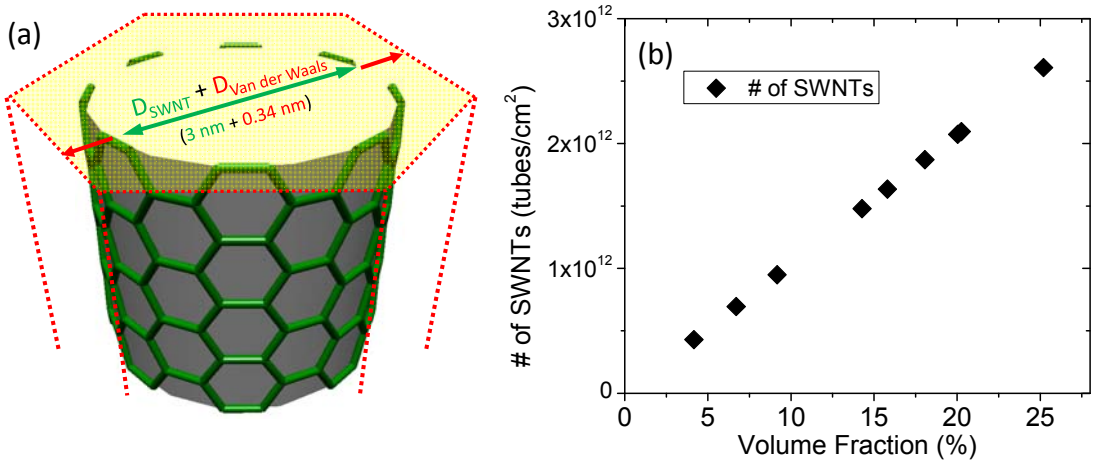

Figure 2.3.1: (a) Employed cross-sectional diameter of a single SWNT to calculate its volume, and (b) the number of SWNTs at each volume fraction of the forest. The employed diameter of cross-section involves the average diameter of an SWNT is 3.0 nm and 0.34 nm of Van der Waals diameter. As-grown VASWNT forest with 4.15 % volume fraction contains 4.30×10^{11} of SWNTs.

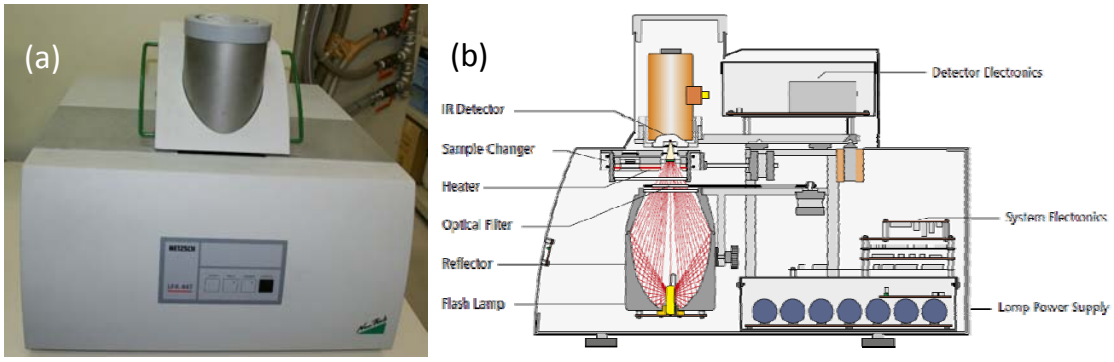

Figure 2.3.2: (a) View of NanoFlash thermal diffusivity analyzer used in this study, and (b) schematic of LFA 447/2 Nanoflash. Reproduced with permission from the brochure for LFA 477/2 at http://www.netzsch.com. Copyright, NETZSCH.

number of SWNTs and the volume of an SWNT, it is able to assume the volume fraction representing how many SWNTs occupy the forest. Figure 2.3.1(b) indicates the dependence of the number of SWNTs on the estimated volume fraction that the forests contain the number of SWNTs corresponding to 4.30×10^{11} in as-grown forest with 4.15 % of V_f and 2.61×10^{12} in the most densified forest with 25.20 % of V_f. With the obtained information above, a density of a single SWNT can be determined by dividing the number of SWNTs by weight of SWNT forest, which is an essential factor to calculate thermal conductivity of an individual SWNT.

2.3.2 Measurement of Thermal Diffusivity by Laser Flash Analysis (LFA)

The contact-free laser flash analysis (LFA) technique proposed by Parker *et al* [72] is a credible standard method to measure thermal diffusivity of solid materials [73], which was employed in this study to measure that of VACNT forest (see Figure 2.3.2(a)). Figure 2.3.2(b) shows schematic arrangement of LFA 447/2 Nanoflash. The light pulse is produced by Xenon flash lamp with the wavelength ranging from 150 to 2000 nm placed within a parabolic mirror.

Table 2.1: Specification of LFA (LFA 447/2).

	Supplied Pulse Source
Light Source	Xenon flash lamp (150 nm ~ 2000 nm)
Pulse Width (ms)	0.1, 0.2, 0.4
Pulse Energy (Joules)	~ 10

	IR Detector
Type	InSb Detector (0.6 mm)
Cooling Type	Liquid Nitrogen
Wavelength (μm)	2 ~ 5

All the specification of LFA 447 are shown in Table 2.1. Through the software, the released energy of the flash lamp can be adjusted up to 10 Joule, and also the width of the heat pulse can be set 0.1, 0.2, and 0.4 ms. During the measurement, the flash lamp, sample, and the infrared detector are vertically arranged by the automatic sample changer. The liquid nitrogen cools InSb infrared detector measures the temperature rise of at rear surface of CNT forest after the light pulse. In addition, the measurable range of thermal diffusivity is from 0.01 to 1000 mm^2/s.

Figure 2.3.3(a) shows the principle of LFA technique. Briefly, if a sample is heated at the front surface, the temperature rise at the rear surface at the time t can be written as

$$\frac{\Delta T}{\Delta T_{\max}} = 1 + 2\left[\sum_{n=1}^{\infty}(-1)^n \exp\left(\frac{-n^2 2\pi^2 \alpha \cdot t}{L^2}\right)\right] \tag{2.1}$$

where ΔT and $\Delta T_{\max}$ are the temperature and maximum temperature at the rear surface, respectively. α, t and L are the thermal diffusivity, time after heating, and thickness of the measured sample.

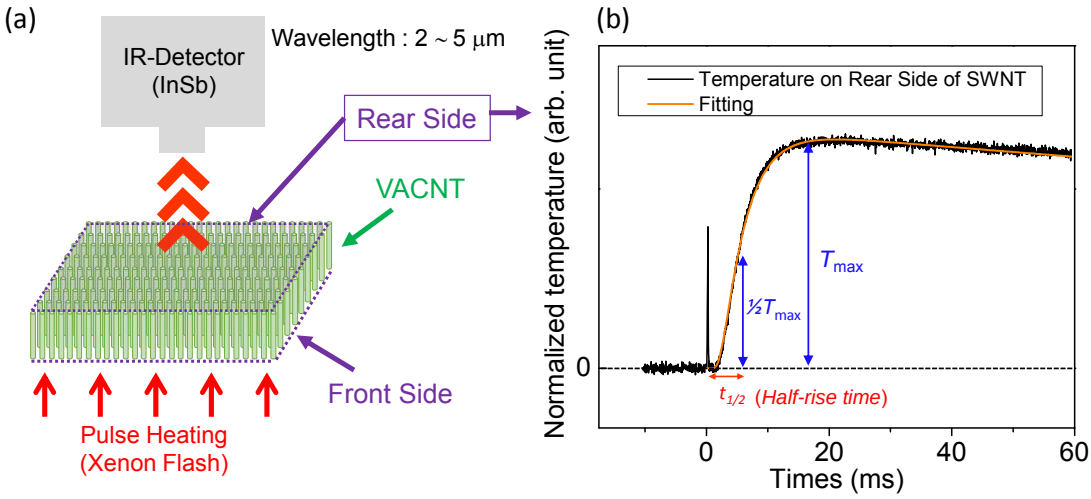

Figure 2.3.3: (a) Concept of laser flash analysis (LFA) technique, and (b) temperature history (black) of rear surface of VASWNT forest and fitting line (red). The LFA method utilizes Xenon flash lamp with the pulse width of 0.1, 0.2, and 0.4 ms, and a liquid nitrogen cools InSb infrared detector ranging from 2 to 5 μm. Cowan model was employed as a mathematical model to fit the obtained data of the temperature rise at the rear surface.

Figure 2.3.3(b) shows an example for temperature history at rear surface of SWNT forest. When $\Delta T/\Delta T_{max}$ corresponds to 1/2, the taken time is called *half-rise time*. Using the half-rise time, thermal diffusivity can be obtained by the relation as below [72]:

$$\alpha = \frac{1.38 \cdot L^2}{t_{1/2}} \tag{2.2}$$

There are several different evaluation models, with and without correction considering heat losses. In this study, Cowan model [74] as a mathematical model was chosen to consider non-negligible heat losses with a finite pulse duration.

2.3.3 Mechanical Densification of VACNT Forest

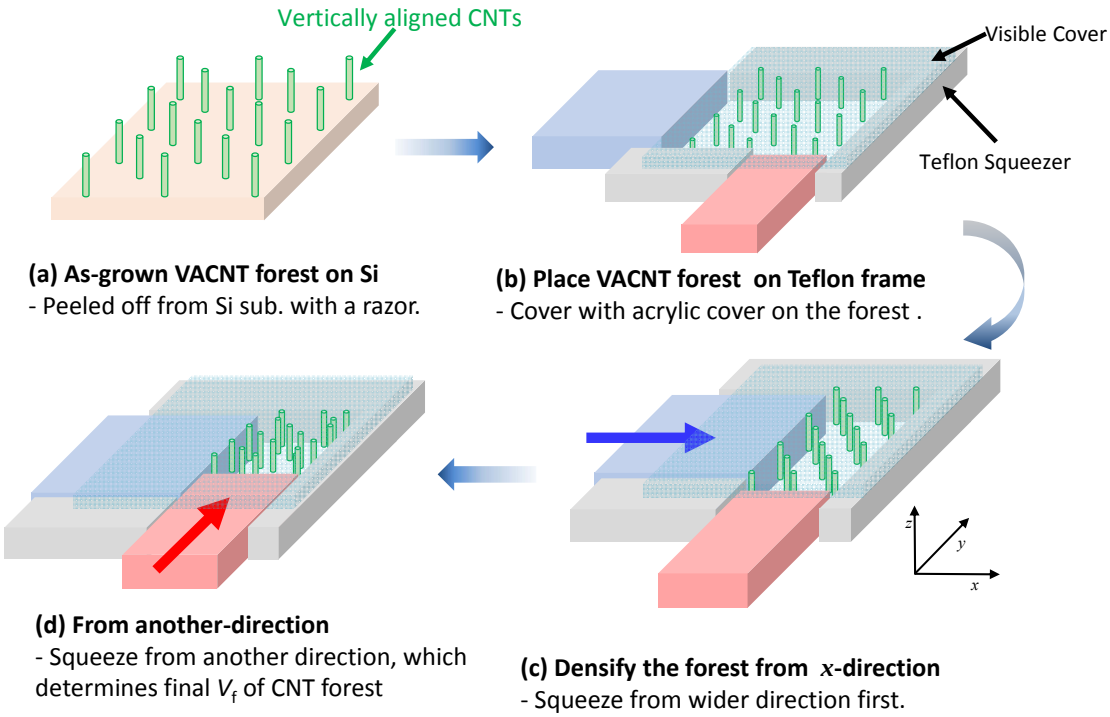

Figure 2.3.4: Mechanical densification process to vary volume fraction of the CNT forest. (a) As-grown VACNT forest with 4.15% of V_f was peeled off from Si substrate, and (b) placed on the squeezer made of Teflon. (c) The forest was densified from one direction (x-direction), and (d) perpendicular direction (y-direction) to previous direction in order.

The term of 'volume fraction' used in this study represents the degree of the number of CNTs occupying the forest with unit volume. In general, the volume fraction of as-grown CNT forest varies at most up to ~5 % of V_f [71]. CNT forest with relatively higher volume fraction expected to be higher thermal property than as-grown CNT forest considering remarkable intrinsic thermal conductivity of an individual CNT. The volume fraction of the CNT forest was controlled through mechanical densification developed by Wardle *et al* [75]. They reported mechanical densification that mechanical compression in two orthogonal directions increased V_f of free-standing CNT forest

placed in Teflon squeezers [57].

As described in Ch. 2.3.1, the volume fraction is 4.15 % for as-grown SWNT forest. The mechanical densification performed based on the as-grown SWNT forest to vary volume fraction of SWNT forest. Figure 2.3.4 shows the process of mechanical densification. The free-standing CNTs were obtained to squeeze to vary V_f of CNT forest that the synthesized mm-long CNT forests were easily delaminated from the Si substrate by a razor [76] or a tweezer with light contact. First, CNT forest without Si substrate was placed on the Teflon squeezer, and then covered with transparent acrylic cover. The cover enables both to estimate roughly volume fraction by observing the area CNT forest, and to see morphology of CNTs during the densification process. Placed CNT forest with cover is squeezed from one (x) lateral direction to axis of VACNTs, and then from perpendicular (y) direction with keeping from x-direction. The maximum obtainable volume fraction of CNT forest was up to 25.20 % for SWNTs, 17.88 % for MWNTs by the mechanical densification in this study.

2.3.4 Thermal Diffusivity and Conductivity of SWNT Forests

The laser flash analysis technique directly determines thermal diffusivity which indicates the rapidity of the heat propagation thorough a material. Thermal diffusivity for SWNT forest with various volume fraction were measured using LFA technique, and found dependence of thermal diffusivity on V_f of SWNT forest. Figure 2.3.5 shows the dependence of thermal diffusivity (black triangles for left axis) on V_f of SWNT forest that the as-grown SWNT forest has thermal diffusivity of 33.71 mm^2/s, which tends to

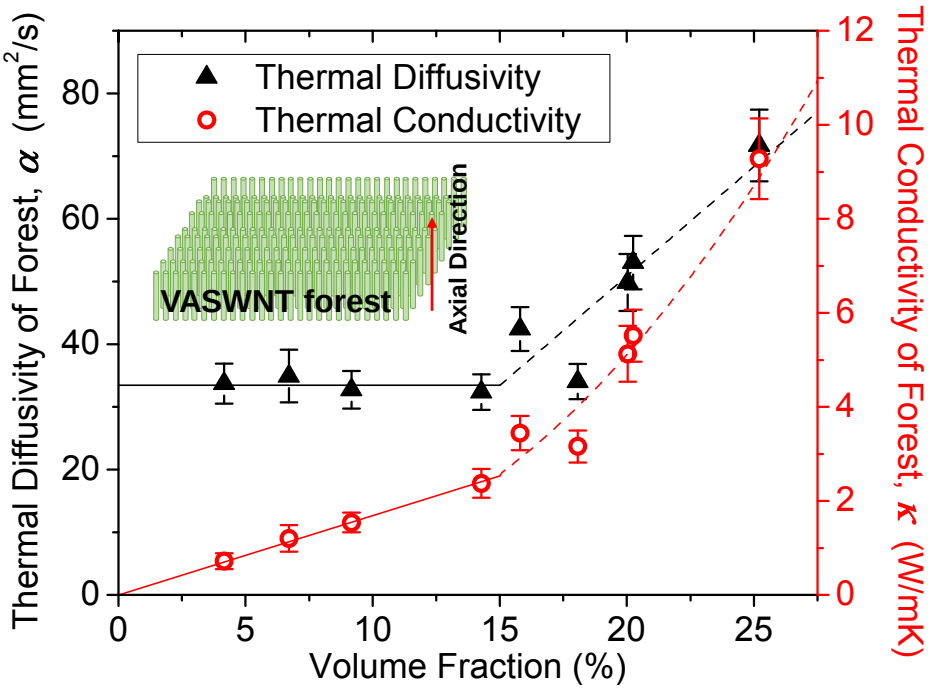

Figure 2.3.5: Volume fraction dependent thermal diffusivity and conductivity of VASWNT forests. Thermal diffusivity increased around 15 % V_f. On the other hand, thermal conductivity of VASWNT forest increased progressively with V_f, derived with additional information such as specific heat, and density. (The solid and dash lines are just guide for eyes.)

increase around at 15 % of volume fraction up to 71.69 mm^2/s at 25.20 % volume fraction.

Since thermal diffusivity is intrinsic thermal property of a material, SWNTs should have had same thermal diffusivity even though they are in different volume fraction. Hence, the result is unnatural that the increase of volume fraction resulted in high thermal diffusivity of SWNT forests. This phenomenon possibly can be explained by the suspending SWNTs in the forest that nanotubes not directly involved in the thermal propagation from front to rear surfaces during the measurement of LFA, become to contribute for thermal transfer rather than to disturb, which causes to increase thermal

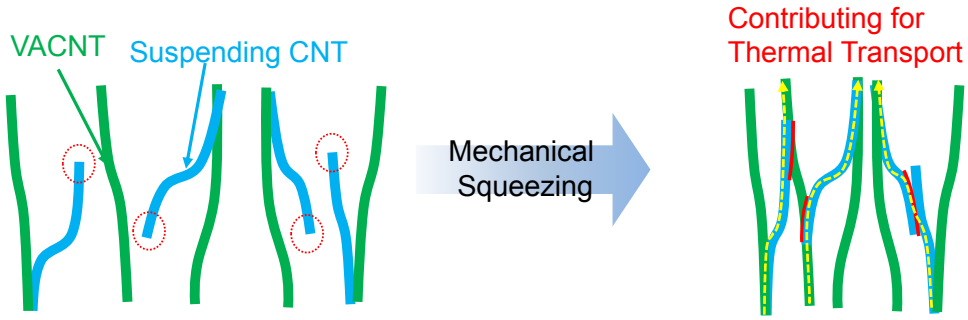

Figure 2.3.6: Schematic for effect of mechanical squeezing on suspending CNTs, which turned to be directly involved in the thermal propagation (yellow arrows).

diffusivity as shown in Fig. 2.3.6.

Dividing total mass of SWNT forest by a single SWNT can suggest the number of total SWNTs resulting in the estimation of inter-tube distance, which was 15.25 nm as shown in Fig. 2.3.7(a). Einarsson *et al* reported "bundling" in as-grown SWNT forest of which average was six-bundling-SWNT [77]. With the consideration of the bundling, the inter-tube distance was estimated to be 158.50 nm in as-grown SWNT forest with 4.15 % V_f as shown in Fig. 2.3.7(b). Figure 2.3.7(c) shows the estimation of inter-tube distance with various volume fraction. Threshold for increase of thermal diffusivity was around at 15 % volume fraction of SWNT forest as described in Fig. 2.3.5 of which distance was estimated to be 84 nm. At 15 % V_f of SWNT forest, the dispersed suspending SWNTs began to be contacted by mechanical squeezing, and then turned to contribute for thermal transfer as shown in Fig. 2.3.8, which lead to increase thermal diffusivity.

On the other hand, indirectly, thermal conductivity of SWNT forest can be derived with additional information such as the specific heat and density by using the relation as

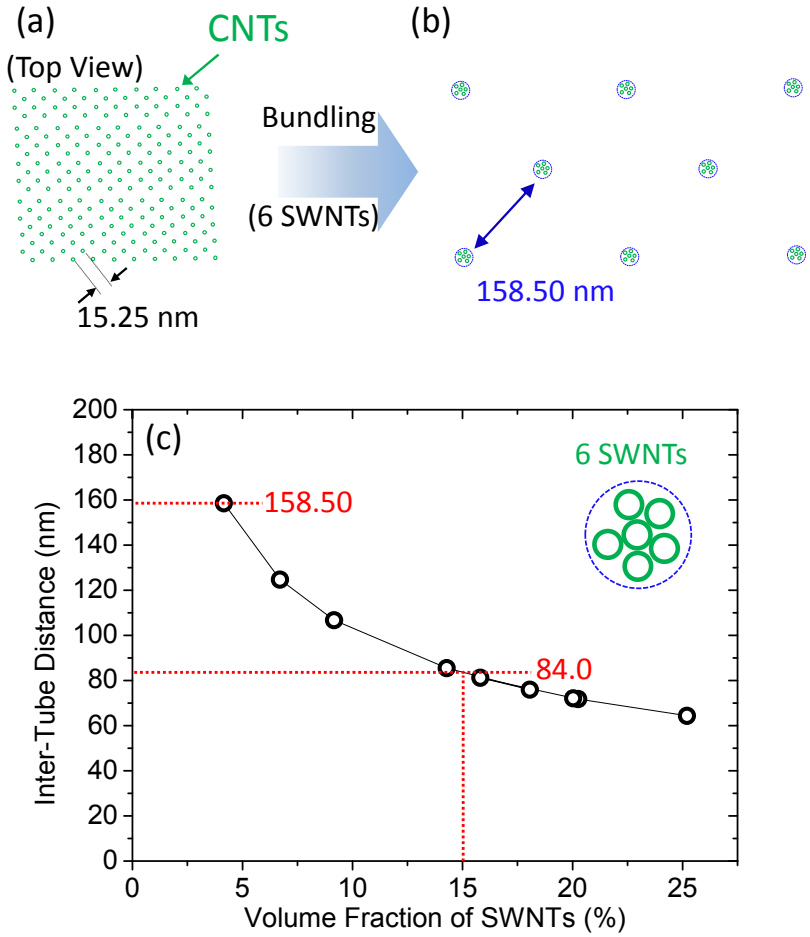

Figure 2.3.7: Estimation of inter-tube distance (a) by simple division with total mass of SWNT forest, and (b) by the consideration of bundling which assumed to be batched with surrounding 6 SWNTs. (c) The estimation of inter-tube distance with various volume fractions.

below,

$$\kappa = \alpha \times \rho \times C_p \tag{2.3}$$

where κ, α, ρ, and C_p are thermal conductivity, thermal diffusivity, density and specific heat, respectively. α and ρ are experimentally measured values. Since SWNTs composes a six-carbon ring same as graphite, C_p is quoted from the of graphite, 0.709 J/gK [78,79].

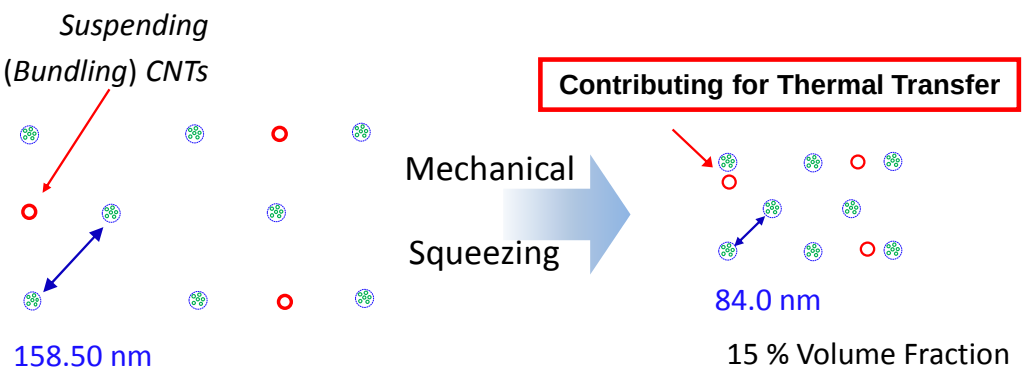

Figure 2.3.8: Schematic for the threshold at 15 % volume fraction for increase of thermal diffusivity. From the estimation of distance with each volume fraction as shown in Fig. 2.3.7, inter-bundling-tube distance was about 84 nm in 15 % V_f of SWNT forest by mechanical squeezing. Dispersed suspending CNTs became to contact, and then turned to contribute for thermal transfer.

Volume fraction of SWNT forest has an effect on thermal conductivity, similar to thermal diffusivity as shown in Fig. 2.3.5(red circles for right axis). As-grown SWNT forest with 4.15 % of volume fraction holds thermal conductivity of 0.72 W/mK, which ascended up to that of 9.28 W/mK at 25.20 % of volume fraction. The increasing tendency of thermal conductivity differs a little from that of thermal diffusivity that rose around 15 % volume fraction since thermal conductivity was multiplied by the density, which was linear and nonlinear, before and after 15 % volume fraction, respectively. Of course, the density in high volume fraction led to increase thermal conductivity which provided more channel for thermal transfer, however nonlinear increase after 15 % volume fraction resulted from suspending SWNTs in forest.

As a result, it is potentially concluded that SWNT forest with higher volume fraction holds better performance for thermal transport as considered from the aspect of both

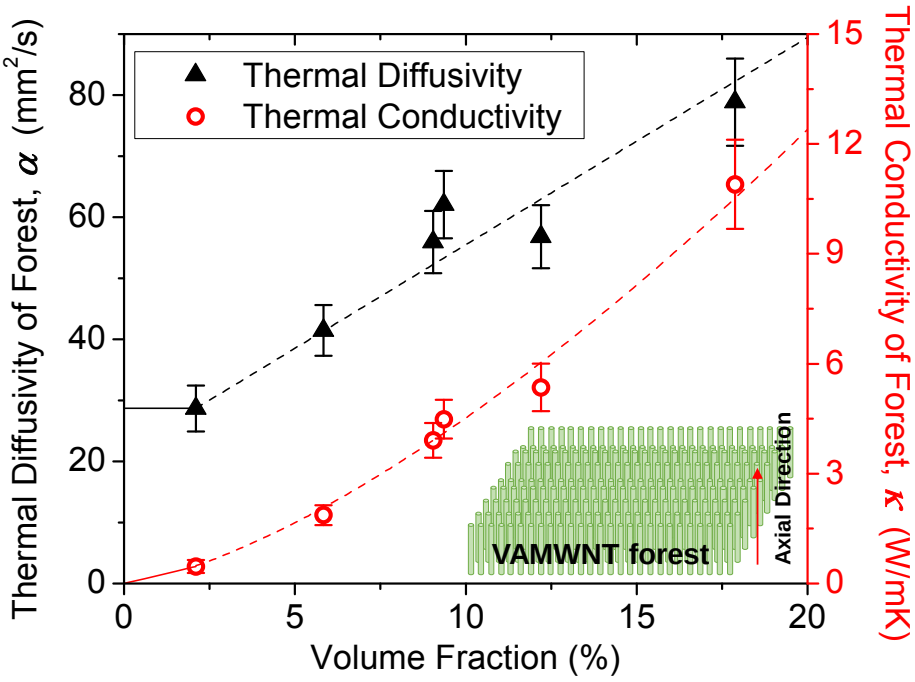

Figure 2.3.9: Thermal diffusivity and conductivity of MWNT forest increase linearly with volume fraction, ranging from 28.67 to 78.86 mm^2/s, and from 0.47 to 10.90 W/mK, respectively. (The solid and dash lines are just guide for eyes.)

thermal diffusivity and conductivity. These findings of volume fraction dependent thermal property represents for SWNT forest, potentially can help to understand the thermal behavior of composing forest for the suitable uses in thermal applications.

2.3.5 Thermal Diffusivity and Conductivity of MWNT Forests

As described in previous section, millimeter-long MWNT forest synthesized with 2.0 nm-thick-layer of Fe catalyst consisted of mostly double-, triple-, and quadruple- walled CNTs. For MWNT forest, volume fraction was calculated by using the diameter of the outer-most wall of each CNT including Van der Waals distance. As-grown MWNT forest was 2.10 % of volume fraction, and the maximum volume fraction of

mechanically squeezed MWNT forest increased up to 17.88 %. Figure 2.3.9 shows thermal diffusivity (black triangles for left axis), measured by LFA technique, and derived thermal conductivity for MWNT forest (red circles for right axis). Thermal diffusivity of as-grown MWNT forest is 28.67 mm^2/s, which seemed to increase linearly to volume fraction up to 78.86 mm^2/s at 17.88 %, obtainable maximum volume fraction. The increased tendency of thermal diffusivity of MWNT forest seemed to be different from that of SWNT forest turning to increase around 15% volume fraction. However, this work believes that the increase of thermal diffusivity of MWNT forests took place immediately after the densification, just different threshold rather than different tendency. The reason for the difference is considered to result from structural difference of vertically aligned SWNTs and MWNTs, and the more details will be discussed in next chapter.

In addition, thermal conductivity was calculated for MWNT forest with additional information using Eq. (2.3), as described in previous section. Thermal conductivity is proportional to volume fraction of MWNT forest that 0.47 W/mK at 2.10 % for as-grown MWNT forest linearly increased up to 10.90 W/mK at 17.88 %. Those obtained values of MWNT forest are higher than that of SWNT forest, and difference between maximum and minimum thermal conductivity of SWNT forest is similar to that of MWNT forest.

2.3.6 Comparison Thermal Properties of between SWNT and MWNT Forests

Comparison of thermal properties between SWNT and MWNT forest were performed

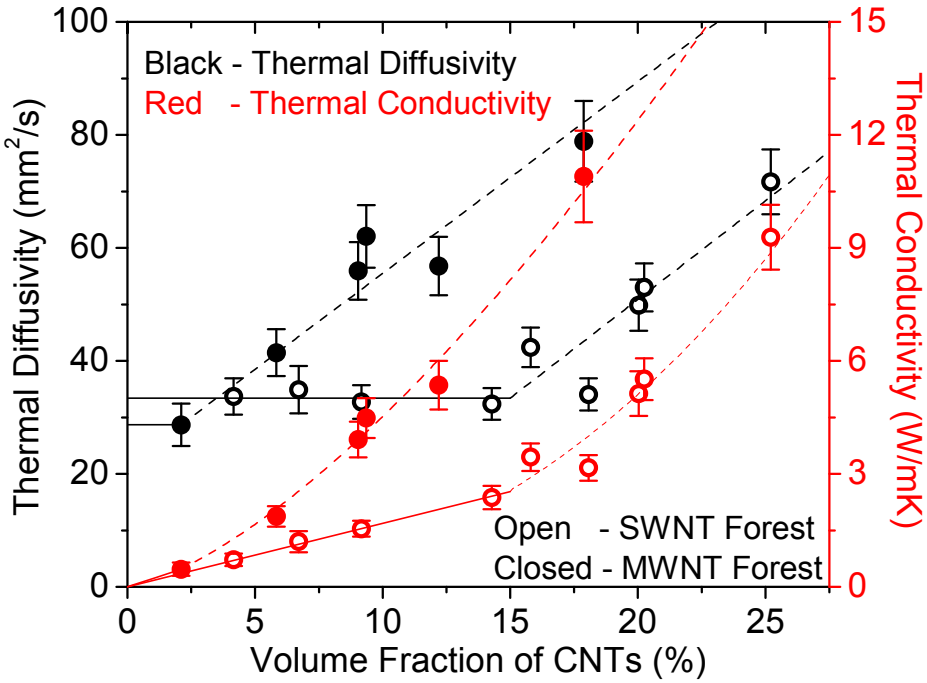

Figure 2.3.10: Comparison of thermal diffusivity (black for left axis) and conductivity (red for right axis) between SWNT (open circle) and MWNT (closed circle) forests. Both thermal diffusivity and conductivity of SWNT forest is found to be higher than those of MWNT forest at each volume fraction. (The solid and dash lines are just guide for eyes.)

as one of the main aims for this thesis. The comparison can suggest a better material between them to be used for potential thermal applications. Figure 2.3.10 shows the comparison of thermal properties of between SWNT and MWNT forests with various volume fraction, was reproduced from Fig. 2.3.5 for SWNT and Fig. 2.3.9 for MWNT forest. Thermal diffusivity of 33.71 mm^2/s for as-grown SWNT forest nonlinearly increased around at 15 % of volume fraction, and reached up to 71.69 mm^2/s at 25.20 %, however that of MWNT forest varied from 28.67 to 78.86 mm^2/s with volume fraction ranging from 2.10 to 17.88 % volume fraction which tends to increase immediately right after mechanical densification.

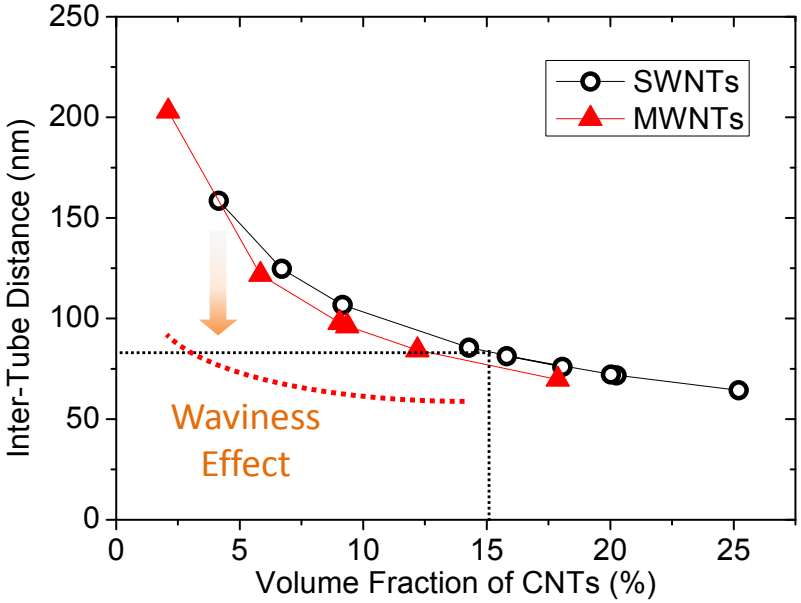

Figure 2.3.11: Comparison of inter-tube distance of between SWNT and MWNT forests with various volume fractions. The tendency of thermal diffusivity of MWNTs differs from that of SWNTs because of the different degree of waviness as shown SEM images in Fig. 2.3.12 for SWNTs and Fig. 2.3.13 for MWNTs.

Thermal diffusivity represents only the speed of thermal transfer through axial direction of CNT forest, hence it is not enough information to conclude of which CNTs thermally performs better. For that, thermal conductivity needs to be compared each together which can suggest more normalized information, considering other physical properties such as density, and specific heat. All of thermal conductivities for SWNT and MWNT forest with obtainable volume fraction, were derived from thermal diffusivities with additional information such density and specific heat. Thermal conductivity of as-grown SWNT forest has 0.72 W/mK which is 154 % higher than that of MWNT although each volume fraction for SWNT and MWNT forest is different, and the difference of them increased with volume fraction.

The comparison indicates that the CNT forest when composed of MWNTs has higher thermal properties than SWNTs at same volume fraction. Marconnet *et al* [56] reported the role of inner-walls of MWNTs for thermal transfer that conduct phonons efficiently with less interacting to surrounding materials than outer shell. Although the CNTs are standing without any surrounding material, the obtained result in this study can be potentially consistent with the previous report that that MWNTs performs to transport heat more efficiently than SWNTs. To conclude better thermal properties either SWNT or MWNT, however, it is necessary to be studied with more suitable CNTs which exclude crucial factors impacting on thermal properties such as waviness, or obtainable volume fraction.

Figure 2.3.11 shows comparison of inter-tube distance of between SWNT and MWNT forests with various volume fractions assuming six-CNT-bundling structure. This study believes that the difference of the threshold for the increase of thermal diffusivity of SWNT and MWNT forests resulted from the structural difference that SWNTs are apparently vertically aligned more straight than MWNTs as shown in Fig. 2.3.12 for SWNTs and Fig. 2.3.13 for MWNTs. Considering the contribution of suspending CNTs in the forests, having more waviness of MWNTs composing forests resulted in the earlier threshold for the increase of thermal diffusivity than SWNTs.

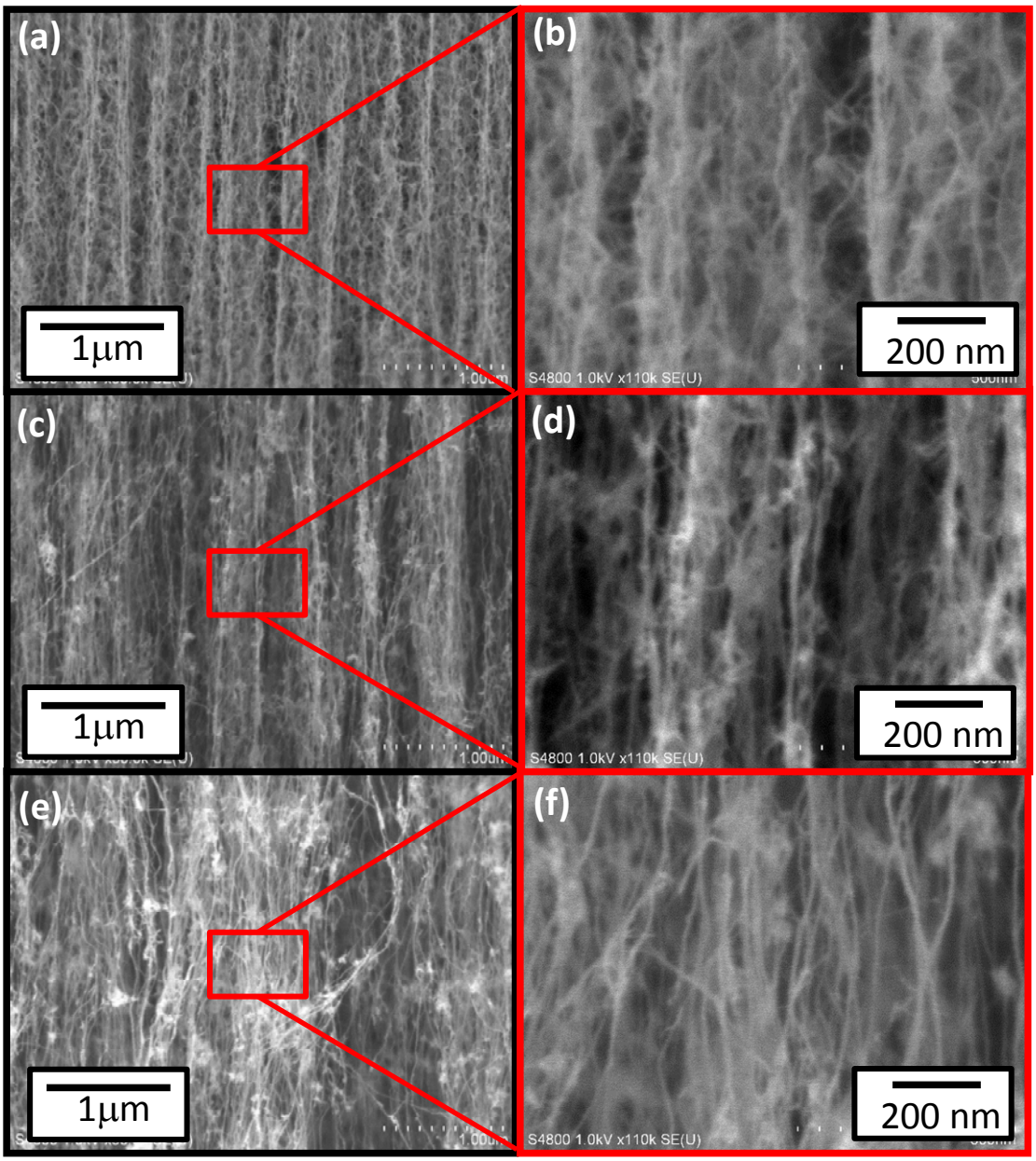

Figure 2.3.12: Cross-sectional SEM images of vertically aligned SWNT forest: (a) Top, (c) middle, and (e) bottom of the forest and each of their enlarged images (b), (d), and (f), respectively.

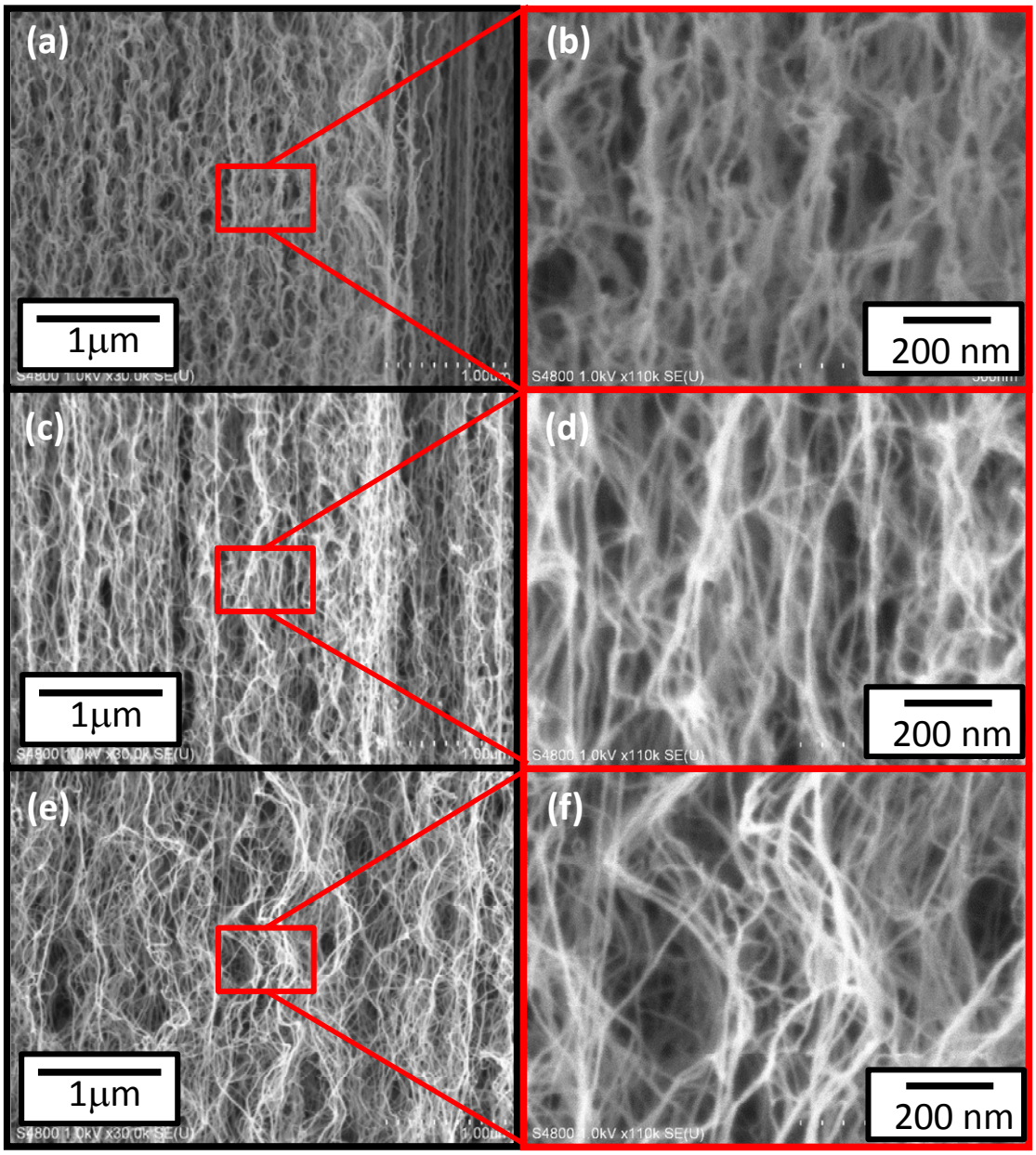

Figure 2.3.13: Cross-sectional SEM images of vertically aligned MWNT forest: (a) Top, (c) middle, and (e) bottom of the forest and each of their enlarged images (b), (d), and (f), respectively.

Table 2.2: Specification and measured thermal properties of single-walled carbon nanotube forests.

	SWNT Forests				A Single SWNT	
Volume Fraction (%)	Density (kg/m^3)	Number of SWNTs ($\times 10^{11}$)	Thermal Diffusivity (mm^2/s)	Thermal Conductivity (W/mK)	Density (kg/m^3)	Thermal Conductivity (W/mK)
4.15	30.09	4.30	33.71	0.72	950.122	22.71
6.70	48.57	6.94	34.90	1.20		23.51
9.16	66.39	9.48	32.74	1.54		22.05
14.3	103.44	14.8	32.37	2.37		21.80
18.1	130.89	18.7	34.05	3.16		22.94
15.8	114.50	16.4	42.43	3.44		28.58
20.3	146.74	21.0	53.02	5.52		35.72
20.0	145.13	20.7	49.85	5.13		33.58
25.2	182.58	26.1	71.70	9.28		48.29

Table 2.3: Specification and measured thermal properties of multi-walled carbon nanotube forests.

	MWNT Forests				A Single MWNT	
Volume Fraction (%)	Density (kg/m^3)	Number of CNTs ($\times 10^{11}$)	Thermal Diffusivity (mm^2/s)	Thermal Conductivity (W/mK)	Density (kg/m^3)	Thermal Conductivity (W/mK)
2.10	22.92	0.87	28.67	0.47	1281.78	26.05
5.84	63.64	2.43	41.45	1.87		37.67
9.04	98.58	3.76	55.93	3.91		50.82
9.36	101.98	3.89	62.06	4.49		56.39
12.20	132.96	5.07	56.80	5.35		51.62
17.88	194.89	7.43	78.86	10.90		71.67

2.4 Derivation of Thermal Conductivity of an Individual CNT

2.4.1 Thermal Conductivity of an Individual CNT

With thermal diffusivity of SWNT forest, specific heat quoted from graphite, and density of an SWNT calculated as described in chapter 2.1, thermal conductivity of a single SWNT was obtained using Eq. (2.3). Figure 2.4.1 shows thermal conductivity of a single SWNT (blue squares for left axis) and that of SWNT forest (red circles for right axis). The volume fraction led to increase thermal diffusivity and conductivity of the forest. Here, considering CNT forest varied by mechanical densification without any

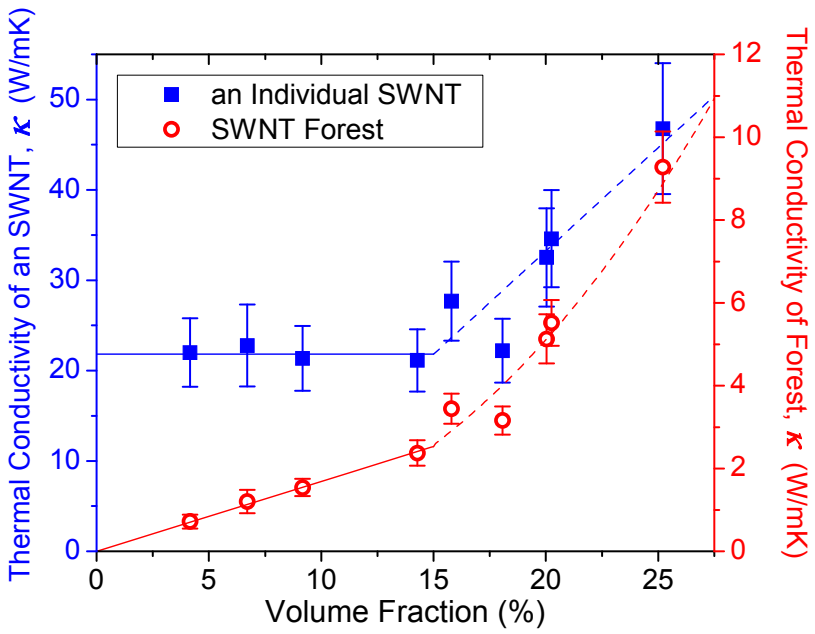

Figure 2.4.1: Thermal conductivity of an individual SWNT (blue squares for left axis), and SWNT forests (right circle for right axis) in various volume fractions. Although every single SWNT in the forest is identical, thermal conductivity of an individual SWNT increased from 20.71 to 48.29 W/mK around 15 % volume fraction. (The solid and dash lines are just guide for eyes.)

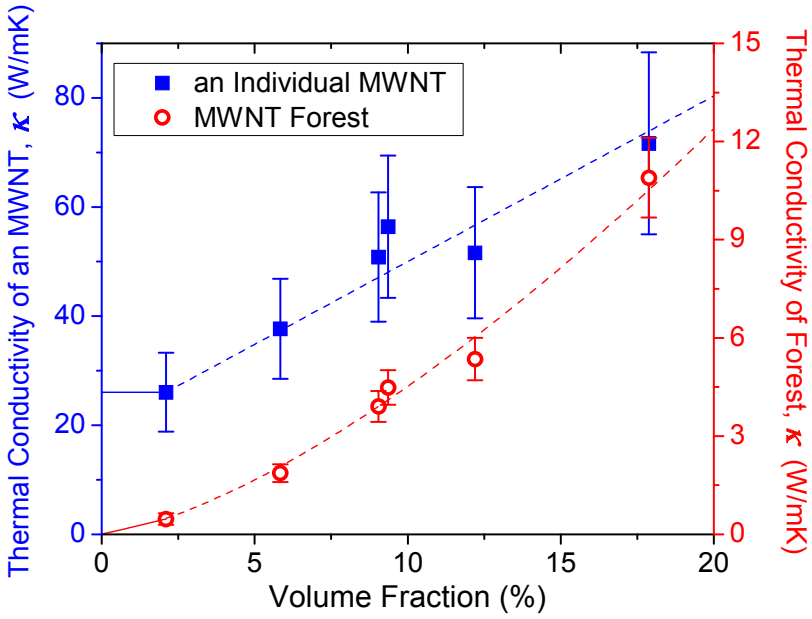

Figure 2.4.2: Thermal conductivity of an individual MWNT (blue squares for left axis), and MWNT forests (right circle for right axis). The density of a single MWNT to calculate thermal conductivity was estimated the consideration of the wall-number-distribution in forest with the diameter ranging from 4.7 to 7.5 nm. (The solid and dash lines are just guide for eyes.)

structural damage during the process, CNTs composing forest are identical in each volume fraction, and also each of their thermal conductivities should be equivalent regardless of the volume fraction. However, the result indicates that obtained thermal conductivity of a single SWNT increases with densification of the forest, ranging from 22.71 to 48.29 W/mK.

Also, thermal conductivities of a single MWNT were obtained for each volume fractions that increased 26.05 to 71.67 W/mK, higher than SWNTs comparing at a same volume fraction (see Fig. 2.4.2). To derive thermal conductivity, it is necessary to find density of a single MWNT which varies according to the number of wall in each CNT

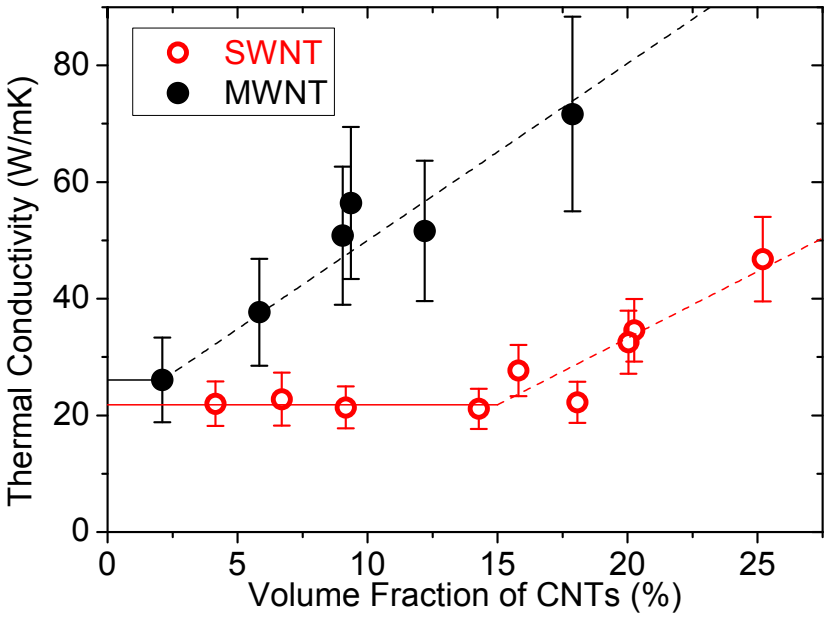

Figure 2.4.3: Comparison thermal conductivity of between a single SWNT and MWNT.

comparing to simple estimation of density for an SWNT. Here, it is obtained by the consideration of wall-proportion in forest counted using TEM images (see Fig. 2.2.3(b)). Basically, the derived values for an individual SWNT are much lower than literature values [19,64,65,80], which leads to suspicious on the quality of SWNTs. However, it is acceptable due to the aim for this thesis to understand the influence of structural change of SWNTs on thermal properties with various volume fractions.

These results can be discussed with the distribution of suspending CNTs for thermal transfer resulting from mechanical densification, and extended to the influence of the thermal boundary conductance between individual CNTs, in terms of thermal boundary resistance, as a factor to have an effect on thermal conductivity.

2.4.2 Possible Reasons for the Increase of Thermal Conductivity for a Single CNT

Thermal conductivity of a single CNT was calculated with same thermal diffusivity and specific heat as CNT forest. The density of a single CNT for the calculation was employed instead of the CNT forest, hence the tendency for the thermal conductivity of a single CNT is equivalent to thermal diffusivity of CNTs. However, this chapter described from the perspective for the thermal conductivity of a single CNT. MWNT forests showed higher thermal conductivities than SWNT forests at any range of volume fraction. If the only difference between SWNTs and MWNTs was the existence of inner-walls inside CNTs, they would played to enhance thermal transfer through CNTs. When CNTs are surrounded by materials such polymer matrix, the inner-wall of MWNTs can possibly transport phonons efficiently [56].

Thermal boundary resistance (TBR) indicates a significant temperature difference [81] occurred during the process of thermal transfer at interface, herein, between individual CNTs since CNTs in forest are basically standing wavy or bundled each other. The TBR is strongly considered as one of the factors to undervalue when structuring forest. Through nonequilibrium molecular dynamics simulation, Zhong and Jenifer reported the effect of TBR between SWNTs resulting from several factors such as distance, contact area, length. The result revealed the TBR was relieved by the three factors of relatively longer CNTs, increased overlap area, and closer spacing between SWNTs [9].

The mechanical densification employed to enhance the volume fraction of the CNT forest with lateral direction to axis of VACNTs, forces the individual CNTs closer, and has the overlap area between them increased. Consequently, as the expended overlap area relieved the TBR, thermal conductivity of an individual CNT increased with the

enhancement of volume fraction. The structural changes during the process of densification of CNT forests such as the interstitial distance and overlap area of CNTs diminished the TBR in good agreement with the assumed tendency inferred from the reported numerical data [9], and this can potentially be one of the reasons that the thermal conductivity of an CNT was dependent on the volume fraction of the CNT forest.

2.5 Summary

This chapter investigated the effect of volume fraction of CNT forest on thermal properties. Single- and multi-walled carbon nanotubes were obtained from CVD method with different size of Fe catalyst of which volume fraction was varied by the mechanical densification, introduced by Wardle *et al* that squeezes interstitial spaces between vertically aligned CNTs without any structural collapse.

With various volume fractions, thermal diffusivity of the CNT forests along axial direction were measured by laser flash analysis technique, and then thermal conductivity were derived with additional information such as specific heat and density, which potentially estimates the role of suspending CNTs in forest for thermal transfer. As a result, thermal diffusivity of SWNT forests tends to increase around 15 % of volume fraction. Since thermal diffusivity is intrinsic thermal property of a material, SWNTs should have had same thermal diffusivity even though they are in different volume fraction. Hence, the result is unnatural that the increase of volume fraction resulted in high thermal diffusivity of SWNT forests. This is probably because the suspending SWNTs in the forest, not directly involved in the thermal propagation from front to rear surfaces during the measurement by LFA, become to contribute for thermal transfer rather than to disturb, which causes to have higher thermal diffusivity. On the other hand, the structural changes during the process of densification of CNT forests such as the interstitial distance and overlap area of CNTs diminished the TBR, and this can be one of the reasons that the thermal conductivity of a single CNT was dependent on the volume fraction of the CNT forest.

Chapter 3:

Enhanced Thermal Properties of PDMS Composites with Vertically Aligned CNT Forest

3.1 Prior Works of Enhanced Thermal Properties of Polymer Composites with Vertically Aligned CNTs

Many studies have been reported for the enhancement of thermal property of polymer composites with CNTs [22,23,26,56,82–84] due to their outstanding thermal property. In particular, thermal property along axial CNTs is much better than transversal due to their quasi-one-dimensional structure with anisotropic thermal property [61]. Huang *et al* [23] reported anisotropic thermal property of CNTs in polymer matrix that thermal conductivity of aligned CNTs in polymer matrix has been enhanced at least three times larger than those of dispersed. Marconnet *et al* [56] reported the enhanced thermal conductivity by vertically aligned CNTs that 1 % V_f of aligned CNTs doubled that of base polymer.

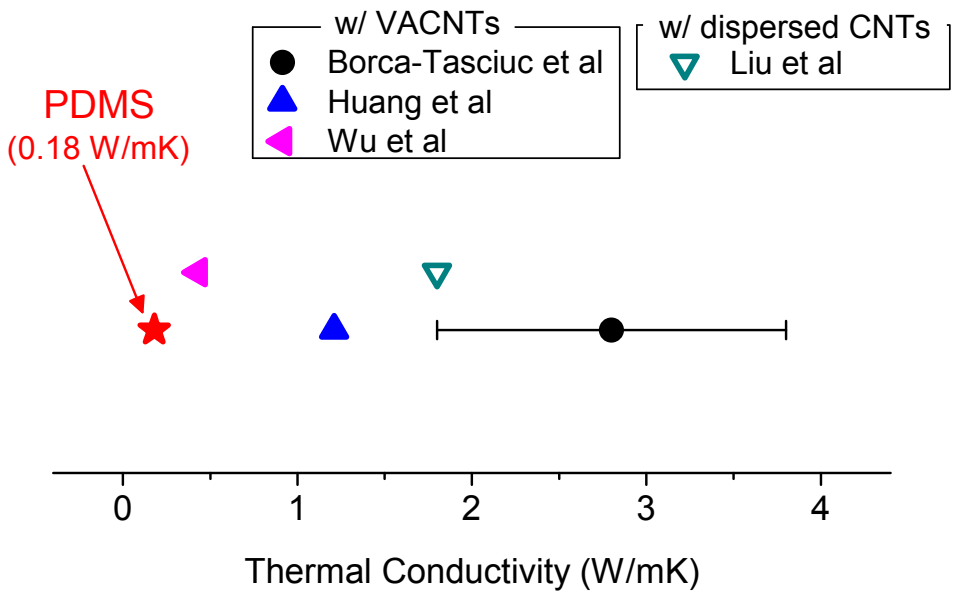

Figure 3.1.1: Experiment data in prior works on enhanced thermal conductivity of PDMS composites by dispersed [21] and vertically aligned carbon nanotubes [22–24].

Polydimethylsiloxane (PDMS), mainly used polymer in this study, is a potential candidate for PDMS-based applications such as thermal interface materials due to its physical behavior during cross-linking process. However, its low thermal conductivity ~0.18 W/mK [55] has been a critical obstacle to be used in thermal applications.

The material in thermal application is essentially to have high thermal properties. For that, several studies have been reported on enhanced thermal conductivity of PDMS composites with dispersed [21] and vertically aligned carbon nanotubes [22–24] (see Fig. 3.1.1), scattered from 2 to 20 times of enhancement than that of PDMS. Borca-Tasciuc *et al* [23] reported the great model for PDMS composite with vertically aligned CNTs that thermal diffusivity of the composite was enhanced up to 4.20 mm^2/s, measured maximum value. The composite were fabricated with suitable frame for synthesized VACNT forest using spin-coating to infiltrate PDMS into the forest. Although it was uneasy to be fully infiltrated into the forest due to its high viscosity, the composite was regarded as the most ideal model for thermal application such thermal interface material which is able to take their advantages of outstanding elasticity from PDMS and high thermal conductivity from axial CNTs. The experiment data from prior works will be compared to the obtained result in this study in chapter 3.3.

3.2 Fabrication of PDMS Composites with VACNT Forests

3.2.1 Fabrication Process of the Composite

Using suitable fabrication method is one of the most important to obtain the desired composites. In general, there are several categorized methods for fabrication of polymer composites such as solution mixing, melt blending, in-situ polymerization, latex technology, and resin transfer molding [85].

Solution mixing is the most common method to fabricate polymer composite containing CNTs, which goes through with three steps procedure. CNTs are dispersed in appropriate solvent, and then stirred mechanically, magnetically or using sonication with temperature control. This method is also applied to fabricate composite film.

Melt blending is also one of the most common methods for fabrication of the composites, which is employed to obtain most of thermoplastic polymers such as polypropylene and polystyrene. The important advantage of this method is not to require solvent, but to use high temperature and shear force for dispersion of CNTs. In addition, the method is frequently used to produce polymer composite fiber with CNTs in present industrial fields. However, melt blending is not effective comparing to solution mixing since increased viscosity in high CNT contents limits the concentration of dispersed CNTs in polymer to be low.

In-situ polymerization is considered as a very effective method to improve the

dispersion of CNTs and to enhance the interaction between CNTs and polymer. First, CNTs are dispersed in monomers, and then they are polymerized through the addition, or condensation reaction. The big advantage of *in-situ* polymerization is to have covalent bonds between functionalized CNTs and polymer, which results in the composite with improved physical properties.

On the other hand, latex technology is a relatively new method with obvious advantages: easy, versatile, uniform incorporation of individual CNTs into a highly viscous polymer matrix. Latex technology enables SWNTs and MWNTs to be dispersed within most of the polymers produced by emulsion polymerization. Difference of this

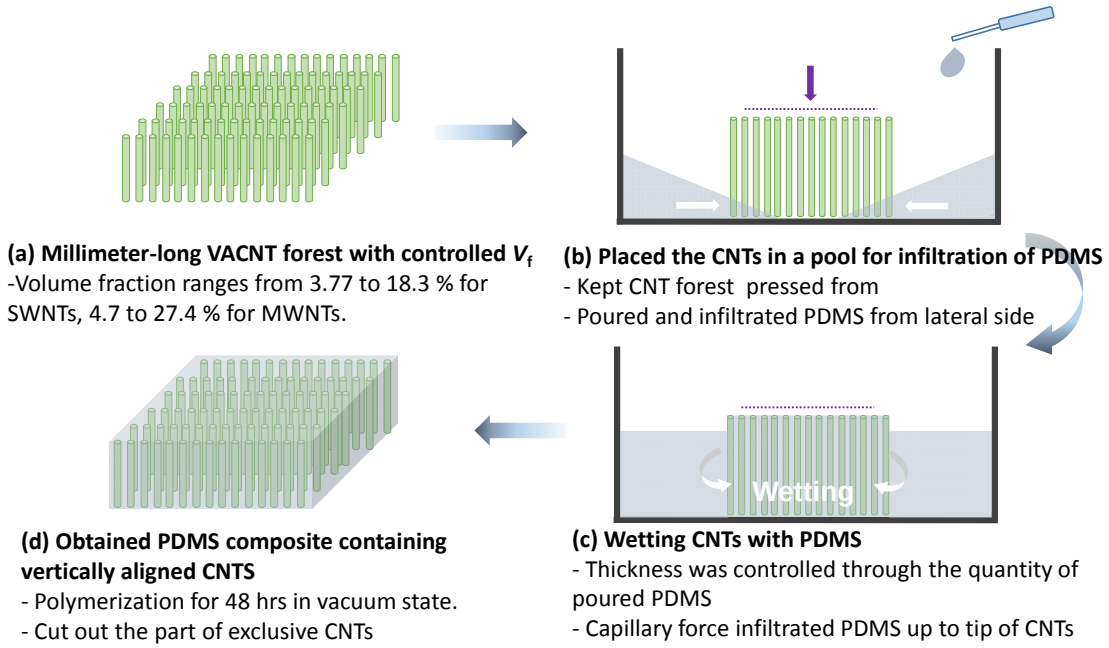

Figure 3.2.1: The process of fabrication for PDMS composites containing mm-long VACNTs with various volume fractions. (a) Controlled volume fraction of VACNT forest is (b) placed in a pool for pouring PDMS. (c) CNTs are wetting PDMS up to the tip by capillary force. Eventually, (d) composites are obtained after cross-linking for 48 hours in vacuum state.

method from the *in-situ* polymerization is that the addition of CNTs occurs after the polymer has been synthesized. Besides, there is another method to fabricate the composites such as resin transfer molding used in fabrication of fiber reinforced polymer composites.

In this study, the wetting CNTs phenomenon of PDMS is apparently close to the *in-situ* polymerization except the functionalized surface that CNTs are incorporated into liquefied polymer matrix in which cross-linking agent was added, resulting from capillary motion. Figure 3.2.1 shows the fabrication process that polymer composites containing VACNT forests with various volume fractions are fabricated through the several steps. Millimeter-long vertically aligned CNT (SWNT and MWNT) forests were synthesized on Si substrates from catalysts CVD, and peeled off by using a razor or a light tweezer contact. Volume fractions of the VACNT forests are controlled by mechanical densification as described in chapter 2. The CNT forests with controlled volume fraction were placed in a plastic pool, and then liquefied PDMS wetted from the side, perpendicular to the axial direction of CNTs. The slow infusion of PDMS from the side direction potentially leads to prevent the composites from void-trap. Since the thickness of the CNT forests are relatively long up to about 1 mm, it is possible to fully wet the CNT forests, up to the tip, by controlling quantities of PDMS [86–88]. Remained voids trapped in the composites are removed by giving enough time to polymerize in a vacuum desiccator.

3.2.2 Characterization of PDMS Infiltration into CNT Forests by SEM

The infiltration condition of polymer is one of the main factors to determine the quality of the desired composites for the enhancement of physical properties of polymer composites containing vertically aligned CNT forests. *In-situ* polymerization pours PDMS into interstitial space between VACNTs with relatively high volume fraction ~ 5 % for as-grown forest in contrast to solution mixing method that disperses CNTs into

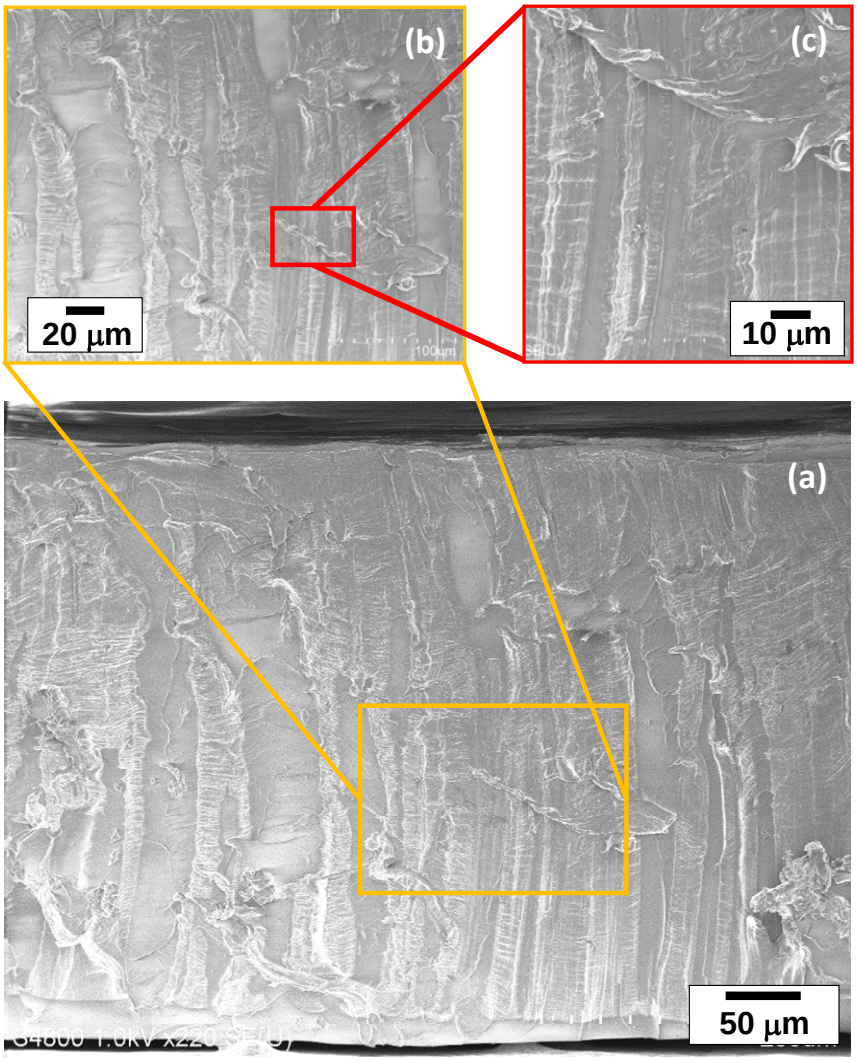

Figure 3.2.2: SEM images for characterization of PDMS infiltration into VASWNTs and their vertical alignment. (a) PDMS infiltrated into interstitial VASWNTs with no voids and excess region on up and down. (b), and (c) shows the enlarged images from (a).

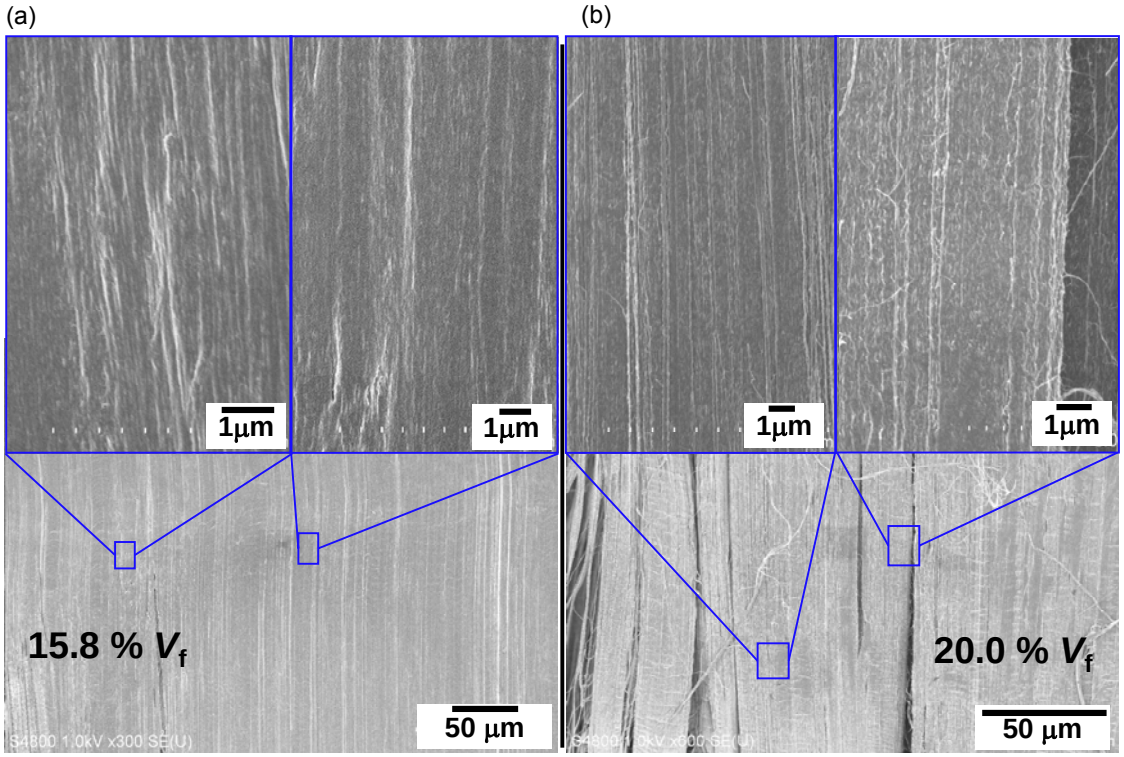

Figure 3.2.3: Cross-sectional SEM images of PDMS composite containing (a) 15.8 % V_f, and (b) 20.0% V_f of VASWTs.

polymer matrix with adjusting the quantity. To obtain the purposed composite with physical properties, it is necessary to characterize the infiltration of the composites. This study employed scanning electron microscopy (SEM) which is the most common in several methods for the characterization to distinguish the void-trapped in the composites through SEM images.

Borca-Tsuic *et al* [22] employed the spin-coating to infiltrate PDMS into VACNTs, and measured thermal property of the composites. PDMS fully infiltrated well into the top of the forest, but not into bottom. Figure 3.2.2(a) shows cross-sectional SEM images of the polymer composites with as-grown SWNT forest which is as long as as-grown SWNTs, and little excess PDMS region on up and down of the composite. Through

enlarged SEM images (see Fig. 3.2.2(b), and (c)), it demonstrates that there are no voids in observable scale by SEM, and the vertical alignment of SWNTs are preserved in the composite.

Interstitial distance between CNTs decreased with the increase of volume fraction of CNT forests. Hence, the infiltration of PDMS poured into higher volume fraction of CNT forests needs to be characterized. In this study, the composites with each 15.8, 20.0, and 25.2 % volume fraction of SWNT forests, obtained by mechanical densification as described in chapter 2 were fabricated and characterized the infiltration by SEM.

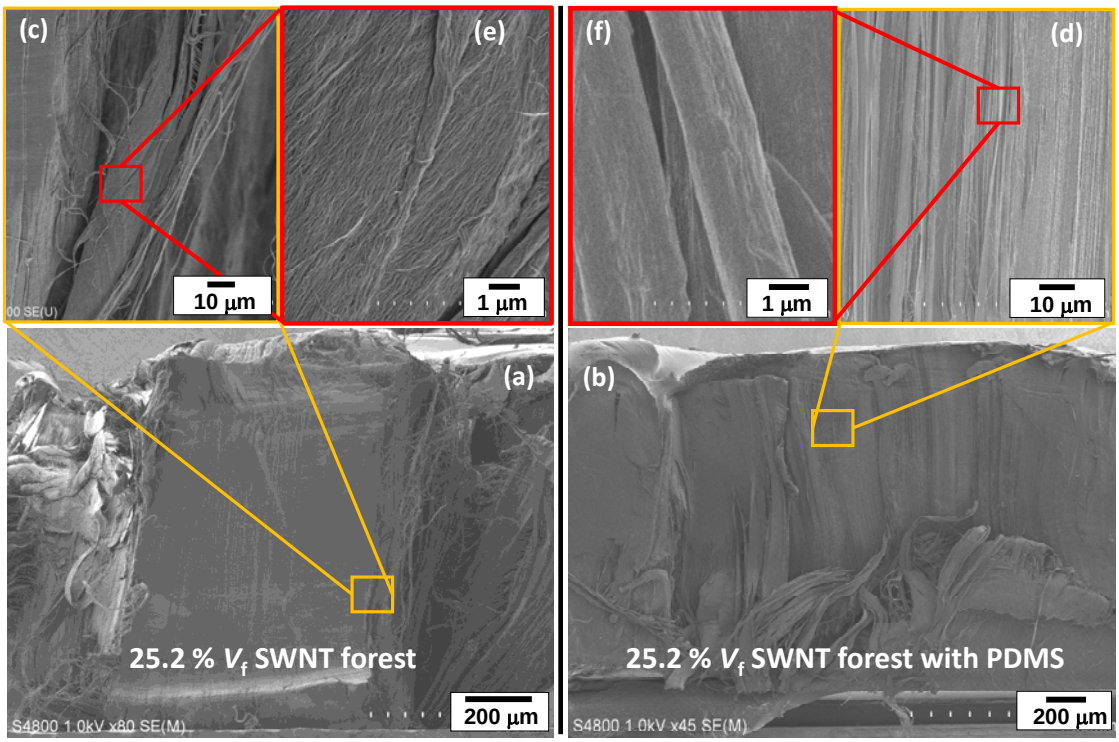

Figure 3.2.4: Cross-sectional SEM images for characterization of PDMS infiltration: (a), (c), and (e) for VASWNT forest and (b), (d), and (f) for the composite with the highest obtainable volume fraction.

Figure 3.2.3(a) and (b) show the cross-sectional SEM images of PDMS composites with 15.8 and 20.0 % V_f, respectively, and no distinguishable voids through the enlarged SEM images. There are, however, cracks along the axial CNTs which possibly resulted from phase separation which prefers to incorporate composite with specific proportion of CNTs and polymer. This can lead to explain the matrix-rich areas in PDMS composite with as-grown SWNTs. As another possible reason, they simply came from the cutting process for the composites, or pressing force after polymerization leading to tear them.

On the other hand, the maximized volume fraction of the VACNT forest was up to 25.2 % by mechanical squeezing in this study. Figure 3.2.4(a), (c), and (e) show SEM images of 25.2 % volume fraction of SWNT forest that it is uneasy to identify CNTs due to close interstitial space, but they appear like aligned threads as shown in the enlarged image of Fig. 3.2.4(e). With this VASWNT forest with 25.2 % volume fraction, the PDMS composite were fabricated, and characterized the infiltration. Figure 3.2.4(b), (d), and (f) shows the infiltration of PDMS that infiltrated into the VASWNT forest, and threads-like CNTs were not observed in the enlarged image of Fig. 3.2.4(f) comparing to Fig. 3.2.4(e) in same scale.

3.3 Enhanced Thermal Properties of PDMS Composite Containing CNT Forests with Various Volume Fractions

3.3.1 Enhanced Thermal Properties of PDMS Composite with SWNT Forests

Using laser flash analysis technique introduced in chapter 2, thermal diffusivity of PDMS composite containing as-grown SWNT forest was directly measured, and compared to those of as-grown SWNT forest and PDMS (see Fig. 3.3.1). Thermal diffusivity of each SWNT forest with 4.15 % V_f, PDMS, and the composite is 29.44, 0.12, and 1.118 mm^2/s, respectively, at room temperature. All of them have no significant dependence on the temperature ranging from 25 to 110 °C. For LFA

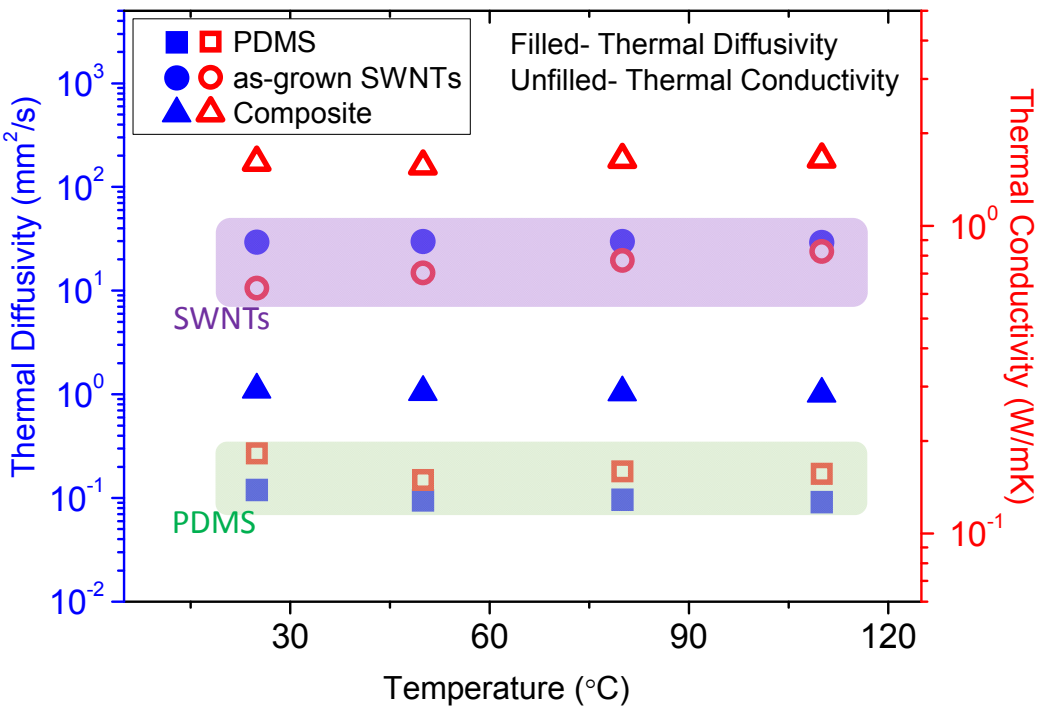

Figure 3.3.1: Comparison of thermal diffusivity and conductivity for as-grown SWNT forest, PDMS, and the composite.

measurement, titanium as adhesive layer and aluminum to prevent from penetration of xenon flash through the composite, were deposited on both front and rear sides of the composite with the thickness of 20 and 200 nm, respectively. In addition, each thermal conductivity of them was obtained with addition information such as specific heat and density. Thermal conductivities were 0.63, 0.18, and 1.61 W/mK for as-grown SWNT forest, PDMS, and the composite, respectively. Thermal diffusivity and conductivity of the composite were enhanced up to 931 and 883 %, respectively, by as-grown SWNT forest than those of PDMS. Although SWNT forest has higher thermal diffusivity than the composite, thermal conductivity of the composite is higher than that of SWNT forest since the density of an SWNT is much lower than the composite. Comparing to required thermal conductivity > 4 W/mK [89], it is not enough to be used for such thermal applications.

3.3.2 Enhanced Thermal Diffusivity and Conductivity of PDMS Composites Containing SWNTs and MWNTs with Various Volume Fractions

Thermal conductivity of polymer composites containing CNTs was more enhanced with the increase of the dispersed amount of CNTs [90], which contributes to heat transfer in polymer matrix. In this study, CNTs are vertically aligned and mm long structure, which results in exposed tips on both top and bottom after the fabrication of the composites. For the phenomenon of thermal transport in this structure, CNTs are directly involved in heat transfer along the axial direction. Two types of CNTs, SWNTs and MWNTs, were employed to investigate the influence of CNTs' inner walls for thermal transfer in the composite.

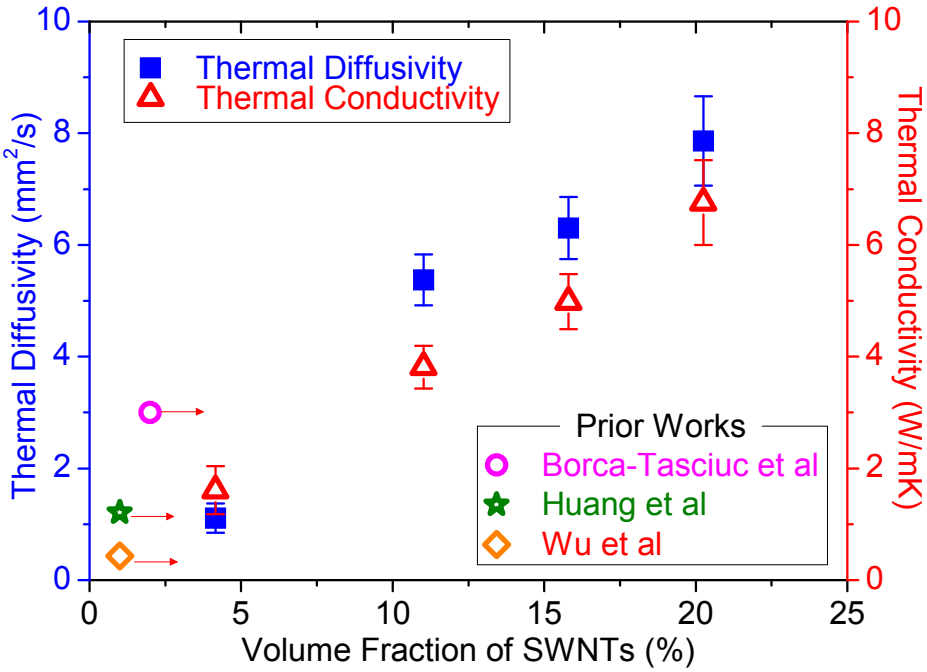

Figure 3.3.2: Prior works for enhanced thermal conductivity by aligned as-grown CNTs [22–24], and enhanced thermal properties dependence of PDMS composites on the volume fraction of SWNT forest, increased up to 7.86 and 6.76 W/mK for thermal diffusivity and conductivity, respectively.

This work has investigated the dependence of thermal properties of the composites on the volume fraction of VACNTs controlled by the mechanical densification. Thermal diffusivity and conductivity of the composites was measured and estimated, respectively, containing VACNT forests with the volume fraction ranging from 4.15 to 20.03 % for SWNTs, and 2.10 to 12.20 % for MWNTs. Density of the composites was directly measured to estimate thermal conductivity, and specific heat was calculated by considering the mixing ratio of SWNTs and PDMS.

Figure 3.3.2 shows the dependence of thermal properties on volume fraction that thermal diffusivity of the composites increased from 1.11 to 7.86 mm^2/s with the

Table 3.1: Thermal properties of PDMS composites with SWNTs and MWNTs.

V_f (%)	Composites with SWNTs	
	Thermal Diffusivity (mm^2/s)	Thermal Conductivity (W/mK)
4.15	1.11	1.61
11.02	5.37	3.81
15.80	6.30	4.99
20.03	7.86	6.76

V_f (%)	Composites with MWNTs	
	Thermal Diffusivity (mm^2/s)	Thermal Conductivity (W/mK)
2.10	0.32	0.53
5.84	2.69	3.17
9.36	5.31	5.51
12.20	6.65	5.83

volume fraction ranging from 4.15 to 20.03 % of SWNTs, which led to give more channels for thermal transport. There have been several reports for enhanced thermal conductivity of PDMS composites by CNTs that they varied 0.43 to 3 W/mK of as-grown SWNT forest although each volume fraction is different [22–24]. Estimated thermal conductivity with density and specific heat of the composites also increased from 1.61 to 6.76 W/mK with volume fraction of SWNTs. Comparing to thermal properties of PDMS, thermal diffusivity of the composite was enhanced up to 6605 %, and thermal conductivity up to 3714 % at 20.03 % volume fraction of SWNT forest. Table 3.1 shows the obtained result for the enhanced thermal properties of PDMS composites by VASWNTs and VAMWNTs.

On the other hand, thermal properties of the composites containing MWNT forests were evaluated by the same way as SWNT forests (see Fig. 3.3.3). Volume fraction of MWNTs ranged from 2.10 to 12.20 % in the composites. Thermal diffusivity and conductivity were 0.32 mm^2/s and 0.53 W/mK with as-grown MWNT forest, and increased up to 6.65 mm^2/s and 5.83 W/mK with 12.20 % volume fraction. Volume fraction of CNTs determined the degree of thermal transfer in composites since CNTs

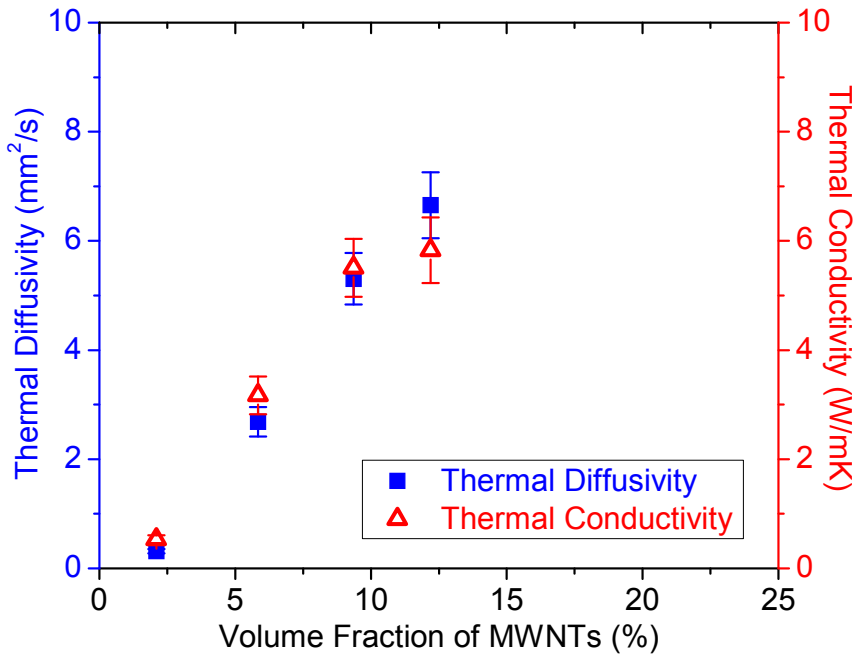

Figure 3.3.3: Enhanced thermal diffusivity and conductivity of PDMS composites by VAMWNTs, which depends on volume fractions. They increased up to 6.65 for thermal diffusivity, and 5.83 W/mK for thermal conductivity.

performs to transport phonon much better than PDMS due to the molecular structure [61,91]. Basically, the increase of volume fraction led to provide more channels for thermal transfer in the composites, which resulted in enhanced thermal conductivity. Comparing SWNTs and MWNTs at same volume fraction, thermal properties of MWNT forests are higher than those of SWNT forests. If filling PDMS matrix into the interstitial space in CNT forest enabled to remove the effect from intrinsic waviness on thermal properties, inner-walls of MWNTs is considered as the only reason to transport phonon effectively [56].

3.3.3 Thermal Conductivity Dependence on Temperature

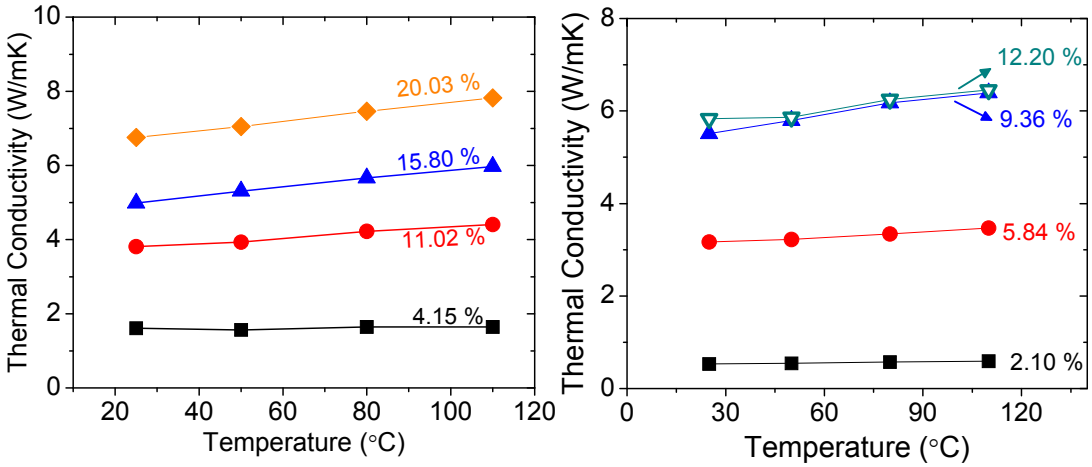

Figure 3.3.4: The composites containing (a) SWNTs and (b) MWNTs are thermally stable although thermal conductivity depends a little on volume fraction.

For the potential application in cooling solution on integrated micro/nano chips such as thermal interface materials, thermal stability needs to be considered during the performance of device. This work evaluated thermal properties of the composites with SWNT and MWNT forests from room temperature (25 °C) to 110 °C, which is apparently high enough than practical temperature of the device processing. Figure (a) and (b) shows thermal properties dependence of the composites with SWNT and MWNT forest on temperature, respectively. Both of them are thermally stable even though thermal conductivity increased a little with higher volume fraction of CNT forests.

3.4 Theoretical Prediction Model for Polymer Composites Containing CNTs

3.4.1 Theoretical Prediction Models for Polymer Composites

There are conventional theoretical prediction models for polymer composites with enhanced thermal property by adding particles into polymer. Maxwell model [92] estimated enhanced thermal property of composite with round –shape particles, and Hamilton-Crosser model [93] with stick-shape of particles. On the other hand, Nan *et al* [94] proposed effective medium theory (EMT) that applied the practical shape of CNTs as additives into polymer matrix, and even suggested several interesting types such as aligned continuous fibers, laminated flat plates, spheres, and completely disoriented ellipsoidal particles. The enhanced thermal conductivity for this model is written as follows:

$$\frac{K_e}{K_m} = \frac{3 + (\beta_x + \beta_z)}{3 - f\beta_x} \tag{3.1}$$

with

$$\beta_x = \frac{2(K_{11}^C - K_m)}{K_{11}^C + K_m}, \quad \beta_z = \frac{K_{33}^C}{K_m} - 1 \tag{3.2}$$

Where f is the volume fraction of the nanotubes; K_m is the thermal conductivity of base polymer, and K_{11}^C and K_{33}^C are thermal conductivities along transverse and longitudinal axes of CNTs, respectively.

In addition, Nan *et al* [95] reported modified EMT which involves the consideration of interface effect on thermal conductivity of composite such as thermal boundary resistance and aspect ratio, as follows:

$$\frac{K_e}{K_m} = 1 + \frac{fp}{3} \frac{K_C/K_m}{p + \frac{2a_k}{d}\frac{K_C}{K_m}} \tag{3.3}$$

where p and d are the aspect ratio and diameter of the nanotube, respectively. a_k is the Kapitza radius defined as the product of thermal boundary resistance (TBR) and the thermal conductivity of polymer (a_k =TBR × K_m).

3.4.2 Enhanced Thermal Conductivity of the Composite by CNTs and Theoretical Prediction Models

Both top and bottom of tips for vertically aligned CNTs are exposed out of the polymer composites fabricated in this study, hence the theoretical prediction model for *aligned*

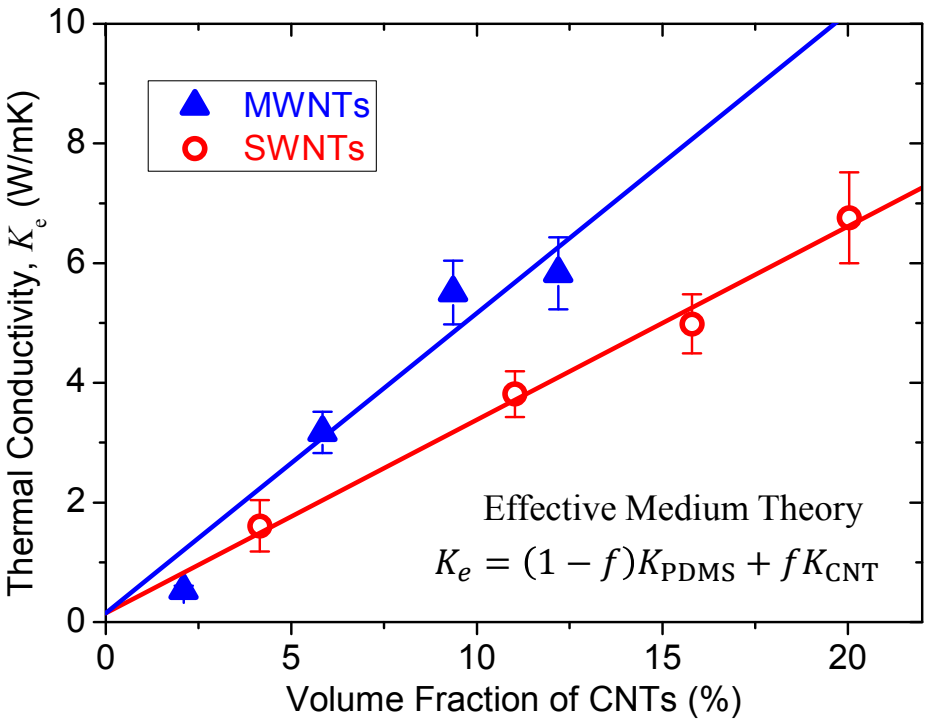

Figure 3.4.1: Enhanced thermal conductivity of PDMS composite containing vertically aligned CNTs (SWNTs and MWNTs) with effective medium theory.

continuous fibers are applicable due to almost infinite aspect ratio of CNTs. The effective medium theory can be simplified as [94],

$$K_e = (1-f)K_m + f \cdot K_{CNT} \tag{3.4}$$

Thermal conductivity of CNTs has been investigated experimentally and theoretically, but largely scattered (see Fig. 2.1.1 and Fig. 2.1.2 in chapter 2). This study estimated thermal conductivity of an SWNT and MWNT with various volume fraction ranging from 22 – 72 W/mK in chapter 2. On the other hand, the prediction model enables to estimate thermal conductivity of CNT which represents the degree of contribution by CNTs in the composite for thermal transfer. Figure 3.4.1 shows enhanced thermal conductivity of PDMS composite containing vertically aligned CNTs (SWNTs and MWNTs) with EMT model for *aligned continuous fibers* proposed by Nan *et al* [94].

By fitting obtained data to EMT model, thermal conductivity of each SWNTs and MWNTs can be estimated to be 32.47 and 50.30 W/mK in PDMS composites, respectively. Comparing to thermal conductivity of a single SWNT and MWNT estimated in chapter 2, they are higher than those in low volume fraction of the forest and lower than those in high volume fraction. Incorporating PDMS enabled suspending CNTs in forest to be bundling each other or to adhere to polymer matrix, which resulted in contributing thermal transfer. On the other hand, thermal conductivity of the composites with MWNTs is higher than with SWNTs because of the different degree of waviness for each SWNTs and MWNTs as described in chapter 2. In addition, the existence of inner-walls in MWNTs potentially led to transport phonon better without the influence of surrounding polymer matrix [56].

3.5 Summary

In summary, thermal properties of PDMS composites containing vertically aligned CNT forests were investigated with various volume fractions. PDMS composite with VACNT forest were fabricated that the phenomenon of PDMS wetting CNTs is apparently close to the in-situ polymerization except the functionalized surface that CNTs are incorporated into liquefied polymer matrix in which cross-linking agent was added, resulting from capillary motion. The degree of PDMS infiltration in CNT forest was characterized by SEM since the infiltration of polymer matrix into CNT forest is one of the main factors to determine the quality of the composite when using the technique to pour polymer on to CNT forest. Remained voids trapped in the composites are removed by giving enough time to polymerize in a vacuum desiccator.

On the other hand, thermal diffusivity of the composites with various volume fraction of VACNT forests was measured by using LFA, which enhanced up to 7.86 mm^2/s at 20.3 % for SWNTs, and 6.65 mm^2/s with 12.2 % for MWNTs. Derived thermal conductivity of each SWNT and MWNT forest was discussed by comparing to the theoretical prediction model of the composite for aligned continuous CNTs proposed by Nan *et al* [94].

Chapter 4:

Development of Fabrication Method for Polymer Composites with Reduced-Size CNT Forest

4.1 Synthesis of CNTs from Alcohol Catalytic Chemical Vapor Deposition (ACCVD)

Impurities such as amorphous carbon, structural defects, and catalyst particles are always produced during the formation of nanotubes synthesized with various methods. However, using ethanol (or alcohol) as carbon feedstock gas enables to minimize the impurities [25], and Fig. 4.1.1 demonstrate three-dimensional structural formula illustrated by *Jmol* and the Lewis structure of ethanol. The CNTs synthesized from alcohol contains highly pure SWNTs with less impurity. Since OH radical of decomposed substances from ethanol reacts with carbon molecules that have dangling bonds and etches them away, and it leads to have less amorphous carbon [25,96]. The CVD method using ethanol as carbon feedstock is called alcohol catalytic chemical vapor deposition (ACCVD). Due to lost-cost for synthesis of highly pure SWNTs, it has become one of the most popular methods. The mechanism of ACCVD process has still been investigated by many different methods including molecular dynamics simulations

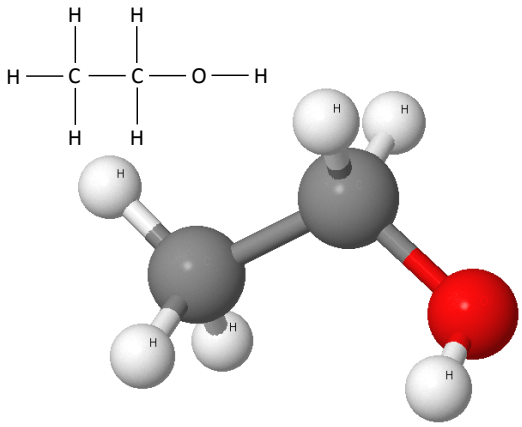

Figure 4.1.1: Illustration of three-dimensional structural formula and the Lewis structure of ethanol.

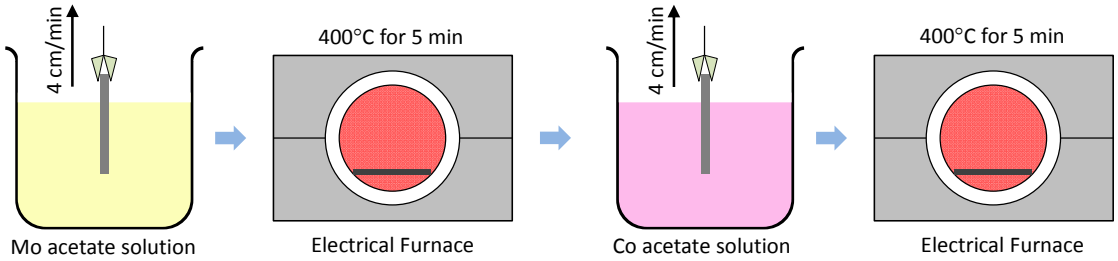

Figure 4.1.2: Dip-coating process with bimetal catalysts of Mo/Co.

[97].

A dip-coating method is a relatively simple process to be performed at atmospheric pressure (see Fig. 4.1.2) [98]. It is already well-known method to produce vertically aligned SWNT forest which can be obtained by supported catalysts of cobalt and molybdenum [98,99]. Initially, 89 mg of molybdenum (II) acetate dimer [$(CH_3COOH)_2Mo$] are dissolved in 40 g of ethanol, and then molybdenum acetate solution with the concentration of 0.01 wt.% is obtained after the process of bath sonication. In the same way, cobalt acetate solution is made by dissolving 129 mg cobalt (II) acetate tetrahydrate [$(CH_3COOH)_2Co{\cdot}4H_2O$] in 40 g of ethanol. Impurities on the Si

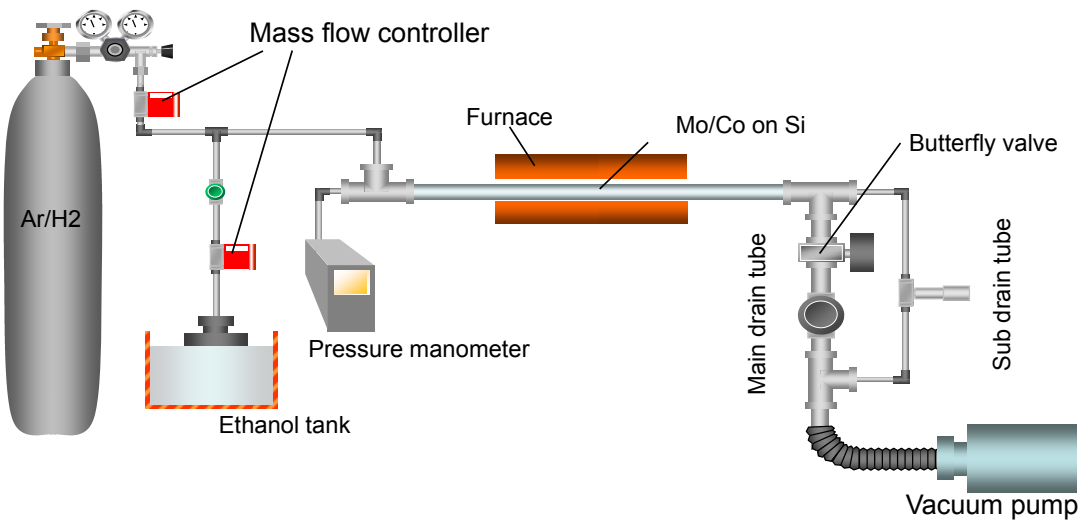

Figure 4.1.3: Schematic of alcohol catalytic CVD apparatus [25].

substrate are removed at 500 °C for 5 min in the electric furnace before the process. The clipped substrate is immersed into molybdenum acetate solution for 5 min, and withdrawn from the solution at speed of 4 cm/min, and then baked in air at 400 °C for 5 min to remove the acetate and oxidize the metals. The process is repeated with cobalt acetate solution. The dip-coated metal catalysts of Co/Mo on substrate are uniformly loaded with mono-dispersed catalyst particles 105 particles/μm^2 with diameters of approximately 1.5 nm [100].

Figure 4.1.3 shows the apparatus of ACCVD method which involves quarts tubes as a chamber, vacuum pump, mixture gas of argon with 3 % H_2, ethanol for carbon source, and electric furnaces to heat up the chamber. The flow rate of the mixture gas of Ar/H_2 and ethanol are controlled by mass flow controller. In addition, there are two tubes connected from vacuum pump to main valve and needle valve, which control the pressure in a chamber.

4.1.1 SWNT and MWNTs

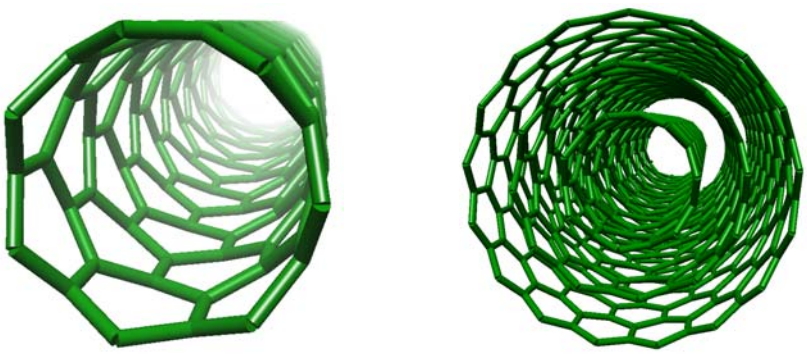

Figure 4.1.4: Structure of single-walled carbon nanotube (left) and multi-walled carbon nanotube (right).

As described in chapter 1, CNTs can be categorized by the number of layers such as single-, double-, few-, and multi-walled carbon nanotube (SWNT, DWNT, FWNT, and MWNT, respectively). To simplify, CNTs are classified into SWNTs or MWNTs in this study (see Fig. 4.1.4). The number of layers of CNTs is controlled by synthesis condition of the CVD method, such as pressure, reaction time, temperature, and size of catalysts.

Two types of CNTs, VASWNTs and VAMWNTs, were employed to study the influence of CNT length, diameter and wall-number on the fabrication of composites. We synthesized VASWNTs using a previously reported ACCVD method [99], which utilizes a dip-coating method with bimetal catalysts of Co/Mo [98] on a Si substrate. Table 4.1 shows the synthesis condition for each VASWNTs and VAMWNTs. To prepare for CNT growth using ACCVD, the quartz tube is heated under Ar containing 3% of H_2 at a flow rate of 300 sccm and at a pressure of 40 kPa. At 800 °C, the growth temperature for CNTs, ethanol with a flow rate of 450 sccm is introduced to substrates with catalysts for 10 min under 1.3 kPa. The length of the grown VASWNTs ranges from 15 to 25 μm. Also, VAMWNTs were synthesized by ACCVD using a Si substrate that was sputtered with 0.5 nm of Co and 15 nm of Al_2O_3. During VAMWNTs growth,

Table 4.1: CVD conditions for synthesis of VASWNTs and VAMWNTs.

	VASWNTs	VAMWNTs
Catalysts	Co / Mo	Co / Al_2O_3
Pressure (kPa)	1.3	3.3
Flow Rate of EtOH (sccm)	450	50
Temperature (°C)	800	850
Synthesis Time (min)	10	20

Table 4.2: Specification of synthesized single- and multi-walled CNT forests.

	VASWNTs	VAMWNTs
Diameter of CNTs (nm)	~1	3 – 10
Number of Walls	1	1 – 5
Thickness of Forest (μm)	15 – 25	40 – 300

at 800 °C, ethanol was flowed at a rate of 50 sccm for 15 min. The length of grown VAMWNTs ranges from 40 to 300 μm. Table 4.2 shows the specification of each synthesized SWNT and MWNT forests such as diameter, number of walls, and thickness of forest.

4.1.2 Characterization of CNTs by Scanning Electron Microscopy (SEM), Raman Spectroscopy, and Transmission Electron Microscopy (TEM)

Since the orientation of CNTs is important to determine their physical properties, there have been developed various techniques in nanoscale to obtain information. Scanning

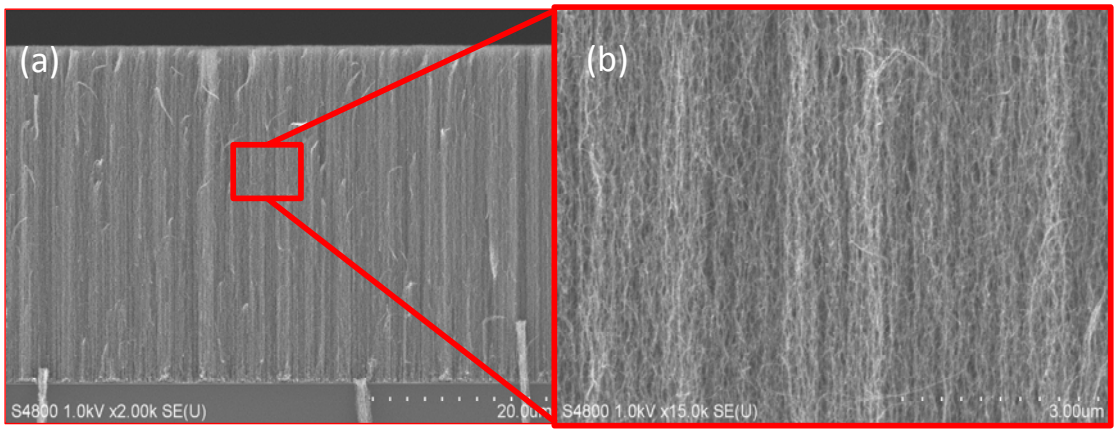

Figure 4.1.5: (a) Cross-section SEM image of a VASWNT forest, and (b) enlarged image.

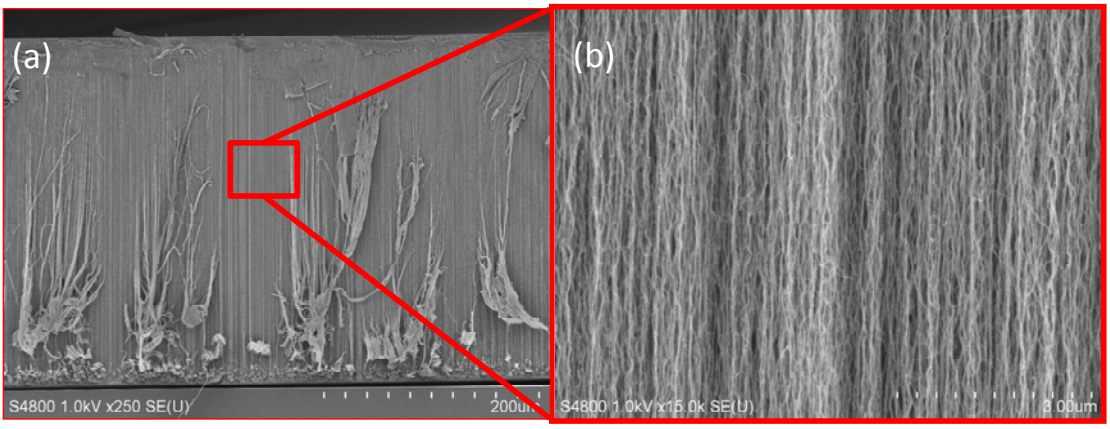

Figure 4.1.6: (a) Cross-section image of a VAMWNT forest and (b) enlarged image.

electron microscopy (SEM) is one of the most common methods for characterization of CNT samples, which produce the image of solid surface around 10 nm, structural information, and spatial distribution. Most of electron energy irradiated on a sample from electron beam is lost as a thermal energy. Some of them are either taken to excite atoms composing the sample or scattered from the sample.

Secondary electrons generated near ~10 nm of surface of the sample are mainly used in SEM. Using secondary electrons restrains damage on the sample of which generation efficiency is high despite of low accelerating voltage and low illumination current. The deep focus also enables to observe three-dimensional structure. Only secondary electrons generated on or inside the sample enter into vacuum, and then they are collected by the detectors generating an electric field. Contrast of the SEM image, regarded as the generated amount of secondary electrons, is determined by an angle of incident electron, a shape roughness of surface, and atoms of structure. The amounts of generated secondary electrons simply increase with an increase of acceleration voltage. However, the increase have the penetration depth of incident electron more deep, which

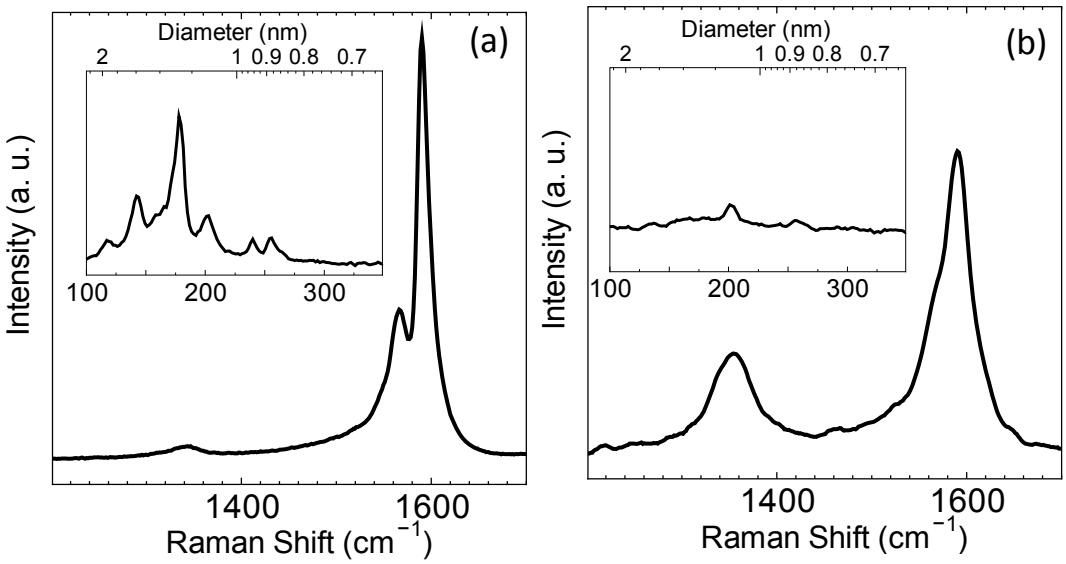

Figure 4.1.7: Resonance Raman spectra of (a) SWNTs and (b) MWNTs synthesized from ACCVD. The D-band and G-band peaks are shown. Both insets shows radial breathing mode (RBM), which each tendency differs from the number of walls.

leads either to decrease the amount of generated secondary electrons on the surface, or to have maximized value resulting in critical damage into the sample. Using SEM enables to observe three-dimensional structure because it detects electrons scattered on the surface of the sample. In addition, it directly observes the sample without any treatment, and keeps the shape of as-synthesized state.

Figure 4.1.5(a) shows the SEM image of cross-section of 25 μm-long SWNT forest vertically aligned on Si substrate. The information such as the distance between SWNTs, or their waviness of bundling SWNTs can be obtained and confirmed with the enlarged image (see Fig. 4.1.5(b)). Figure 4.1.6(a) and (b) shows the cross-sectional and enlarged image of vertically aligned MWNT forest with the length of about 300 μm, respectively. MWNT forest is more uniformly grown than SWNT forest.

Raman spectroscopy as a fast and nondestructive method is one of the most powerful tools to characterize the structure of CNTs. Raman spectroscopy gives the information such as diameter, the wall-number of CNTs, and even the existence of amorphous carbons. There are four distinctive characteristics of CNTs obtained from Raman spectrum.

First, radial breathing mode (RBM) is shown in CNTs at low frequency ranging from 100-400 cm^{-1}, which corresponds to coherent atomic vibration of carbon atoms in radial direction. RBM band is used to distinguish SWNTs that vibrates perpendicular to lattice plane and opposite to G-band mode [101]. On the other hand, the frequency of RBM depends on the diameter of an SWNT, which described as below [102],

$$\omega_{RBM} = \frac{217.8}{d} + 15.7 \tag{4.1}$$

where ω and d are corresponding to frequency of RBM and the diameter of an SWNT, respectively. D-band, a strong peak shown between 1250 and 1350 cm^{-1}, results from a disordered symmetric hexagonal graphene arrangement, which is found in all types of nanotubes as well as other types of graphitic materials. It also arises from amorphous carbon non-contributing to compose carbon nanotubes. Only with the intensity of D-band, therefore, it is difficult to determine the disorderness of carbon nanotubes.

A strong peak which occurs at 1582 cm^{-1} in graphite is termed the G-band. The structure of SWNT differs the axial and transverse in-plane vibrational modes from that of graphite, hence the tangential G-band mode of nanotubes appears multiple peaks between 1550 and 1600 cm^{-1}. The G-band is split into two-peaks due to energy difference: G^+ and G^- bands with separation of 20 cm^{-1}, where the frequency of G^+ is

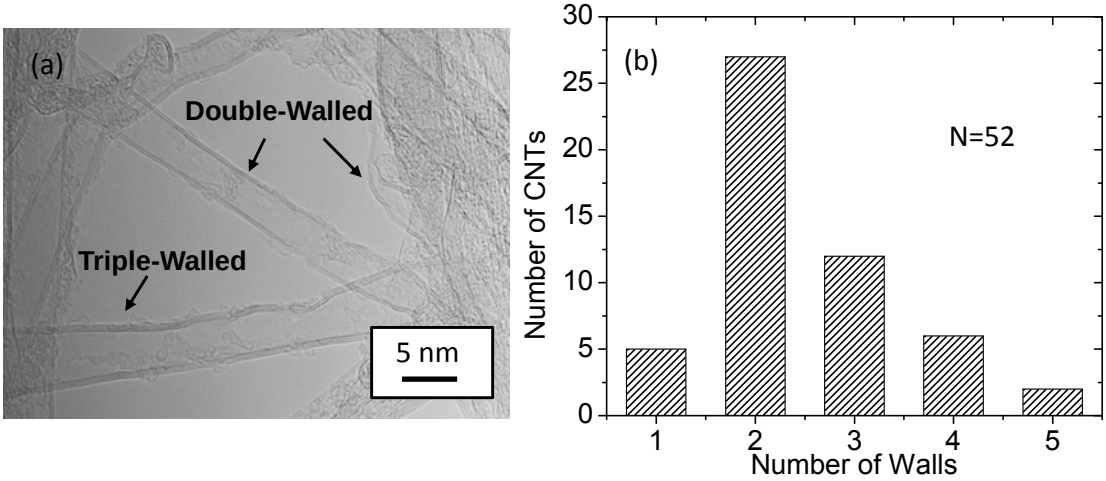

Figure 4.1.8: (a) TEM image of MWNTs. (b) Wall-number distribution of CNTs demonstrates that the VAMWNTs consist mostly of double-/triple walled CNTs.

has higher energy at higher position than G^-. In addition, the shape of G^- band can be used to determine if a nanotube is semiconducting or metallic. On the other hand, the relative intensity of D-band/G-band ratio is occasionally used to qualify the purity of carbon nanotubes. Figure 4.1.7 shows Raman spectra for (a) SWNTs with clear RBM and low ratio of D-band/G-band representing the quality, and for (b) MWNT with ambiguous RBM and relatively high ratio of D-band/G-band.

Transmission electron microscopy (TEM) produce images using more intensified electronic beam. For observation of CNTs in atomic scale, it is the most powerful imaging tool. The study of CNTs by TEM provides much information such as wall-number, diameter, and defects in the structure of CNTs. This work investigated wall-distribution of CNTs using TEM (JEM-2000EX, JEOL Ltd, 120 kV acceleration voltage).

Figure 4.1.8(a) shows TEM images of CNTs with the diameter of 5 nm. From the TEM examination, they mostly consist of double-/triple- walled CNTs with their diameter ranging from 5 to 10 nm, hence this thesis named them 'VAMWNT' for simplicity in this study although they include a few SWNTs.

4.2 *Side-Intrusion* Method for Fabrication of PDMS Composite with Reduced-Size CNT Forest

As ideal fillers in polymer nanocomposite, aligned carbon nanotube (CNTs) with extraordinary physical properties have been promising materials for various potential application [38], such as reinforced mechanical property of polymer nanocomposites with aligned CNTs tailored for advanced surface materials of an aircraft [57], and high intrinsic thermal conductivity of CNTs [90], potentially leads the polymer nanocomposite to the solution for thermal management of micro-/nano-sized electronic devices [103]. Several fabrication methods have been suggested to have thin nanocomposite containing well-aligned and dispersed CNTs such as fitting frames to vertically-aligned (VA) CNTs [51], or polishing the over-layer of polymer on the composite after the fabrication [57] to have the CNTs dominate the physical property of the nanocomposites.

The orientation of CNTs in polymer have a critical effect on the enhancement of their mechanical [51], thermal [23], and electrical [104] properties, to be specific, since the axial physical properties of CNTs are more excellent than the transversal or random direction, vertical alignment of CNTs in polymer matrix has more enhanced them than random orientation. Thus, it is necessary to find and decide a suitable way to disperse or align CNTs in polymers for the fabrication of nanocomposites in order to utilize full anisotropic properties of CNTs.

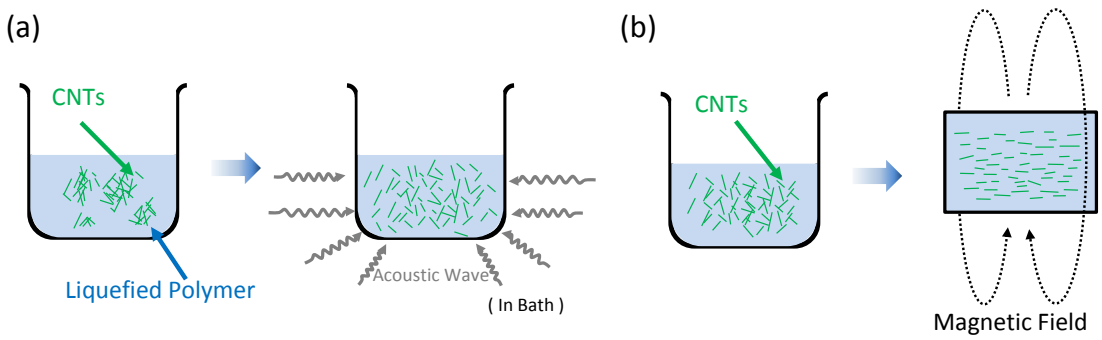

Figure 4.2.1: (a) Sonication for dispersion of CNTs [26,27]. Reproduced with permission. Copyright 2009, John Wiley and Sons. Copyright 2008, Elsevier. (b) Magnetic field to align CNTs dispersed in solution [28]. Reproduced with permission. Copyright 2002, John Wiley and Sons.

For the dispersion of CNTs in polymer matrix, using sonication [26,27]is one of the widely accepted ways (see Fig. 4.2.1(a)), however, which requires CNTs to be relatively small quantities. With a high volume fraction of aligned CNTs homogeneously dispersed in polymers [75], only using the sonication limits to have the nanocomposite with desired morphology resulting from the relation between the high concentration and bundle configuration of CNTs [105], which potentially takes nanocomposites away from the desired physical properties.

Kimura *et al* [28] employed strong magnetic field to align CNTs dispersed in solution to take advantages of exceptional anisotropic physical properties (see Fig. 4.2.1(b)), but available for low amount of CNTs. Wardle *et al*, utilized capillary-induced wetting of epoxy into interstitial VACNTs, which relieved the confined length of CNT forests up to hundreds of μm or mm [75] instead of the concept of dispersing CNTs into polymer matrix to fabricate nanocomposites. This method can make the nanocomposite contain well-dispersed, highly-aligned, and high volume fraction of CNT forests. It seems the

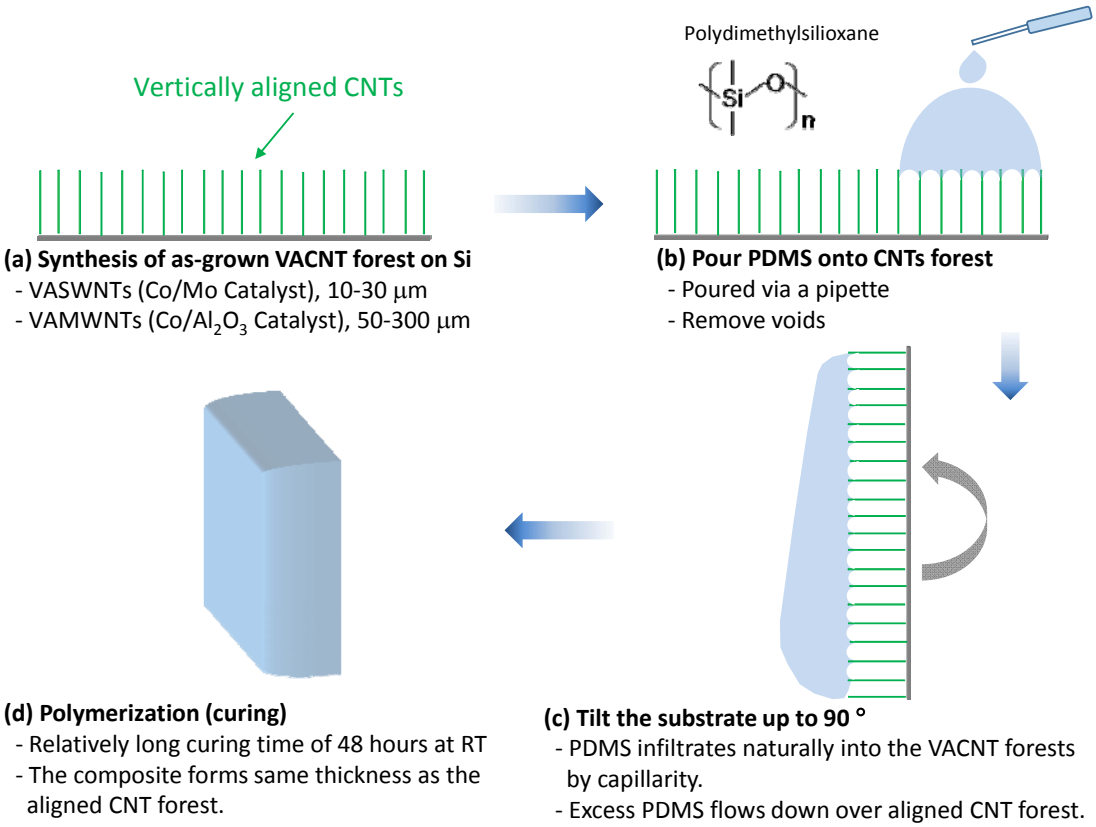

Figure 4.2.2: Schematic illustration for the fabrication process of PDMS composites containing vertically aligned CNT forest by the side-intrusion method.

best way, however, certain treatments is still required to prevent ununiformity of CNTs in polymer nanocomposites such as polishing [57] or using the frame for polymer pouring [52] for the thickness reduction of CNT forests less than hundreds μm. Moreover, even with using such treatments it is impracticable to have CNTs dispersed and distributed without morphological destruction

In this study, a facile method proposed, called *side-intrusion method*, is proposed to fabricate uniformly well-infiltrated PDMS nanocomposites into vertically aligned single- and multi-walled carbon nanotube (SWNT and MWNT) films with the thickness ranging from 15 to 300 μm without additional treatment process. Figure 4.2.2 shows the

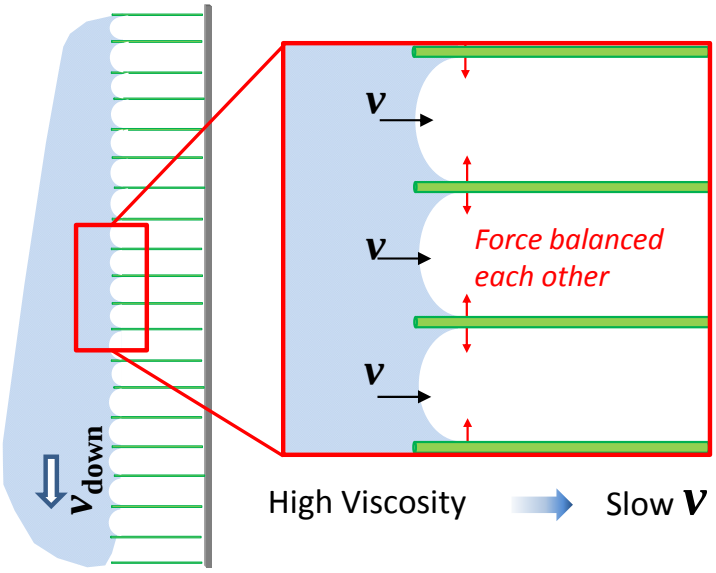

Figure 4.2.3: Possible mechanism for each part of PDMS infiltration into CNTs. Due to high viscosity of PDMS, capillary flow of PDMS occurs together at the same time with balanced force acting on each nanotube leading to no structural collapse.

fabrication process of VACNT-PDMS nanocomposites using the side-intrusion method. Liquefied PDMS after curing agent added into the base matrix of PDMS is poured to an as-grown VACNT forest on a Si substrate via a pipette, however it hardly infiltrates into the VACNT forest due to high viscosity which lead to slow down the speed of the infiltration (see Fig. 4.2.3). The excess PDMS remained on the top of the CNT forest is removed by tilting the substrate by 90 ° from the horizontal. Once complete PDMS coverage of the VACNT forests is achieved, which is cured in vacuum at room temperature for 48 hours, to allow the complete polymerization of the PDMS. The condition chosen in this study with relatively long curing time of 48 hours gives enough time for the excess PDMS placed over the aligned CNT forest to flow down and to form same thickness as the aligned CNT forest. Although the fabrication process is clearly shown, it is necessary to understand the mechanism for the side-intrusion method with physical approach.

The Washburn's equation, known as *Lucas-Washburn equation*, describes the capillary flow rate of fluid in a bundle of parallel cylindrical tubes [106]. Applying Poiseuille's law for fluid motion in a circular tube with a fully wettable capillary, the equation can be dscribed as below,

$$l = \sqrt{\frac{r\gamma\cos\theta}{2\eta}t} \tag{4.2}$$

where l and t are penetration distance and time for a liquid of dynamic viscosity, respectively. r, γ, θ, and η are corresponding to radius of cylinder, surface tension, contact angle of the liquid on the capillary, respectively. The capillary flow rate of fluid, dl/dt is

$$\frac{dl}{dt} = v = \frac{1}{2}\left(\frac{r\gamma\cos\theta}{2\eta}\right)^{\frac{1}{2}} t^{\frac{1}{2}} \tag{4.3}$$

The flow rate of PDMS can be estimated with the Eq. (4.3). r, γ, and η of PDMS are 26 nm in six-bundling state [77], 0.0251 N/m [55], 5 N·s/m^2 [107], respectively. On the

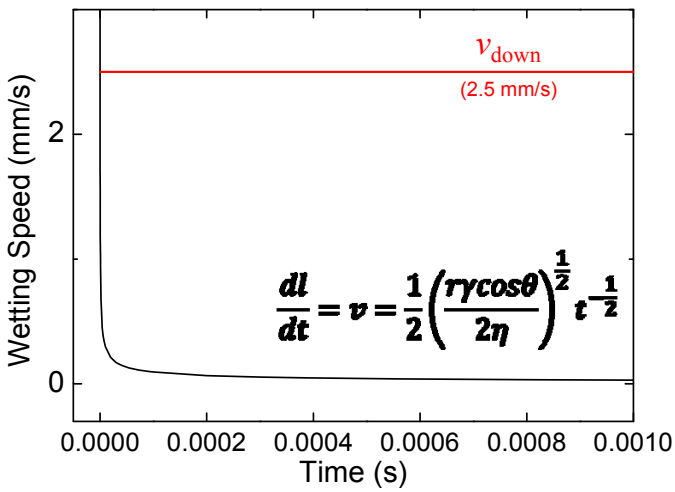

Figure 4.2.4: The speed of capillary flow into CNT forest and flow down during side-intrusion method.

other hand, the flowing down speed of liquefied PDMS was about 2.5 mm/s, roughly measured during the fabrication process by side-intrusion method. Figure 4.2.4 shows the comparison that the speed of PDMS flowing down was much faster than that of the capillary flow due to high viscosity of PDMS, which means that capillary flow occurs together at the same time with balanced force acting on each nanotube leading to no structural collapse. Viscosity of ethanol is 0.001 $N \cdot s/m^2$ [108], which the infiltration into VACNTs happened very fast leading to zipping CNTs each other due to unbalanced force acting on each vertically aligned CNT.

In addition, wettability of liquid is also one of the main factors having an effect on the structural preservation of VASWNTs. Contact angle of PDMS is close to 0 ° [109] which enabled the wetting on nanotubes well. In general, contact angle of liquid or polymer matrix on CNTs is an indicator to represent whether it wets or not. However, since contact angle can be dependent on the several conditions such as the type and quality of CNTs, this study employed the term of wettability on CNTs instead of contact angle to understand the mechanism for the fabrication of polymer composite containing CNTs.

The speed of capillary flow and wettability are the factors which directly determine on the structural preservation of CNTs during incorporation process in fabrication of composite. On the other hand, shrinkage of polymer also determines the structural preservation of CNTs, meaning volumetric change during polymerization or drying. PDMS shrinks less than 1% during the polymerization transition [110], the orientation of CNTs can be preserved during the fabrication process for PDMS composite. Since

polyvinyl alcohol (PVA) has high viscosity close to PDMS, the composite can be fabricated with the preserved orientation of CNTs if incorporated with hydrophilic CNTs. However, dry volume of PVA is compressed to less than one tenth of its wet volume [111], hence PVA composite hardly avoid the structural change of CNTs. Considering above main factors in the fabrication of polymer composite with aligned CNTs, enables to control the structure of the composite for specific purpose such as well-distributed and -aligned, but highly zipped CNTs in composite.

Fabricated PDMS composites with reduced-size CNT forests using by side-intrusion method in this study are characterized the infiltration of the polymer, the preservation of CNT orientation, and the uniformity of the nanocomposite, by using Raman scattering spectroscopy, polarized Raman spectroscopy, and cross-sectional SEM, respectively.

4.3 Characterization of the Composite by SEM and Raman Spectroscopy

4.3.1 Raman spectra and Cross-Sectional SEM Images of Before and After the Fabrication

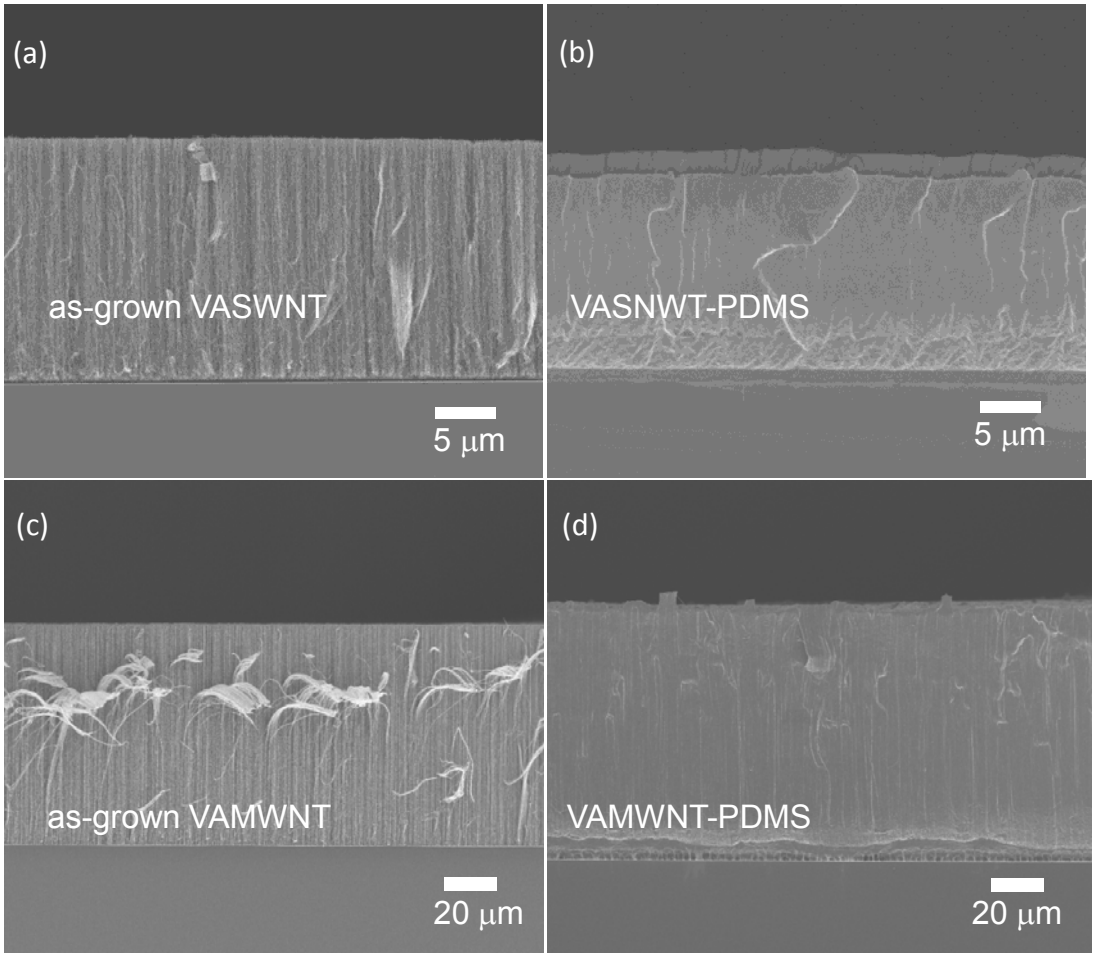

Figure 4.3.1: (a) Cross-sectional SEM images of 20-22 μm-long as-grown VASWNT forest and (b) PDMS nanocomposite with the forest fabricated by the side-intrusion method. This shows the thickness of nanocomposite is same as the as-grown VASWNT forest without over-layer PDMS. (c) Those of 90-95 μm-long as-grown VAMWNT forest, and PDMS nanocomposite with it, (d) PDMS nanocomposite with the VAMWNT forest. By comparing to each other, the nanocomposite has the same thickness as VAMWNT.

Figure 4.3.1(a) and (b) shows cross-sectional SEM images of as-grown VASWNTs and the nanocomposite on substrates, respectively. The comparison reveals that the PDMS completely infiltrated into the VASWNT forest, and with height of 20 to 22 μm, the nanocomposites have the same thickness as the as-grown VASWNTs. PDMS was optimally blended with the same thickness as the VASWNT forest without any treatment after the fabrication despite of the relatively shorter length of VASWNT forests.

On the other hand, the thickness of as-grown VAMWNT forests was observed to range from 90 to 95 μm (see Fig. 4.3.1(c)). Figure 4.3.1(d) shows the cross-sectional image of the nanocomposite that was also fabricated with the same thickness as the relatively longer VAMWNT forest. This work have performed the fabrication of nanocomposites

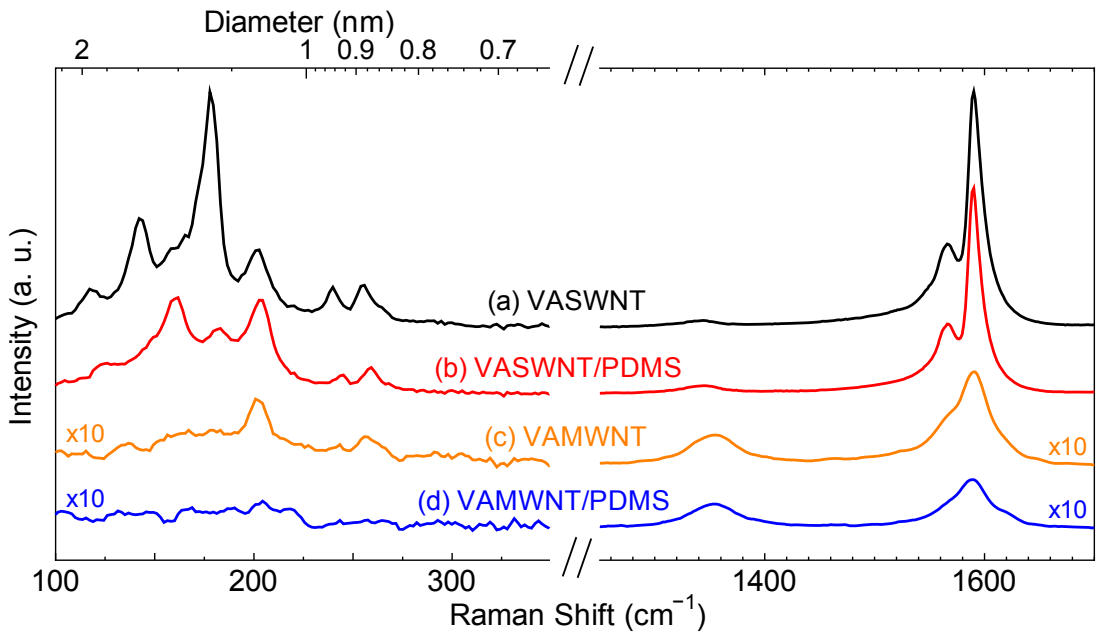

Figure 4.3.2: Raman scattering spectra of RBM and D-band/G-band for (a) as-grown VASWNTs, (b) VASWNTs in PDMS composite, (c) as-grown VAMWNTs, and (d) VAMWNTs in PDMS composite.

with VACNT forests ranging from 15 to 300 μm and potentially conclude that the side-intrusion method is useful for shorter VACNT forests than about 100 μm.

Figure 4.3.2 shows the Raman scattering spectra with RBM band, D-band, and G-band of both as-grown VASWNT and VAMWNT, and each of them in PDMS nanocomposite. As-grown VASWNTs are characterized RBM and G^- and G^+ peaks (see spectrum (a) in Fig. 4.3.2). Since surrounding PDMS have an effect on the radial vibration mode of CNTs, there is a little change in the shape of RBM band (see spectrum (b) in Fig. 4.3.2). In addition, by the comparison of the ratio of D-band and G-band, the VASWNTs have no damage during the fabrication. Spectrum (c) in Fig. 4.3.2 shows the Raman spectra of VAMWNT with RBM, D-/G-peak ratio, and G^-/G^+, and spectrum (d) of the PDMS nanocomposite containing VAMWNTs present almost no difference from as-grown VAMWNT, which intends no damage during the fabrication.

4.3.2 Infiltration of PDMS into CNT Forest

The infiltration of PDMS into the VASWNT forest was investigated by scanning the cross-section of the nanocomposite using Raman spectroscopy, and quantitative thickness characterization of the nanocomposite as well. The nanocomposite was scanned along the axial direction of VASWNTs from below the interface to the Si substrate. Typical Raman peaks of Si, G-band of SWNT, and PDMS peak characterized the infiltration of PDMS into the VASWNT forest, which are visible at 520, 1593, and 2096 cm^{-1}, respectively (see Fig. 4.3.3(a)).

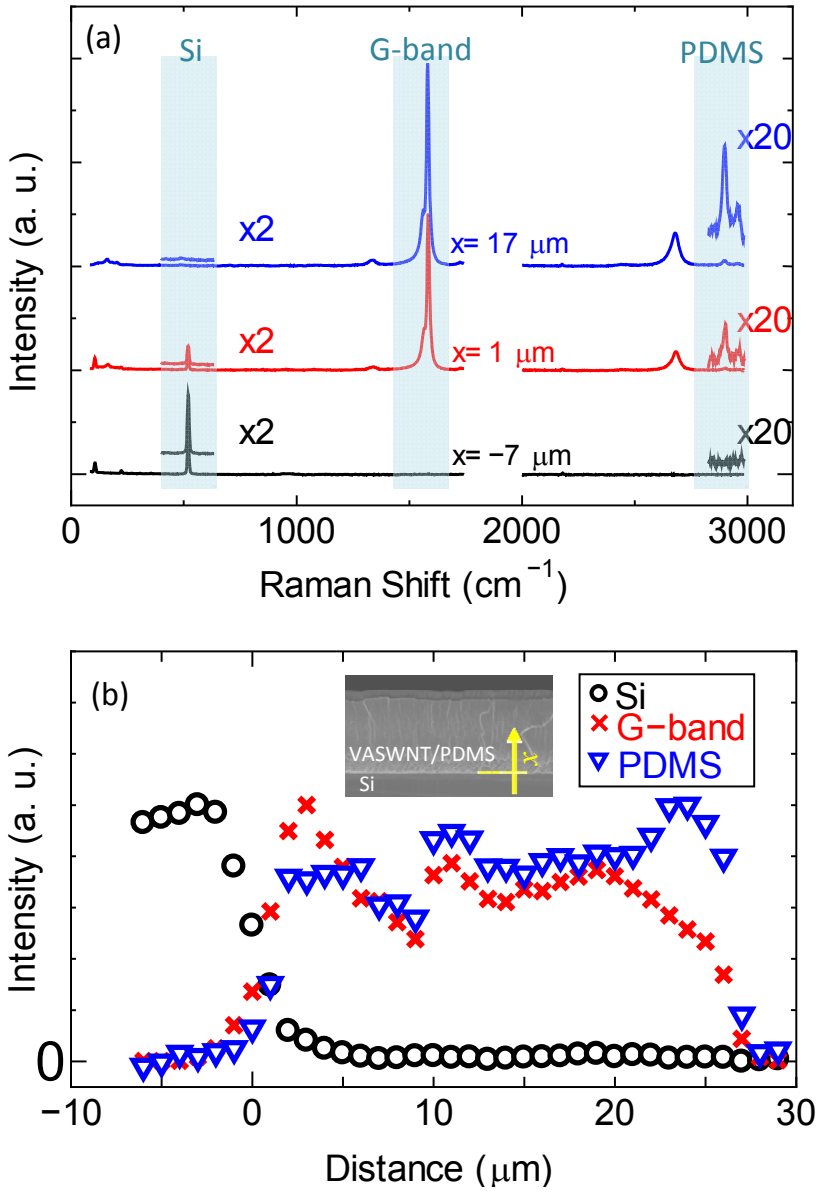

Figure 4.3.3: (a) Raman scattering spectra of Si, G-band of SWNTs and PDMS, and (b) spatial intensity distribution of Raman scatterings along the vertical direction of nanocomposite. The presence at same point of both G-band of SWNTs and PDMS peaks indicates the complete infiltration of PDMS along the full thickness of the film. SEM image (inset) demonstrates the origin and direction for scan.

Figure 4.3.3(b) reveals that the Si peak disappears at the origin, where both G-peak by VASWNTs and PDMS peaks appear. The appearance of G-band and PDMS peak and disappearance of Si occurs at the same point, which indicates that the PDMS reached the SWNT-Si interface and no over-layer of PDMS, respectively. For the appearance of PDMS peaks at the same point with VASWNT peaks, if the polymer does not well-infiltrated uniformly into the VACNT forest, the composite possesses over- or underestimated physical properties than the fully well-infiltrated composite [22].

On the other hand, the disappearance of G-band and PDMS at the same point demonstrates that is a key evidence to determine if the nanocomposite with or without over-layer. In particular, it becomes more important for the length reduction of VACNTs. Even though it can be regarded as the matter of controlling amount to pour polymer, however, it is practically difficult to adjust the exact amount of the polymer on tens-of-μm VACNT forests. In addition, polishing is a widely used method to remove the over-layered polymers, but it cannot be applied for soft polymer such as PDMS.

4.3.3 The Orientation of SWNTs in PDMS Matrix

The orientation of CNTs in the PDMS matrix plays an important role, which can bring more enhanced physical properties of the nanocomposite arising from the anisotropic structure CNTs [23,27,51]. Thus, vertical alignment of the CNT forest with preserved as grown morphology in PDMS matrix can achieve maximized performance as a nanocomposite. The intensity of G-band in SWNTs depends on the polarization of incident light in Raman spectroscopy, which is found to be the strongest when the

polarized incident light corresponds to the axial direction of SWNTs in contrast to be minimized when perpendicular to transversal direction [112].

Using the polarization dependence of Raman scattering spectroscopy characterized the orientation investigation of VASWNTs in PDMS nanocomposite fabricated by the side-intrusion method. To the given polarized incident laser, the G-band of SWNTs was measured with varied angle at 0°, 30°, 60°, and 90° by rotating the continuous ration stage. Figure 4.3.4(a) shows the intensity dependence of the G-band on the polarization of the Raman laser with the angle θ. The intensity of the G-band gradually decreases with the increase of the angle, maximized at 0 ° and minimized at 90 °as shown in the inset of Fig. 4.3.4(a). On the other hand, Figure 4.3.4(b) shows the intensities of the

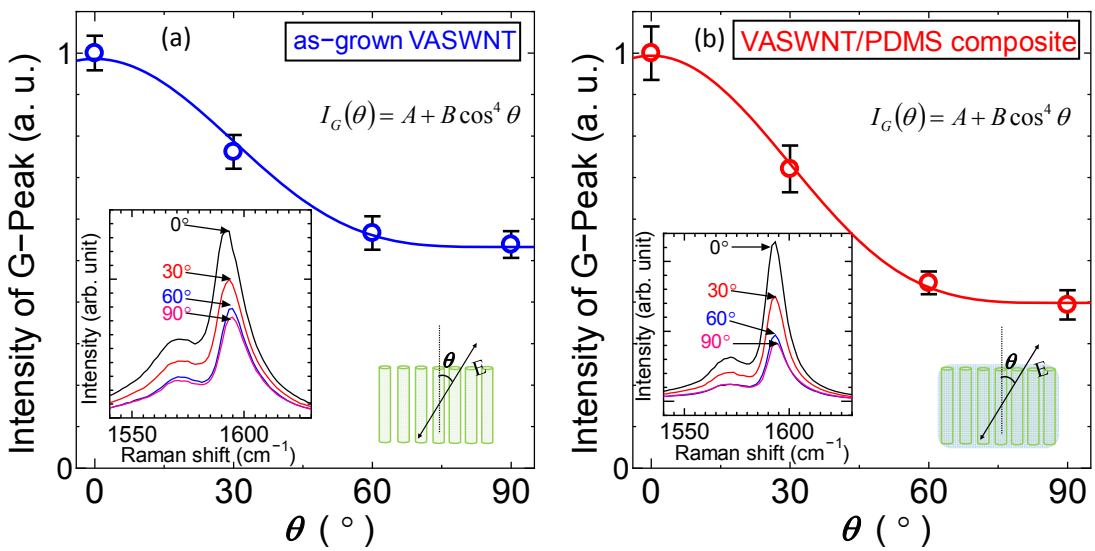

Figure 4.3.4: Raman spectra of (a) as-grown VASWNTs and (b) VASWNTs in PDMS matrix by polarized Raman spectroscopy. The original vertical alignment of as-grown CNTs was preserved in the PDMS matrix, as illustrated by comparing the G-band intensities of VASWNTs. Both insets shows Raman scattering spectra as a function of polarization angle (θ) of the excitation laser.

G-peaks of the VASWNTs that are embedded in the nanocomposite. Similar intensity variation as a function of θ for both cases demonstrates that the original vertical alignment of the as-grown CNTs was preserved in the PDMS matrix. Each inset in Fig. 4.3.4(a) and (b) shows Raman scattering spectra as a function of the polarization angle of the excitation laser.

4.4 Summary

For the effective use of polymer composites containing CNTs for thermal applications, the quality of CNTs is better to be highly pure with less impurities, and to be ranged up to tens of μm long which is practical size and in thermal interface materials for such integrated chips. There have been reported several fabrication methods for composites, however they have limits to apply for nanocomposite with reduced-size CNT forest. In this chapter, a facile method was proposed, so-called *side-intrusion method*, to fabricate uniformly well-infiltrated polymer composites containing VACNTs synthesized through ACCVD with the thickness ranging from 15 to 300 μm, and requires no additional treatment process.

The composites fabricated from the side-intrusion method were characterized the degree of PDMS infiltration into CNT forest, and vertical alignment of CNTs in PDMS composite by Raman spectroscopy. As a result, PDMS fully infiltrated along vertically aligned CNT forest by capillary motion, which was characterized by scanning the cross-section of the nanocomposite using Raman spectroscopy. In addition, using polarized Raman spectroscopy characterized the orientation of vertically aligned CNTs that was preserved during fabrication process by side-intrusion method.

Chapter 5:

Conclusions

The generation of micro/nanotechnology has required "*cooling*" as one of the major challenges. In the field of micro and nano electronics, those devices undoubtedly produce heat, which need to be minimized with efficient cooling to prevent the failure of performance. For decade, electronic devices such as integrated chips tend to reduce size and increase the speed and performance, which drive the thermal management more important due to the necessity for the sufficient cooling system. Thermal interface materials (TIMs) are one of the main bottlenecks for efficient heat transfer from integrated chips to heat sinks and ambient environment by filling micro-gap-interface between two contacting materials to improve thermal conduction instead of air gap.

Carbon nanotubes (CNTs) with high thermal conductivity and high aspect ratio is one of the most expected candidates among carbon allotropes-based TIMs, acting as fillers since they enables to extend the study down to a further smaller scale than before. However, thermal properties of CNTs have been investigated by theoretical simulation and calculation since it is difficult to measure directly thermal properties of an individual CNT due to the technical difficulties in nanoscale. Thermal conductivity of CNTs has been measured up to ~ 6000 W/mK surpassing that of diamond, even though the results of measured thermal conductivities are largely scattered.

First, thermal behavior of CNT forest without polymer were investigated with several potential factors such as volume fraction, types of CNTs, and temperature prior to study for the thermal performance of the composite. The effect of volume fraction of CNT forest on thermal properties was investigated with single- and multi-walled carbon nanotubes synthesized from CVD method with different size of Fe catalyst. Volume

fraction was varied by the mechanical densification, introduced by Wardle *et al* that squeezes interstitial spaces between vertically aligned CNTs without any destruction. Thermal diffusivity of the CNT forests along axial direction were measured by laser flash analysis technique, and then thermal conductivity were derived with additional information such as specific heat and density, which potentially estimates the role of suspending CNTs in CNT forest for thermal transfer.

As a result, thermal diffusivity of SWNT forests tends to increase around 15 % of volume fraction. Since thermal diffusivity is intrinsic thermal property of a material, SWNTs should have had same thermal diffusivity even though they are in different volume fraction. Hence, the result is unnatural that the increase of volume fraction resulted in high thermal diffusivity of SWNT forests. This is potentially because the suspending SWNTs in the forest, not directly involved in the thermal propagation from front to rear surfaces during the measurement of LFA, become to contribute for thermal transfer rather than to disturb, which causes to have higher thermal diffusivity. In addition, the structural changes during the process of densification of CNT forests such as the interstitial distance and overlap area of CNTs diminished the TBR, and this can also be one of the reasons that the thermal conductivity of a single CNT was dependent on the volume fraction of the CNT forest.

Second, thermal properties of polymer composite containing CNT forest was evaluated to be used for potential thermal applications. PDMS composite with VACNT forest were fabricated that the phenomenon of PDMS wetting CNTs is apparently close to the in-situ polymerization except the functionalized surface that CNTs are incorporated into

liquefied polymer matrix in which cross-linking agent was added, resulting from capillary motion. The slow infusion of PDMS from the side direction potentially leads to prevent the composites from void-trap. Since the thickness of the CNT forests are relatively long up to about 1 mm, it is possible to fully wet the CNT forests, up to the tip, by controlling quantities of PDMS. Remained voids trapped in the composites are removed by giving enough time to polymerize in a vacuum desiccator. Since the infiltration of polymer matrix into CNT forest is one of the main factors to determine the quality of the composite when using the technique to pour polymer on to CNT forest, scanning electron microscopy characterized the degree of PDMS infiltration in CNT forest.

Thermal diffusivity of the composites was enhanced by the various volume fractions of VACNT forests up to 7.86 mm^2/s with 20.3 % of SWNTs, and 6.65 mm^2/s with 12.2 % for MWNTs. Derived thermal conductivity of each SWNT and MWNT forest was discussed by comparing to the theoretical prediction model of the composite for aligned continuous CNTs proposed by Nan *et al* [82].

At last, this thesis work also focused on the development for the fabrication method of polymer composite with CNT forests in relatively smaller size up to tens of μm to enhance thermal transfer, which is expected to be practical size-scale in thermal interface materials for such integrated chips, called *side-intrusion* method. The method enabled to make the polymer composite uniform and well-aligned, but requires no treatment. The composites fabricated from the side-intrusion method were characterized the degree of PDMS infiltration into CNT forest, and vertical alignment of CNTs in

PDMS composite by Raman spectroscopy. As a result, it was confirmed that PDMS uniformly infiltrated into the VACNT forest by capillarity even without deteriorating the aligned morphology.

The obtained result in this thesis work can potentially provide engineering knowledge to understand thermal behavior of aligned CNT forests, and polymer composite containing VACNT forests, which possibly help to imagine various applications with improved thermal property by using the composites in the field of micro and nanotechnology.

Bibliography

[1] P.-C. Ma, N. A. Siddiqui, G. Marom, J.-K. Kim, Dispersion and functionalization of carbon nanotubes for polymer-based nanocomposites: A review, *Compos. Part A Appl. Sci. Manuf.* **41** (2010) 1345–1367.

[2] E.J. Garcia, B.L. Wardle, A. John Hart, Joining prepreg composite interfaces with aligned carbon nanotubes, *Compos. Part A Appl. Sci. Manuf.* **39** (2008) 1065–1070.

[3] S. Berber, Y. Kwon, D. Tomanek, Unusually high thermal conductivity of carbon nanotubes, *Phys. Rev. Lett.* **84** (2000) 4613–6.

[4] M. Osman, D. Srivastava, Temperature dependence of the thermal conductivity of single-wall carbon nanotubes, *Nanotechnology* **12** (2001) 21–24.

[5] C.W. Padgett, D.W. Brenner, Influence of Chemisorption on the Thermal Conductivity of Single-Wall Carbon Nanotubes, *Nano Lett.* **4** (2004) 1051–1053.

[6] J. F. Moreland, the Disparate Thermal Conductivity of Carbon Nanotubes and Diamond Nanowires Studied By Atomistic Simulation, *Microscale Thermophys. Eng.* **8** (2004) 61–69.

[7] S. Maruyama, A Molecular Dynamics Simulation of Heat Conduction of a Finite Length Single-Walled Carbon Nanotube, *Microscale Thermophys. Eng.* **7** (2003) 41–50.

[8] J. Che, T. Cagin, W. A. Goddard III, Thermal conductivity of carbon nanotubes, *Nanotechnology* **11** (2000) 65–69.

[9] H. Zhong, J. Lukes, Interfacial thermal resistance between carbon nanotubes: Molecular dynamics simulations and analytical thermal modeling, *Phys. Rev. B.* **74** (2006) 125403.

[10] J. Hone, M. C. Llaguno, N. M. Nemes, A. T. Johnson, J. E. Fischer, D. A. Walters, M. J. Casavant, J. Schmidt, R. E. Smalley, Electrical and thermal

transport properties of magnetically aligned single wall carbon nanotube films, *Appl. Phys. Lett.* **77** (2000) 666.

[11] C. Yu, L. Shi, Z. Yao, D. Li, A. Majumdar, Thermal conductance and thermopower of an individual single-wall carbon nanotube., *Nano Lett.* **5** (2005) 1842–6.

[12] E. Pop, D. Mann, Q. Wang, K. Goodson, H. Dai, Thermal conductance of an individual single-wall carbon nanotube above room temperature., *Nano Lett.* **6** (2006) 96–100.

[13] Z. L. Wang, D. W. Tang, X. B. Li, X. H. Zheng, W. G. Zhang, L. X. Zheng, Y. T. Zhu, A. Z. Jin, H. F. Yang, C. Z. Gu, Length-dependent thermal conductivity of an individual single-wall carbon nanotube, *Appl. Phys. Lett.* **91** (2007) 123119.

[14] Z. Wang, D. Tang, X. Zheng, W. Zhang, Y. Zhu, Length-dependent thermal conductivity of single-wall carbon nanotubes: prediction and measurements, *Nanotechnology* **18** (2007) 475714.

[15] M. T. Pettes, L. Shi, Thermal and Structural Characterizations of Individual Single-, Double-, and Multi-Walled Carbon Nanotubes, *Adv. Funct. Mater.* **19** (2009) 3918–3925.

[16] M. Fujii, X. Zhang, H. Xie, H. Ago, K. Takahashi, T. Ikuta, H. Abe, T. Shimizu, Measuring the Thermal Conductivity of a Single Carbon Nanotube, *Phys. Rev. Lett.* **95** (2005) 065502.

[17] T.-Y. Choi, D. Poulikakos, J. Tharian, U. Sennhauser, Measurement of the thermal conductivity of individual carbon nanotubes by the four-point three-omega method, *Nano Lett.* **6** (2006) 1589–93.

[18] M. A. Panzer, G. Zhang, D. Mann, X. Hu, E. Pop, H. Dai, E. Goodson, Thermal Properties of Metal-Coated Vertically Aligned Single-Wall Nanotube Arrays, *J. Heat Transfer.* **130** (2008) 052401.

[19] D. Yang, Q. Zhang, G. Chen, S. Yoon, J. Ahn, S. Wang, Q. Zhou, Q. Wang, J. Q. Li, Thermal conductivity of multiwalled carbon nanotubes, *Phys. Rev. B.* **66** (2002) 165440.

[20] H. Sugime, S. Noda, S. Maruyama, Y. Yamaguchi, Multiple "optimum" conditions for Co–Mo catalyzed growth of vertically aligned single-walled carbon nanotube forests, *Carbon* **47** (2009) 234–241.

[21] C. H. Liu, H. Huang, Y. Wu, S. S. Fan, Thermal conductivity improvement of silicone elastomer with carbon nanotube loading, *Appl. Phys. Lett.* **84** (2004) 4248.

[22] T. Borca-Tasciuc, M. Mazumder, Anisotropic thermal diffusivity characterization of aligned carbon nanotube-polymer composites, *J. Nanosci. Nanotechnol.* **7** (2007) 1581–1588.

[23] H. Huang, C. H. Liu, Y. Wu, S. Fan, Aligned Carbon Nanotube Composite Films for Thermal Management, *Adv. Mater.* **17** (2005) 1652–1656.

[24] Y. Wu, C. H. Liu, H. Huang, S. S. Fan, Effects of surface metal layer on the thermal contact resistance of carbon nanotube arrays, *Appl. Phys. Lett.* **87** (2005) 213108.

[25] S. Maruyama, R. Kojima, Y. Miyauchi, Low-temperature synthesis of high-purity single-walled carbon nanotubes from alcohol, *Chem. Phys. Lett.* **360** (2002) 229–234.

[26] M. Bozlar, D. He, J. Bai, Y. Chalopin, N. Mingo, S. Volz, Carbon nanotube microarchitectures for enhanced thermal conduction at ultralow mass fraction in polymer composites., *Adv. Mater.* **22** (2010) 1654–8.

[27] A. Allaoui, S. Hoa, M. Pugh, The electronic transport properties and microstructure of carbon nanofiber/epoxy composites, *Compos. Sci. Technol.* **68** (2008) 410–416.

[28] T. Kimura, H. Ago, M. Tobita, S. Ohshima, M. Kyotani, M. Yumura, Polymer Composites of Carbon Nanotubes Aligned by a Magnetic Field, *Adv. Mater.* **14** (2002) 1380–1383.

[29] R. Prasher, Thermal Interface Materials: Historical Perspective, Status, and Future Directions, *Proc. IEEE.* **94** (2006) 1571–1586.

[30] E. Samson, S. Machiroutu, Interface Material Selection and a Thermal Management Technique in Second-Generation Platforms Built on Intel® Centrino™ Mobile Technology., *Intel Technol. J.* **9** (2005) 75–87.

[31] O.L. Blakslee, Elastic Constants of Compression-Annealed Pyrolytic Graphite, *J. Appl. Phys.* **41** (1970) 3373.

[32] P.-C. Ma, N. A. Siddiqui, G. Marom, J.-K. Kim, Dispersion and functionalization of carbon nanotubes for polymer-based nanocomposites: A review, *Compos. Part A Appl. Sci. Manuf.* **41** (2010) 1345–1367.

[33] I. Kang, Y. Y. Heung, J. H. Kim, J. W. Lee, R. Gollapudi, S. Subramaniam, S. Narasimhadevara, D. Hurd, G. R. Kirikera, V. Shanov, M. J. Schulz, D. Shi, J. Boerio, S. Mall, M. Ruggles-Wren, Introduction to carbon nanotube and nanofiber smart materials, *Compos. Part B Eng.* **37** (2006) 382–394.

[34] C. Lee, X. Wei, J. W. Kysar, J. Hone, Measurement of the elastic properties and intrinsic strength of monolayer graphene, *Science* **321** (2008) 385–8.

[35] Z.-S. Wu, W. Ren, L. Gao, J. Zhao, Z. Chen, B. Liu, D. Tang, B. Yu, C. Jiang, H.-M. Cheng, Synthesis of graphene sheets with high electrical conductivity and good thermal stability by hydrogen arc discharge exfoliation, *ACS Nano.* **3** (2009) 411–7.

[36] S. Iijima, Helical microtubules of graphitic carbon, *Nature* **354** (1991) 56–58.

[37] S. Iijima, T. Ichihashi, Single-shell carbon nanotubes of 1-nm diameter, *Nature* **363** (1993) 603–605.

[38] M. S. Dresselhaus, G. Dresselhaus, P. C. Eklund, Science of fullerenes and carbon nanotubes, Academic Press, New York (NY), San Diego (CA), 1996.

[39] P. G. Collins, P. Avouris, Nanotubes for electronics., *Sci. Am.* **283** (2000) 62–9.

[40] T. Guo, P. Nikolaev, A. Thess, Catalytic growth of single-walled manotubes by laser vaporization, *Chem. Phys. Lett.* **243** (1995) 49–54.

[41] D. Qian, G. J. Wagner, W. K. Liu, M.-F. Yu, R. S. Ruoff, Mechanics of carbon nanotubes, *Appl. Mech. Rev.* **55** (2002) 495.

[42] S. Hong, S. Myung, Nanotube electronics: a flexible approach to mobility, *Nat. Nanotechnol.* **2** (2007) 207–8.

[43] P. Kim, L. Shi, A. Majumdar, P. McEuen, Thermal Transport Measurements of Individual Multiwalled Nanotubes, *Phys. Rev. Lett.* **87** (2001) 19–22.

[44] S. Maruyama, A molecular dynamics simulation of heat conduction in finite length SWNTs, *Phys. B Condens. Matter.* **323** (2002) 193–195.

[45] M. A. Stroscio, M. Dutta, D. Kahn, K. W. Kim, Continuum model of optical phonons in a nanotube, *Superlattices Microstruct.* **29** (2001) 405–409.

[46] M. Grujicic, G. Cao, B. Gersten, Atomic-scale computations of the lattice contribution to thermal conductivity of single-walled carbon nanotubes, *Mater. Sci. Eng. B.* **107** (2004) 204–216.

[47] S. P. Hepplestone, A. M. Ciavarella, C. Janke, G. P. Srivastava, Size and temperature dependence of the specific heat capacity of carbon nanotubes, *Surf. Sci.* **600** (2006) 3633–3636.

[48] C. Nan, A simple model for thermal conductivity of carbon nanotube-based composites, *Chem. Phys. Lett.* **375** (2003) 666–669.

[49] G. M. Whitesides, The origins and the future of microfluidics, *Nature* **442** (2006) 368–73.

[50] F. Schneider, J. Draheim, R. Kamberger, U. Wallrabe, Process and material properties of polydimethylsiloxane (PDMS) for Optical MEMS, *Sensors Actuators A Phys.* **151** (2009) 95–99.

[51] A. T. Sepúlveda, R. Guzman de Villoria, J. C. Viana, A J. Pontes, B. L Wardle, L. A Rocha, Full elastic constitutive relation of non-isotropic aligned-CNT/PDMS flexible nanocomposites, *Nanoscale* **5** (2013) 4847–54.

[52] A. T. Sepúlveda, R. G. De Villoria, J. C. Viana, A. J. Pontes, B. L Wardle, L. A Rocha, Flexible Pressure Sensors: Modeling and Experimental Characterization, *Procedia Eng.* **47** (2012) 1177–1180.

[53] D. Kim, J. Han, H. Park, K. Yun, Simple and low-cost patterning of carbon nanotube on PDMS for flexible MEMS, *Solid-State Sensors*, *Actuators Microsystems Conf.* (2011) 2355–2358.

[54] L. Chen, C. Liu, K. Liu, C. Meng, C. Hu, J. Wang, High-Performance, Low-Voltage, and Easy-Operable Bending Actuator Based on Aligned Carbon Nanotube/Polymer Composites, *ACS Nano* **5**(3) (2011) 1588–1593.

[55] J. Mark, Polymer data handbook, Oxford University Press, 1999.

[56] A. M. Marconnet, N. Yamamoto, M. A Panzer, B. L Wardle, K. E. Goodson, Thermal conduction in aligned carbon nanotube-polymer nanocomposites with high packing density, *ACS Nano* **5** (2011) 4818–25.

[57] H. Cebeci, R. G. De Villoria, A. J. Hart, B. L Wardle, Multifunctional properties of high volume fraction aligned carbon nanotube polymer composites with controlled morphology, *Compos. Sci. Technol.* **69** (2009) 2649–2656.

[58] Q. Wang, J. Dai, W. Li, Z. Wei, J. Jiang, The effects of CNT alignment on electrical conductivity and mechanical properties of SWNT/epoxy nanocomposites, *Compos. Sci. Technol.* **68** (2008) 1644–1648.

[59] E. J. Garcia, B. L Wardle, A. John Hart, Joining prepreg composite interfaces with aligned carbon nanotubes, *Compos. Part A Appl. Sci. Manuf.* **39** (2008) 1065–1070.

[60] T. Souier, C. Maragliano, M. Stefancich, M. Chiesa, How to achieve high electrical conductivity in aligned carbon nanotube polymer composites, *Carbon* **64** (2013) 150–157.

[61] J. Hone, M. Whitney, C. Piskoti, A. Zettl, Thermal conductivity of single-walled carbon nanotubes, *Phys. Rev. B.* **59** (1999) R2514–R2516.

[62] H. Xie, A. Cai, X. Wang, Thermal diffusivity and conductivity of multiwalled carbon nanotube arrays, *Phys. Lett. A.* **369** (2007) 120–123.

[63] J. Hone, M. C. Llaguno, N. M. Nemes, A. T. Johnson, J. E. Fischer, D. A. Walters, M. J. Casavant, J. Schmidt, R. E. Smalley, Electrical and thermal

transport properties of magnetically aligned single wall carbon nanotube films, *Appl. Phys. Lett.* **77** (2000) 666.

[64] S. Shaikh, L. Li, K. Lafdi, J. Huie, Thermal conductivity of an aligned carbon nanotube array, *Carbon* **45** (2007) 2608–2613.

[65] X. J. Hu, A. A. Padilla, J. Xu, T.S. Fisher, K. E. Goodson, 3-Omega Measurements of Vertically Oriented Carbon Nanotubes on Silicon, *J. Heat Transfer.* **128** (2006) 1109.

[66] S. Noda, Y. Tsuji, Y. Murakami, S. Maruyama, Combinatorial method to prepare metal nanoparticles that catalyze the growth of single-walled carbon nanotubes, *Appl. Phys. Lett.* **86** (2005) 173106.

[67] S. Noda, H. Sugime, T. Osawa, Y. Tsuji, S. Chiashi, Y. Murakami, S. Maruyama, A simple combinatorial method to discover Co–Mo binary catalysts that grow vertically aligned single-walled carbon nanotubes, *Carbon* **44** (2006) 1414–1419.

[68] S. Noda, K. Hasegawa, H. Sugime, K. Kakehi, Z. Zhang, S. Maruyama, Y. Yamaguchi, Millimeter-Thick Single-Walled Carbon Nanotube Forests: Hidden Role of Catalyst Support, *Jpn. J. Appl. Phys.* **46** (2007) L399–L401.

[69] K. Hasegawa, S. Noda, H. Sugime, K. Kakehi, S. Maruyama, Y. Yamaguchi, Growth window and possible mechanism of millimeter-thick single-walled carbon nanotube forests., *J. Nanosci. Nanotechnol.* **8** (2008) 6123–8.

[70] K. Hasegawa, S. Noda, Millimeter-tall single-walled carbon nanotubes rapidly grown with and without water., ACS Nano. 5 (2011) 975–84. doi:10.1021/nn102380j.

[71] D. N. Futaba, K. Hata, T. Namai, T. Yamada, K. Mizuno, Y. Hayamizu, M. Yumura, S. Iijima, 84% Catalyst Activity of Water-Assisted Growth of Single Walled Carbon Nanotube Forest Characterization By a Statistical and Macroscopic Approach, *J. Phys. Chem. B.* **110** (2006) 8035–8.

[72] W. J. Parker, R. J. Jenkins, C. P. Butler, G. L. Abbott, Flash Method of Determining Thermal Diffusivity, Heat Capacity, and Thermal Conductivity, *J. Appl. Phys.* **32** (1961) 1679–1684.

[73] M. Akoshima, T. Baba, Thermal Diffusivity Measurements of Candidate Reference Materials by the Laser Flash Method, *Int. J. Thermophys.* **26** (2005) 151–163.

[74] R. D. Cowan, Pulse Method of Measuring Thermal Diffusivity at High Temperatures, *J. Appl. Phys.* **34** (1963) 926.

[75] B. L Wardle, D. S. Saito, E. J. García, A. J. Hart, R. G. de Villoria, E. A. Verploegen, Fabrication and Characterization of Ultrahigh-Volume- Fraction Aligned Carbon Nanotube-Polymer Composites, *Adv. Mater.* **20** (2008) 2707–2714.

[76] K. Hata, D. N. Futaba, K. Mizuno, T. Namai, M. Yumura, S. Iijima, Water-assisted highly efficient synthesis of impurity-free single-walled carbon nanotubes, *Science* **306** (2004) 1362–4.

[77] E. Einarsson, H. Shiozawa, C. Kramberger, M. H. Rummeli, A. Gruneis, P. Thomas, S. Maruyama, Revealing the small-bundle internal structure of vertically aligned single-walled carbon nanotube films, *J. Phys. Chem. C.* **111** (2007) 17861–17864.

[78] L. Lu, W. Yi, D. L. Zhang, 3Ω Method for Specific Heat and Thermal Conductivity Measurements, *Rev. Sci. Instrum.* **72** (2001) 2996.

[79] C. Masarapu, L. L. Henry, B. Wei, Specific heat of aligned multiwalled carbon nanotubes, *Nanotechnology* **16** (2005) 1490–1494.

[80] J. Hone, M. C. Llaguno, N. M. Nemes, A. T. Johnson, J. E. Fischer, D. A. Walters, M. J. Casavant, J. Schmidt, R. E. Smalley, Electrical and thermal transport properties of magnetically aligned single wall carbon nanotube films, *Appl. Phys. Lett.* **77** (2000) 666.

[81] E. Swartz, R. Pohl, Thermal boundary resistance, *Rev. Mod. Phys.* **61** (1989) 605–668.

[82] S. D. Kang, J. Joon Yoo, H.-K. Lyeo, J. Yong Song, S. Lee, J. Yu, Assessing the thermal conductivity of non-uniform thin-films: Nanocrystalline Cu composites incorporating carbon nanotubes, *J. Appl. Phys.* **110** (2011) 023506.

[83] J. Hong, J. Lee, C. K. Hong, S. E. Shim, Effect of dispersion state of carbon nanotube on the thermal conductivity of poly(dimethyl siloxane) composites, *Curr. Appl. Phys.* **10** (2010) 359–363.

[84] C.-W. Nan, G. Liu, Y. Lin, M. Li, Interface effect on thermal conductivity of carbon nanotube composites, *Appl. Phys. Lett.* **85** (2004) 3549.

[85] P.-C. Ma, J.-K. Kim, Carbon Nanotubes for Polymer Reinforcement, in: CRC Press, Taylor & Francis Group, LLC, 2011: pp. 117–121.

[86] N. Chakrapani, B. Wei, A. Carrillo, P. M. Ajayan, R. S. Kane, Capillarity-driven assembly of two-dimensional cellular carbon nanotube foams, *Proc. Natl. Acad. Sci. U. S. A.* **101** (2004) 4009–12.

[87] D. N. Futaba, K. Hata, T. Yamada, T. Hiraoka, Y. Hayamizu, Y. Kakudate, O. Tanaike, H. Hatori, M. Yumura, S. Iijima, Shape-engineerable and highly densely packed single-walled carbon nanotubes and their application as super-capacitor electrodes, *Nat. Mater.* **5** (2006) 987–94.

[88] E.J. García, A. J. Hart, B. L Wardle, A H. Slocum, Fabrication of composite microstructures by capillarity-driven wetting of aligned carbon nanotubes with polymers, *Nanotechnology* **18** (2007) 165602.

[89] X. Tian, M. E. Itkis, E. B. Bekyarova, R. C. Haddon, Anisotropic Thermal and Electrical Properties of Thin Thermal Interface Layers of Graphite Nanoplatelet-Based Composites, *Sci. Rep.* **3** (2013) 1–6.

[90] M. J. Biercuk, M. C. Llaguno, M. Radosavljevic, J. K. Hyun, A. T. Johnson, J. E. Fischer, Carbon nanotube composites for thermal management, *Appl. Phys. Lett.* **80** (2002) 2767.

[91] Y. Agari, A. Ueda, Y. Omura, S. Nagai, Thermal diffusivity and conductivity of PMMA/PC blends, *Polymer (Guildf)* **38** (1997) 801–807.

[92] J. Maxwell, A treatise on electricity and magnetism, 2nd ed., Clarendon Press, (1881).

[93] R. Hamilton, O. Crosser, Thermal conductivity of heterogeneous two-component systems, *Ind. Eng. Chem. Fundamen.* **1** (1962) 187–191.

[94] C. W. Nan, R. Birringer, D. R. Clarke, H. Gleiter, Effective thermal conductivity of particulate composites with interfacial thermal resistance, *J. Appl. Phys.* **81** (1997) 6692.

[95] C.-W. Nan, G. Liu, Y. Lin, M. Li, Interface effect on thermal conductivity of carbon nanotube composites, *Appl. Phys. Lett.* **85** (2004) 3549.

[96] Y. Murakami, S. Yamakita, T. Okubo, S. Maruyama, Single-walled carbon nanotubes catalytically grown from mesoporous silica thin film, *Chem. Phys. Lett.* **375** (2003) 393–398.

[97] Y. Shibuta, S. Maruyama, Molecular dynamics simulation of formation process of single-walled carbon nanotubes by CCVD method, *Chem. Phys. Lett.* **382** (2003) 381–386.

[98] Y. Murakami, Y. Miyauchi, S. Chiashi, S. Maruyama, Direct synthesis of high-quality single-walled carbon nanotubes on silicon and quartz substrates, *Chem. Phys. Lett.* **377** (2003) 49–54.

[99] Y. Murakami, S. Chiashi, Y. Miyauchi, M. Hu, M. Ogura, T. Okubo, S. Maruyama, Growth of vertically aligned single-walled carbon nanotube films on quartz substrates and their optical anisotropy, *Chem. Phys. Lett.* **385** (2004) 298–303.

[100] M. Hu, Y. Murakami, M. Ogura, S. Maruyama, T. Okubo, Morphology and chemical state of Co-Mo catalysts for growth ofBsingle-walled carbon nanotubes vertically aligned on quartz substrates, *J. Catal.* **225** (2004) 230–239.

[101] Y. Kawashima, G. Katagiri, Observation of the out-of-plane mode in the Raman scattering from the graphite edge plane, *Phys. Rev. B.* **59** (1999) 62–64.

[102] P. Araujo, S. Doorn, S. Kilina, S. Tretiak, E. Einarsson, S. Maruyama, H. Chacham, M. A. Pimenta, A. Jorio, Third and Fourth Optical Transitions in Semiconducting Carbon Nanotubes, *Phys. Rev. Lett.* **98** (2007) 067401.

[103] R. Mahajan, Emerging directions for packaging technologies, *Intel Technol. J.* 06 (2002) 62–75.

[104] H. Peng, X. Sun, Highly aligned carbon nanotube/polymer composites with much improved electrical conductivities, *Chem. Phys. Lett.* **471** (2009) 103–105.

[105] K. Bui, B. P. Grady, D. V. Papavassiliou, Heat transfer in high volume fraction CNT nanocomposites: Effects of inter-nanotube thermal resistance, *Chem. Phys. Lett.* **508** (2011) 248–251.

[106] E. W. Washburn, The dynamics of capillary flow, *Phys. Rev.* **17** (1921) 273–283.

[107] MSDS for Dow Corning Sylgard 184 Silicone Elastomer, Dow Corning Corporation 2013, www.dowcorning.com

[108] N. Kiuna, C. Lawrence, Q. Fontana, A model for resin viscosity during cure in the resin transfer moulding process, *Compos. Part A Appl. Sci. Manuf.* **33** (2002) 1497–1503.

[109] A. Barber, S. Cohen, H. Wagner, Static and Dynamic Wetting Measurements of Single Carbon Nanotubes, *Phys. Rev. Lett.* **92** (2004) 186103.

[110] Y. Xia, G. Whitesides, Soft lithography, *Annu. Rev. Mater. Sci.* **28** (1998) 153–184.

[111] C. P. Derdeyn, C. J. Moran, D. T. Cross, H. H. Dietrich, R. G. Dacey, Polyvinyl alcohol particle size and suspension characteristics, *AJNR. Am. J. Neuroradiol.* **16** (1995) 1335–1343.

[112] Z. Zhang, E. Einarsson, Y. Murakami, Y. Miyauchi, S. Maruyama, Polarization dependence of radial breathing mode peaks in resonant Raman spectra of vertically aligned single-walled carbon nanotubes, *Phys. Rev. B.* **81** (2010) 165442.

Curriculum Vitae

Education

Current: Ph. D. candidate in Mechanical Engineering

The University of Tokyo, Japan

Thermal properties of PDMS composite containing *aligned CNTs*

Advisor: Prof. Shigeo MARUYAMA

(G.P.A. 3.0/3.0)

MARCH 2011: M. Sc. in Mechanical Engineering

The University of Tokyo, Japan

Molecular dynamics simulation of thermal boundary conductance between SWNT and surrounding fluid

Advisor: Prof. Shigeo MARUYAMA

(G.P.A. 2.83/3.0)

FEBRUARY 2009: B. Sc. in Mechanical Engineering

B. Sc. in Japanese and Japanese Literature

Kyoungpook National University, Korea

(G.P.A. 4.07/4.5, Rank 2/32)

Awards / Scholarships / Honors / Certificates

2012: **2011' Outstanding GMSI Research Assistant Award**

21st Century Global Center of Excellence for Mechanical System Innovation, the University of Tokyo

2012: **Best Poster Award**

4th GMSI International Symposium, Tokyo, Japan

2011 – 2014: **University of Tokyo Fellowship**

Special Scholarship for International Students, the University of Tokyo

2011 – 2012: **Graduate Research Assistant**

21st Century Global Center of Excellence for Mechanical System Innovation (GMSI), the University of Tokyo

2010: **Excellent Poster Award**

A3 Symposium on Emerging Materials 2010 – Nanocarbons and Nanowires for Energy, Jeonju, Korea

2009: **Honors Scholarship** (for Privately Financed International Students)

Japan Student Services Organization (JASSO)

Research Interest

- Enhancement of thermal properties for polymer nanocomposites
- Measurement of physical properties for CNT nanocomposite
- Fabrication of polymer nanocomposite containing CNTs
- Analysis for nanomaterials with molecular dynamics (MD) simulation
- Thermal boundary resistance between CNT and surrounding fluid

Internships

- AUGUST 2012 – FEBRUARY 2013 :

  International research collaboration – 21st Century Global Center of Excellence for Mechanical System Innovation (GMSI)

  at Nano-Engineered Composite aerospace Structures (NECST) Laboratory (Prof. Brian L Wardle)

  Massachusetts Institute of Technology (M. I. T.), Cambridge, Massachusetts, USA

- SEPTEMBER 2010 :

  Institutional program for young researcher overseas visits – Japan Society for the Promotion of Science (JSPS)

  at NanoEngineering Group (Prof. Gang Chen)

  Massachusetts Institute of Technology (M. I. T.), Cambridge, Massachusetts, USA

- MARCH – AUGUST 2006 :

  Short term internship – New University for Regional Innovation, (NURI)

  at Solid Mechanics Laboratory (Prof. Yoji Shibutani)

  Osaka University, Osaka Japan

Languages

KOREAN: Mothertongue

ENGLISH: Fluent

JAPANESE: Fluent